Reports of the Department of Geodetic Science and Surveying

Report No. 360

UPWARD CONTINUATION OF SURFACE GRAVITY ANOMALIES

by

Jaime Y. Cruz and Piotr Laskowski

The Ohio State University
Department of Geodetic Science and Surveying
1958 Neil Avenue
Columbus, Ohio 43210

December 1984

AFGL-TR-84-0331

UPWARD CONTINUATION OF SURFACE GRAVITY ANOMALIES

Jaime Y. Cruz and Piotr Laskowski

The Ohio State University
Research Foundation
Columbus, Ohio 43210

December 1984

Scientific Report No. 8

AIR FORCE GEOPHYSICS LABORATORY
AIR FORCE SYSTEMS COMMAND
UNITED STATES AIR FORCE
HANSCOM AFB, MASSACHUSETTS 01731

Abstract

Investigations on the upward continuation of gravity anomalies given on the surface of the earth's visible topography are reported. Results are compared for three upward continuation procedures: first, the direct Poisson integration of the original terrain-uncorrected surface anomalies; second, the direct Poisson integration of terrain-corrected (i.e., Faye) surface anomalies; and third, the so-called indirect method. In the indirect method the original anomaly field is basically split into three frequency ranges that are then modeled separately: the low frequencies are modeled by spherical harmonics; the medium frequencies are modeled by Poisson integration of residual surface anomalies with long-wavelength terrain correction applied; and the high frequencies are modeled by prism integration of the gravitational effects of certain shallow topographic masses of assumed constant density.

Values of 5'x5' mean anomalies, 5'x5' mean elevations, and 30"x30" point elevations in a 7°x9° area covering both mountainous and smooth topography in New Mexico are used in actual upward continuations. Upward continued values are obtained for test profiles at elevations 30, 10, and 5 km, as well as for points in the float section (30 km elevation) of a balloon-borne gravity measuring project being coordinated by the Air Force Geophysics Laboratory (AFGL). The test profiles resulting from the direct Poisson integration of terrain-uncorrected anomalies are negatively biased (i.e., too low) by about (0.6, 0.5, 0.7) mgal at elevation (30, 10, 5) km compared with the profiles resulting from the direct Poisson integration of terrain-corrected anomalies. There is no detectable bias between the latter set of profiles and those from the indirect method. The standard deviation of the differences among the three upward continuation methods reaches the order of (0.5, 0.6, 1.3) mgal at (30, 10, 5) km elevation, for the profiles tested. Also presented is an analysis of errors associated with upward continued anomalies and with computed normal gravity values. It is projected that values at the AFGL balloon points have been recovered with about 0.9 mgal total standard error in gravity anomaly with data error propagation as dominating error source, and about 0.7 mgal error in normal gravity with vertical position error as dominating error source. In a separate series of tests, it is shown that upward continuations using Fast Fourier techniques produce results that agree with Poisson integration on the level of (0.1, 0.3) mgal at (30, 10) km elevation.

Foreword

This report was prepared by Jaime Y. Cruz and Piotr Laskowski, Graduate Research Associates, Department of Geodetic Science and Surveying, The Ohio State University, under Air Force Contract No. F19268-82-K-0022, The Ohio State University Research Foundation Project No. 714274. This project is under the supervision of Professor Richard H. Rapp. The contract covering this research is administered by the Air Force Geophysics Laboratory, Hanscom Air Force Base, Massachusetts, with Dr. Christopher Jekeli, Scientific Program Officer.

Acknowledgements

The authors gratefully acknowledge the guidance received from Dr. Richard H. Rapp throughout the investigations and writing of the report, and the excellent skill applied by Ms. Laura Brumfield in typing the report.

Table of Contents

	Abstract	ii
	Foreword	iii
	Acknowledgements	iv
1.	Introduction	1
2.	Upward Continuation Formulas	3
	2.1 Spherical-Earth Poisson Integral	3
	2.2 Spherical Harmonics	5
	2.3 Flat-Earth Poisson Integral	7
	2.4 Fourier Transform	8
	2.5 Direct Topographic Mass Effect	10
	2.6 Normal Gravity in Space	12
3.	Upward Continuation of Surface Free-Air Anomalies	15
	3.1 Available Anomalies as Surface Free-Air Anomalies	15
	3.2 Rationale Behind an Indirect Method of Upward Continuation of Surface Anomalies	18
	3.3 Direct and Indirect Upward Continuation	19
4.	Anomaly Field Truncation Theory	25
5.	Global Characterization of Anomaly Fields	34
6.	Error Propagation for Upward Continuation Operator	38
	6.1 Flat-Earth Data Error Propagation	38
	6.2 Spherical-Earth Data Error Propagation	40
	6.3 Flat-Earth Discretization Error Propagation	43
7.	Operational Generation of Anomaly Fields	47
8.	Data Preparation for Upward Continuation Tests in New Mexico	49
	8.1 Available Gravity and Elevation Data	49
	8.2 Data Thinning	51
	8.3 5'x5' Mean Anomalies	51
	8.4 Covariance Function	54
	8.5 Data De-Trending at High Frequencies	55
	8.6 Data De-Trending at Low Frequencies	56
	8.7 Actual Predictions of 5'x5' Mean Anomalies	57

9. Numerical Investigations 68
9.1 Comparison of Direct and Indirect Upward Continuation Results 68
9.2 Other Studies 72
9.3 Fourier Computations 83
10. Applications to Balloon Gravity Project 88
10.1 Preparation of Tracking Data 88
10.2 Reference Systems 89
10.3 Upward Continuation Results 94
10.4 Interpolation of Results at Altitude 94
10.5 Propagation of Tracking Errors 95
10.6 Other Sources of Errors 96
11. Summary and Conclusions 100
Appendix - DFT Program for Upward Continuation 104
References 108

1. Introduction

This report is concerned with the upward continuation of gravity anomaly data given on the surface of the earth. A number of computational procedures to be presented here are offshoots from the studies of Cruz (1985) dealing with modeling the external gravity disturbance vector field.

Various modern possibilities exist to model the external gravity field of the earth for the realistic case of free-air anomalies being given on the surface of the earth's visible topography. These possibilities fall under two general types of modeling approaches: the continuous approach, and the discrete approach. In the continuous approach the free-air anomalies are assumed to be known at every point of the earth's surface, and the Molodensky problem is being solved. In the discrete approach the anomalies are known only at discrete points of the earth's surface, and the Bjerhammar problem is then being solved. In this report we have used the discrete approach, specifically least squares collocation, only in the first stage of data processing, for the purpose of generating an optimal set of mean surface free-air anomalies from the originally given irregular and discrete distribution of point anomaly data. After this, using the optimal set of surface data and concepts from the continuous approach we generated our quantity of interest which is the upward continued anomaly.

The simplest conceptualization of a solution to the (continuous) Molodensky's problem is by means of analytic continuation advocated in Moritz (1969). The external gravity anomaly field is analytically continued to a level surface which may be entirely above, partly above and partly below, or entirely below the earth's surface. Once the level surface anomalies are known, then under a spherical approximation the external gravity field can be generated from these anomalies using classical procedures for data on a sphere. A general procedure for analytical continuation is by means of Taylor series:

$$\Delta g_p^* = \Delta g_s + \frac{\partial \Delta g}{\partial H}(H_p - H_s) + \frac{1}{2}\frac{\partial^2 \Delta g}{\partial H^2}(H_p - Hs)^2 + \ldots \qquad (1.1)$$

where

Δg_s	surface free-air anomaly, defined more precisely in section 3
Δg_p^*	anomaly in the same plumb line as Δg_s, but located on the level surface, to which the surface data are being reduced
H_s	elevation of the surface point to which Δg_s applies
H_p	elevation of the level surface of Δg_p^*
$\frac{\partial \Delta g}{\partial H}$	vertical gradient of the gravity anomaly field

If the level surface to which the data are reduced is entirely below the earth's surface the analytical (downward) continuation may also be done by an inversion, usually by successive approximations, of the classical Poisson

integral (see equation (2.1.13))

$$\Delta g_S = \frac{t^2(1-t^2)}{4\pi} \iint_\sigma \frac{\Delta g_P^*}{D^3}\, d\sigma, \qquad (1.2)$$

in accordance with the procedures of Bjerhammar (1964).

The use of (1.1) presents practical difficulties because the computation of the required vertical gradients of the gravity anomaly field, even just the first gradient and the more so the higher order gradients, poses rather severe requirements on the density and accuracy of gravity data (for a study of numerical evaluation of the gradients, see Noe, 1980). Therefore, the techniques that we have used in this report have a common motivation, namely to avoid altogether the use of correction terms in (1.1) and therefore use only the first term. The different manners in which the correction terms are avoided give rise to three methods for upward continuation which we numerically tested and compared using real gravity and elevation data. The first method, and the crudest, is to simply drop the correction terms and take Δg_P^* to be equal to Δg_S; we therefore simply insert Δg_S directly into the classical Poisson upward continuation integral for data on a sphere. This procedure will obviously be in error especially in areas with rough anomaly field and our numerical study will provide a feeling for the magnitude of this error. The second method is to drop all correction terms, only after the terrain correction has been applied to Δg_S. The application of the terrain correction is viewed as a first order attempt to reduce the surface data Δg_S to a level surface; the reduced data are then inserted into the Poisson upward continuation integral. The third method is to drop the correction terms, only after smoothing the anomaly field by the subtraction of the gravitational effects of certain shallow topographic masses of assumed density. The total upward continued anomaly field is then the sum of two fields: one generated by classical Poisson integration from the residual anomalies left after the removal of topographic masses, and the other is the field generated by integration of the gravitational effects of the removed topographic masses themselves. This third method is in the spirit of the "remove-restore" technique advocated in the works of Tscherning and Forsberg (see Tscherning, 1979; Tscherning and Forsberg, 1983; and Forsberg, 1984, p. 41).

Other concerns of this report include the use of spherical harmonics in anomaly field modeling, the use of Fourier series for upward continuation, and the application of studied modeling techniques to the balloon-borne gravity project being coordinated by the Air Force Geophysics Laboratory (Lazarewicz, et al., 1983).

2. Upward Continuation Formulas

2.1 Spherical-Earth Poisson Integral

Let us use the spherical coordinates r (geocentric radius), $\bar{\Phi}$ (geocentric latitude), and λ (geocentric longitude). The anomalous potential $T(r, \bar{\Phi}, \lambda)$ being a harmonic function in space has surface spherical harmonics $T_n(R, \bar{\Phi}, \lambda)$ attenuating with $r^{-(n+1)}$ (Heiskanen and Moritz, 1967, p. 35):

$$T_n(r, \bar{\Phi}, \lambda) = \left(\frac{R}{r}\right)^{n+1} T_n(R, \bar{\Phi}, \lambda) \qquad (2.1.1)$$

The surface harmonics of the gravity anomaly $\Delta g(r, \bar{\Phi}, \lambda)$ and anomalous potential $T(r, \bar{\Phi}, \lambda)$ are fundamentally related, in a spherical approximation, as follows (ibid., pp. 88-89):

$$\Delta g_n(r, \bar{\Phi}, \lambda) = \frac{n-1}{r} T_n(r, \bar{\Phi}, \lambda) \qquad (2.1.2)$$

The last equation becomes for r=R:

$$\Delta g_n(R, \bar{\Phi}, \lambda) = \frac{n-1}{R} T_n(R, \bar{\Phi}, \lambda) \qquad (2.1.3)$$

Substituting (2.1.1) into (2.1.2):

$$\Delta g_n(r, \bar{\Phi}, \lambda) = \frac{n-1}{R} \left(\frac{R}{r}\right)^{n+2} T_n(R, \bar{\Phi}, \lambda) \qquad (2.1.4)$$

Substituting (2.1.3) into (2.1.4):

$$\Delta g_n(r, \bar{\Phi}, \lambda) = \left(\frac{R}{r}\right)^{n+2} \Delta g_n(R, \bar{\Phi}, \lambda), \qquad (2.1.5)$$

that is, the surface harmonics of Δg attenuate as $r^{-(n+2)}$. The upward continued anomaly $\Delta g(r, \bar{\Phi}, \lambda)$ is found by summing the terms in (2.1.5). After omitting the zero and first degree harmonics as customary:

$$\Delta g(r, \bar{\Phi}, \lambda) = \sum_{n=2}^{\infty} \left(\frac{R}{r}\right)^{n+2} \Delta g_n(R, \bar{\Phi}, \lambda) \qquad (2.1.6)$$

The space domain equivalent of (2.1.6) is:

$$\Delta g(r, \bar{\Phi}, \lambda) = \frac{1}{4\pi} \iint_{\sigma} K(t, \psi)\, \Delta g(R, \bar{\Phi}', \lambda')\, d\sigma \qquad (2.1.7)$$

where

$$t = \left(\frac{R}{r}\right)$$

$$K(t, \psi) = \sum_{n=2}^{\infty} (2n+1)\, t^{n+2}\, P_n(\cos \psi) \qquad (2.1.8)$$

$$\cos \psi = \sin \bar{\Phi} \sin \bar{\Phi}' + \cos \bar{\Phi} \cos \bar{\Phi}' \cos (\lambda' - \lambda) \qquad (2.1.9)$$

A closed form for $K(t, \psi)$ can be obtained using the following relation (ibid., p. 35):

$$\frac{t(1-t^2)}{D^3} = \sum_{n=0}^{\infty} (2n+1)\, t^{n+1}\, P_n(\cos \psi) \qquad (2.1.10)$$

where $D = (1 + t^2 - 2t \cos \psi)^{1/2}$ (2.1.11)

Multiplying (2.1.10) by t, removing the zero and first degree ha monics, and combining with (2.1.8) we get the closed form:

$$K(t, \psi) = \frac{t^2(1-t^2)}{D^3} - t^2 - 3t^3 \cos \psi \qquad (2.1.12)$$

Equation (2.1.7) with (2.1.12) is the same as equation (2.160) in ibid., p. 90, and is in fact the well-known Poisson integral formula for the space domain upward continuation of gravity anomalies given on the surface of a geocentric sphere. Note that the second and third terms of the integral kernel $K(t, \psi)$ are related to the removal of the zero and first degree harmonics from the gravity anomaly field. For our (low altitude) applications, however, these terms have negligible effects and so it is sufficient to retain only the first term of the integral kernel, giving:

$$\Delta g(r, \bar{\Phi}, \lambda) = \frac{t^2(1-t^2)}{4\pi} \iint_{\sigma} \frac{\Delta g(R, \bar{\Phi}', \lambda')}{D^3}\, d\sigma \qquad (2.1.13)$$

Note that (2.1.13) needs gravity anomalies to be given on the surface of a (geocentric) sphere. In practice, we have gravity anomalies given on the surface of a (geocentric) reference ellipsoid (the problem of the topography is taken care of separately). To still use (2.1.13) in practice, we follow the spherical approximation used in Heiskanen and Moritz (1967, p. 241):

Spherical Approximation

$$\Delta g(r, \phi, \lambda) = \frac{t^2(1-t^2)}{4\pi} \int\int_{\sigma} \frac{\Delta g(r_E, \phi', \lambda')}{D^3} \, d\sigma \qquad (2.1.13a)$$

$$t = \frac{R}{R+H_o} \qquad (2.1.13b)$$

$$\cos \psi = \sin \phi \sin \phi' + \cos \phi \cos \phi' \cos(\lambda'-\lambda) \qquad (2.1.13c)$$

where

(r, ϕ, λ)	geocentric radius, and geodetic latitude and longitude of the computation point in space.
(r_E, ϕ', λ')	geocentric radius, and geodetic latitude and longitude of data point on the reference ellipsoid.
R	a mean earth radius, taken as R=6371 km.
H_o	height of the computation point (r, ϕ, λ) above the reference ellipsoid; we will also call H_o the upward continuation distance, i.e. the distance through which the data are upward continued to arrive at the value of anomaly in space.
D	still evaluated by (2.1.11), but now using t from (2.1.13b) and cos ψ from (2.1.13c).

2.2 Spherical Harmonics

The surface spherical harmonics of the anomalous potential $T(r, \Phi, \lambda)$ on a sphere of radius "a" can be written as (Rapp, 1982):

$$T_n(a, \bar{\Phi}, \lambda) = \frac{kM}{a} \sum_{m=0}^{n} (\bar{C}^*_{nm} \cos m\lambda + \bar{S}_{nm} \sin m\lambda)\, \bar{P}_{nm}(\sin \bar{\Phi}) \qquad (2.2.1)$$

where

a	usually an equatorial radius
kM	geocentric gravitational constant
$\bar{C}^*_{nm}$, $\bar{S}_{nm}$	fully normalized potential coefficients with even-degree zonal reference values subtracted
$\frac{kM}{a}\bar{C}^*_{nm}$, $\frac{kM}{a}\bar{S}_{nm}$	spectrum of $T(r, \bar{\Phi}, \lambda)$ on the sphere of radius a
$\bar{P}_{nm}$	fully normalized Legendre functions

The upward continued gravity anomalies from spherical harmonics are obtained by substituting (2.2.1) into (2.1.4) with R=a, then summing the surface harmonics:

$$\Delta g(r, \bar{\Phi}, \lambda) = \frac{kM}{a^2} \sum_{n=2}^{\infty} (n-1)\left(\frac{a}{r}\right)^{n+2} \sum_{m=0}^{n} (\bar{C}^*_{nm} \cos m\lambda + \bar{S}_{nm} \sin m\lambda)\, \bar{P}_{nm}(\sin \bar{\Phi}) \qquad (2.2.2)$$

For the purposes of this report we would like to use spherical harmonics to generate a rigorously self-consistent field of gravity anomalies on the earth's surface and in space. This field is to be used as reference, to be subtracted from the observed field as part of upward continuation procedures. For this purpose (2.2.2) can be used, but during our applications and because we used the Rapp (1981) field we decided to use the following equation instead:

$$\Delta g(r, \phi, \lambda) = \frac{kM}{a^2} \sum_{n=2}^{\infty} (n-1) \left(\frac{a}{a+H_o}\right)^{n+2} \sum_{m=0}^{n} \cdot$$

$$(\bar{C}^*_{nm} \cos m\lambda + \bar{S}_{nm} \sin m\lambda)\, \bar{P}_{nm}(\sin \phi), \qquad (2.2.3)$$

where, as in (2.1.13b), H_o is the height of the computation point (r, ϕ, λ) above the reference ellipsoid.

Equation (2.2.3) was motivated by the fact that for a point on the ellipsoid (i.e., $r = r_E$, $H_o = 0$) (2.2.3) becomes:

$$\Delta g(r_E, \phi, \lambda) = \frac{kM}{a^2} \sum_{n=2}^{\infty} (n-1) \sum_{m=0}^{n} \cdot$$

$$(\bar{C}^*_{nm} \cos m\lambda + \bar{S}_{nm} \sin m\lambda)\ \bar{P}_{nm}(\sin \phi). \qquad (2.2.4)$$

The last equation is essentially the equation inverted in Rapp, 1981, eq. (2) (except that Rapp used the geocentric latitude $\bar{\phi}$ instead of the geodetic latitude ϕ) to compute his coefficients C^*_{nm}, S^*_{nm} from terrestrial data $\Delta g(r_E, \phi, \lambda)$; realizing this we merely constructed (2.2.3) as an upward continued version of (2.2.4) under a spherical approximation. The rationale behind (2.2.3) does not hold at lower degrees (say, $n \leq 36$) of the Rapp-1981 field, these degrees being dominated by satellite derived coefficients $\bar{C}^*_{nm}$, $\bar{S}^*_{nm}$. Nevertheless, we decided to use (2.2.3) entirely, for n=2 to 180°; in any case, (2.2.3) serves our above stated purpose of generating a self-consistent, spatial reference anomaly field from a set of spherical harmonic coefficients.

2.3 Flat-Earth Poisson Integral

For our applications of the Poisson integral (2.1.13a) it is sufficient to use a planar approximation, namely (Rapp, 1966; Hirvonen and Moritz, 1963):

$$\Delta g(r, \phi, \lambda) = \frac{H_o}{2\pi} \iint_A \frac{\Delta g(r_E, \phi', \lambda')}{D_o^3}\, dx\, dy \qquad (2.3.1)$$

where

A	fixed integration area
D_o	$(x^2 + y^2 + H_o^2)^{1/2}$
x	$R \cos \phi' (\lambda' - \lambda)$
y	$R(\phi' - \phi)$

Equation (2.3.1) represents a flat-earth, space domain upward continuation formula for gravity anomalies. This equation is indicated to be valid for a distance up to 20° from the computation point and up to an upward continuation distance of 250 km (Hirvonen and Moritz, 1963, p. 71).

2.4 Fourier Transform

In this section we briefly introduce the 3-dimensional Dirichlet problem for the half-space and state its solution. This forms the theoretical basis on which the Fourier transformation technique can be implemented in upward continuation problems. Fourier technique offers high speeds in computation, requiring no more assumptions than the planar Poisson's integral method does. Now we will state the problem theoretically (refer to later sections for examples of practical implementation).

The Dirichlet problem in three-dimensions consists of the Laplace equation

$$\frac{\partial^2 f}{\partial x^2} + \frac{\partial^2 f}{\partial y^2} + \frac{\partial^2 f}{\partial z^2} = \nabla^2 f = 0$$

within some region V with boundary surface S, together with data prescribed on S.

We will use the usual planar approximation to the earth's surface, where the boundary surface S is the plane z=0 and the volume of interest V is the half-space z>0. The solution to this problem is known in the literature (Robinson E.A., M.T. Silvia, 1981, p. 223) as the Dirichlet integral.

$$f_z(x, y) = f(x, y, z) = \frac{z}{2\pi} \int_{-\infty}^{\infty} \int_{-\infty}^{\infty} \frac{f(\alpha, \beta)\ d\alpha d\beta}{[(x-\alpha)^2 + (y-\beta)^2 + z^2]^{3/2}}\ , \quad z > 0 \tag{2.4.1}$$

where $f(\alpha, \beta) = f(\alpha, \beta, 0)$ are boundary values of f for z=0.

In this report the function f to be upward continued is gravity anomaly function. The gravity anomaly is a harmonic function in case of the planar Dirichlet problem as stated above. We use the fact that in our planar case vertical gravity satisfies the Laplace equation if the potential does. The proof can be found in (Robinson E.A., M.T. Silvia, 1981, p. 213).

The solution (2.4.1) is identical with the Poisson's integral for gravity anomalies introduced in Section 2.3. Poisson's integral can be viewed as a limiting case for the sphere of radius R when $R \to \infty$. On the other hand the Dirichlet solution (2.4.1) is derived for the planar case of half-space z>0 using the Green's second identity (Robinson E.A., M.T. Silvia, 1981, ch. 4). Notice that (2.4.1) represents the 2-dimensional convolution integral.

Equation (2.4.1) can be written in the form:

$$f_z(x, y) = \int_{-\infty}^{\infty} \int_{-\infty}^{\infty} f(\alpha, \beta)\ a(x-\alpha, y-\beta)\ d\alpha\ d\beta \tag{2.4.2}$$

where $$a(x, y) = \frac{z}{2\pi} \frac{1}{(x^2 + y^2 + z^2)^{3/2}} \qquad (2.4.3)$$

a(x, y) can be viewed as the impulse response function of the upward continuation operation (2.4.2).

Now, the 2-dimensional Fourier transform of (2.4.3) is defined as (Robinson E.A., M.T. Silvia, 1981, p. 224):

$$A(k_x, k_y) = \int_{-\infty}^{\infty} \int_{-\infty}^{\infty} a(x, y)\, e^{2\pi i(k_x x + k_y y)}\, dxdy = e^{-z \cdot 2\pi \sqrt{k_x^2 + k_y^2}}, \qquad (2.4.4)$$

for $z > 0$, $i = \sqrt{-1}$

(see equation 7, p. 11 and equation 44, p. 56, Erdelyi et al., 1954).

This is the frequency response or transfer function associated with upward continuation operator. The function $A(k_x, k_y)$ is a spatial frequency function of two continuous variables k_x, k_y representing the frequencies (in cycles per unit length) along x and y directions.

The boundary values $f(\alpha, \beta)$ can be transformed to the frequency domain by means of the Fourier integral:

$$F(k_x, k_y) = \int_{-\infty}^{\infty} \int_{-\infty}^{\infty} f(x, y)\, e^{2\pi i(k_x x + k_y y)}\, dxdy \qquad (2.4.5)$$

Using this transform the equivalence of the Dirichlet integral (2.4.1) in the frequency domain turns out to be the multiplication of the transfer function (2.4.4) and the Fourier transform of the data measured at the boundary surface:

$$F_z(k_x, k_y) = A(k_x, k_y) \cdot F(k_x, k_y) = e^{-z 2\pi \sqrt{k_x^2 + k_y^2}} \cdot F(k_x, k_y) \qquad (2.4.6)$$

Finally, the desired upward-continued function is obtained by the inverse Fourier transform of the frequency function F_z (Bhattacharyya, 1967):

$$f_z(x, y) = \frac{1}{4\pi^2} \int_{-\infty}^{\infty} \int_{-\infty}^{\infty} F_z(k_x, k_y)\, e^{-2\pi i(k_x x + k_y y)}\, dk_x dk_y \qquad (2.4.7)$$

2.5 Direct Topographic Mass Effect

Topographic heights are a much more readily available and cheap type of information than gravity anomalies themselves, and can be effectively utilized in gravity anomaly interpolation and upward continuation problems. The idea is to subtract, from the originally given gravity anomaly boundary values on the earth's surface, the gravity anomaly effects caused by topographic masses of assumed density. The residual anomalies are then smoother and can be much more easily interpolated and upward continued than the original anomalies. The removed effects of the topographic masses are then added back at the interpolation points or at the upward continuation points by direct integration of the gravitational influence of the masses at those points.

Topographic masses of assumed constant density ρ (e.g., ρ=2.67 g/cm^3 is a standard density for land areas) directly generate gravitational attractions at points on or above the earth's surface. Considering the topographic masses as anomalous, we have the following "topographic" anomalous potential generated at the point P in space (Heiskanen and Moritz, 1967, p. 3):

$$T_P^t = k\rho \iiint_v \left(\frac{1}{\ell_Q}\right) dv_Q \qquad (2.5.1)$$

where

k	Newtonian gravitational constant
ρ	constant density of the topographic masses
dv_Q	element of volume
v	volume occupied by the masses
ℓ_Q	$(r_P^2 + r_Q^2 - 2r_P r_Q \cos\psi_{PQ})^{1/2}$, i.e., the spatial distance between P and Q
ψ_{PQ}	angular distance between P and Q
r_P, r_Q	geocentric radius of P, Q.

We have the following fundamental relation between gravity anomaly Δg and anomalous potential T in a spherical approximation (ibid., p. 88):

$$\Delta g = \frac{-\partial T}{\partial r} - \frac{2}{r} T \qquad (2.5.2)$$

Substituting (2.5.1) into (2.5.2), exchanging the order of integration and differentiation, and performing the differentiations, yield:

$$\Delta g_P^t = k\rho \iiint_V \left(\frac{r_P - r_Q \cos \psi_{PQ}}{\ell_Q^3} - \frac{2}{\ell_Q r_P} \right) dv_Q \qquad (2.5.3)$$

The last equation gives the ("topographic") gravity anomaly in space generated by topographic masses of assumed density.

For the generation of topographic gravity anomalies right on the surface of the earth, a special treatment is sometimes convenient. Assuming that the masses referred to are those lying between the actual topography and the geoid we can perform the following split (see ibid., pp. 130-132):

$$\Delta g_Q^t = \Delta g_Q^{BA} - tc_Q \qquad (2.5.4)$$

where

Δg_Q^t	vertical attraction at the surface point Q generated by topographic masses lying between the actual topography and the geoid.
Δg_Q^{BA}	vertical attraction at Q generated by a Bouguer plate through Q.
tc_Q	the well-known gravimetric terrain correction at Q, to account for the difference between the attraction Δg_Q^{BA} caused by the Bouguer plate and the attraction Δg_Q^t caused by the actual topographic masses.

In terms of formulas:

$$\Delta g_Q^{BA} = 2\pi k\rho H_Q \qquad (2.5.5)$$

$$tc_Q = \tfrac{1}{2} k\rho R^2 \iint_\sigma \frac{(H-H_Q)^2}{\ell_0^3} d\sigma \qquad (2.5.6)$$

in which (Moritz, 1966, p. 88):

R	mean earth radius
H	elevation of integration point
H_Q	elevation of computation point
σ	unit sphere
$d\sigma$	element of solid angle
ℓ_0	$2R \sin \psi/2$
ψ	angular distance between Q and $d\sigma$.

The use of the symbol "Δ" in (2.5.4) is intended to suggest that in this report we are using the attractions Δg_Q^t and Δg_Q^{BA} as components of gravity

anomalies at the point Q. This means that we are viewing Δg_Q^t and Δg_Q^{BA} as components of excesses or deficiencies of the actual gravity at the point Q over the normal gravity at the "corresponding" normal point Q' (the correspondence between Q and Q' is that the actual potential at Q is equal to the normal potential at Q', and Q and Q' lie on the same plumb line of the normal field - see Heiskanen and Moritz, 1967, p. 83). In this sense we may also call Δg_Q^t and Δg_Q^{BA} as gravity anomalies generated by the topographic masses and Bouguer plate, respectively.

2.6 Normal Gravity in Space

The spatial relationship between the actual gravity field and the normal gravity field generated by a given ellipsoid of reference is given on the diagram on the next page. The geop passing through point P has the same constant potential as the spherop passing through the point Q, where the geop and spherop are the equipotential surfaces of the actual and ellipsoidal gravity field respectively.

Normal gravity corresponding to a given value of gravity anomaly at a fixed location P in space is defined to be the vertical component of attraction generated by the equipotential ellipsoid of revolution (rotating with the same angular velocity ω as the real earth) at the respective point Q located on the equipotential surface of the ellipsoidal field corresponding to point P. The spatial correspondence between P and Q is uniquely determined by the requirement that the earth's gravity potential at P is equal to the normal gravity potential of ellipsoid at the corresponding point Q. The normal gravity in space is fully determined by the geometric (size and shape) and the physical (surface potential and the rotation) properties of the level ellipsoid. Combined with the gravity anomaly the normal gravity can be used to compute the vertical attraction due to the actual Earth at any location. For the purpose of this report we use the equations by (Hirvonen, 1960), as implemented by (Rapp, Feb. 1966) in his FORTRAN subprogram 'SGAMMT'.

Although the method of Hirvonen was fully described by (Rapp, Jan. 1966) and then fully documented for the computer implementation in (Rapp, Feb. 1966) we decided to state here the equations used by the subprogram 'SGAMMT'. For details the reader is referred to (Hirvonen, 1960) and (Rapp, Jan. 1966).

Suppose we need the vertical component of normal gravity γ_T corresponding to the computation point P having the coordinates ϕ, λ, h, where h is the geometric height of P above the reference ellipsoid. Then, following (Heiskanen and Moritz, 1967, eq. (8-5)) the normal gravity γ_T should be referred to some point Q which is the 'normal' counterpoint of P. Point Q can be found by projecting point P from the geop having potential W_p on to the corresponding spherop having normal potential $U=W_p$ (see diagram below). The distance between P and Q or the geop-spherop separation is called the height anomaly ζ. The geometric height of 'normal' point Q above reference ellipsoid is defined to be the normal height H^* of the corresponding point P.

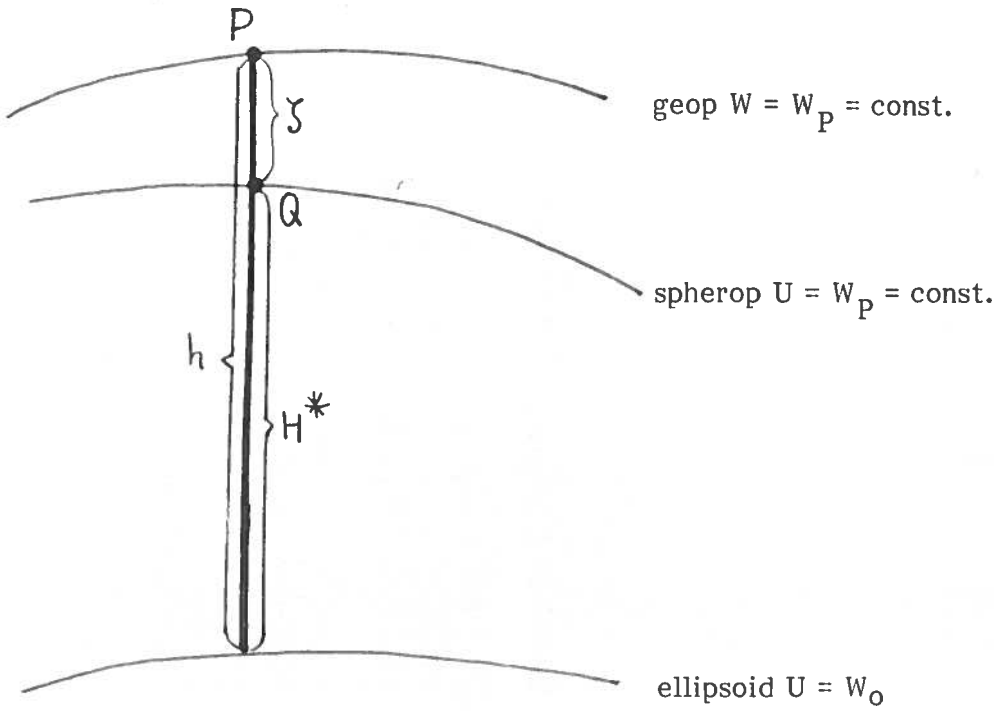

Diagram for Section 2.6

The relation between the geometric height h, normal height H^* and the height anomaly ζ, for a given computation point P in space.

For the computation of normal gravity γ_T we require the normal height H^*. Based on (Heiskanen and Moritz, 1967, eq. (8-5)) H^* can be derived from h and height anomaly ζ according to the formula:

$$H^* = h - \zeta \qquad (2.6.1)$$

For our balloon project we converted the known geometric heights into the normal heights using the height anomalies estimated from the spherical harmonic expansion of gravity field up to degree 180 (Rapp, 1981).

Here we will give a summary of the procedure as presented in (Rapp, January 1966, pp. 14-16):

Input: (ϕ, λ, H^*) plus parameters of the normal ellipsoid.

Compute:

$$X = (N + H^*) \cos \phi \cos \lambda \tag{2.6.2}$$

$$Y = (N + H^*) \cos \phi \sin \lambda \tag{2.6.3}$$

$$Z = (N(1-e^2) + H^*) \sin \phi \tag{2.6.4}$$

$$\text{with } N = a/(1-e^2 \sin^2 \phi)^{\frac{1}{2}} \tag{2.6.5}$$

$$p^2 = X^2 + Y^2 \tag{2.6.6}$$

$$r^2 = p^2 + Z^2 \tag{2.6.7}$$

$$c = ae \tag{2.6.8}$$

$$K^2 = r^2 + c^2 \tag{2.6.9}$$

$$h^2 = K^4 - 4p^2c^2)^{\frac{1}{2}} \tag{2.6.10}$$

$$\sin^2\alpha = \frac{K^2-h^2}{2p^2} \tag{2.6.11}$$

$$\tan \beta = \frac{Z}{p \cos \alpha} \tag{2.6.12}$$

$$q = \tfrac{1}{2} [\alpha - 3 \cot \alpha (1-\alpha \cot \alpha)] \tag{2.6.13}$$

$$q' = \frac{3(1 - \alpha \cot \alpha)}{\sin^2 \alpha} - 1 \tag{2.6.14}$$

$$w = (1 - \sin^2\alpha \cos^2\beta)^{\frac{1}{2}} \tag{2.6.15}$$

$$\Gamma_\alpha = \frac{KM \sin^2\alpha}{c^2 w} + \frac{w^2a^2q' \sin^2\alpha}{2cq_o w} (\sin^2\beta - \frac{1}{3}) \tag{2.6.16}$$

$$\Gamma_\beta = \frac{w^2a^2q \sin \alpha \sin \beta \cos \beta}{cq_o w} \tag{2.6.17}$$

$$\gamma_\alpha = \Gamma_\alpha - \frac{w^2c \cos^2\beta}{w \tan \alpha} \tag{2.6.18}$$

$$\gamma_\beta = -\Gamma_\beta + \frac{w^2c \sin \beta \cos \beta}{w \sin \alpha} \tag{2.6.19}$$

$$\gamma_T = (\gamma_\alpha^2 + \gamma_\beta^2)^{\frac{1}{2}} \tag{2.6.20}$$

where γ_T is the normal gravity in the vertical direction.

3. Upward Continuation of Surface Free-Air Anomalies

In this section we will describe a procedure that can be used for the upward continuation of free-air anomalies given on the surface of the earth. These surface free-air anomalies are boundary values of free-air anomalies in space. Recall from Heiskanen and Moritz (1967, pp. 91, 292) that the gravity anomaly on or above the surface of the earth is defined as follows:

$$\Delta g_P(h, \phi, \lambda) = g_P(h, \phi, \lambda) - \gamma_Q(H^*, \phi, \lambda) \tag{3.1}$$

where (see diagram on p. 13)

Δg_P	gravity anomaly at P
h	height of P above the reference ellipsoid
ϕ, λ	geodetic latitude and longitude of P and Q
Q	normal point of P; point Q is established such that the actual gravity potential W_P at P is equal to the normal gravity potential U_Q at Q, and P and Q lie on the same plumb line of the normal gravity field.
H^*	height of the normal point Q above the reference ellipsoid; H^* is called the normal height of P.
g_P	gravity at P
γ_Q	normal gravity at Q.

Below we first show that operationally available anomalies can be closely interpreted as surface free-air anomalies, and then we describe a strategy for upward continuation of these anomalies combining Poisson integration, spherical harmonics, and topographic mass effects.

3.1 Available Anomalies as Surface Values

In practice, available gravity anomalies had been computed from:

$$\Delta g = g_P(h, \phi, \lambda) - \left(\frac{\partial \gamma}{\partial h}\right)_P H - \gamma_P'(0, \phi, \lambda) \tag{3.1.1}$$

where

h, ϕ, λ	ellipsoidal height, geodetic latitude, and geodetic longitude of a gravity station P
$g_P(h, \phi, \lambda)$	measured gravity at P
H	orthometric height of P

$\left(\frac{\partial\gamma}{\partial h}\right)_P$ vertical gradient of the normal gravity at P

$\gamma_P'(0, \phi, \lambda)$ normal gravity on the ellipsoid, at the point P' that has the same (ϕ, λ) as P.

At this point, assume that we do not know the vertical location of the point at which the Δg found by (3.1.1) applies, and let us find this location. Let H^* be the normal height of P as defined in equation (3.1); we can then perform the following manipulations on (3.1.1):

$$\Delta g = g_P(h, \phi, \lambda) - \left[\gamma_P'(0, \phi, \lambda) + \left(\frac{\partial\gamma}{\partial h}\right)_P H\right]$$

$$= g_P(h, \phi, \lambda) - \left[\gamma_P'(0, \phi, \lambda) + \left(\frac{\partial\gamma}{\partial h}\right)_P H + \left(\frac{\partial\gamma}{\partial h}\right)_P H^* - \left(\frac{\partial\gamma}{\partial h}\right)_P H^*\right]$$

$$= g_P(h, \phi, \lambda) - \left[\gamma_P'(0, \phi, \lambda) + \left(\frac{\partial\gamma}{\partial h}\right)_P H^*\right] + \left(\frac{\partial\gamma}{\partial h}\right)_P (H^*-H) \qquad (3.1.2)$$

The quantity in brackets is the normal gravity, upward continued from the ellipsoidal point P' to the normal point Q of P defined in equation (3.1):

$$\gamma_Q(H^*, \phi, \lambda) = \gamma_P'(0, \phi, \lambda) + \left(\frac{\partial\gamma}{\partial h}\right)_P H^* \qquad (3.1.3)$$

To a good approximation we may assume

$$H \cong H^* \qquad (3.1.4)$$

(see equation (3.1.7) below for an estimate of the actual difference, $H-H^*$). Substituting (3.1.3) into (3.1.2) and neglecting the small third term because of (3.1.4) we get:

$$\Delta g \cong g_P(h, \phi, \lambda) - \gamma_Q(H^*, \phi, \lambda) \qquad (3.1.5)$$

The right side of (3.1.5) is, according to (3.1), the gravity anomaly at the point P, which in the present case is a station on the earth's surface. Therefore we

have found that under the approximation (3.1.4) the Δg as operationally computed from (3.1.1) is a free-air anomaly on the earth's surface. Using a subscript "s" to denote a surface free-air anomaly we finally have the interpretation:

$$\Delta g \cong \Delta g_S(h, \phi, \lambda) \tag{3.1.6}$$

The error of the interpretation (3.1.6) is given by the last term of (3.1.2) arising from the difference between the normal height H^* of P and the orthometric height H of P:

$$\varepsilon = \Delta g_S(h, \phi, \lambda) - \Delta g = -\left[\frac{\partial \gamma}{\partial h}\right]_P (H^* - H) \tag{3.1.7}$$

An estimate of this error can be obtained using the standard normal gradient

$$\frac{\partial \gamma}{\partial h} = -0.3086 \text{ mgal/m} \tag{3.1.8}$$

and an approximate formula for $(H^* - H)$ found in Heiskanen and Moritz (1967, section 8-13):

$$(H^* - H)(\text{meters}) = -\Delta g_{BA}(\text{gals}) \cdot H(\text{km}), \tag{3.1.9}$$

where Δg_{BA} is the Bouguer anomaly given by

$$\Delta g_{BA} = \Delta g - 2\pi k\rho H. \tag{3.1.10}$$

A standard value for $2\pi k\rho$, where k=Newtonian gravitational constant and ρ=density of topographic masses, is

$$2\pi k\rho = 0.1119 \text{ mgal/m}, \tag{3.1.11}$$

corresponding to $k=66.7 \times 10^{-9}$ cm^3/g/sec^2 and $\rho=2.67$ g/cm^3. Using equations (3.1.8) to (3.1.11) into (3.1.7) and using gravity anomaly and elevation data in our test area in New Mexico we found that the error ε has a maximal value of 0.2 mgal, occurring over mountainous terrain of the area.

3.2 Rationale Behind an Indirect Method of Upward Continuation of Surface Anomalies

We are given free-air anomalies Δg_S on the earth's surface,and we want to upward continue them. The difficulty with the use of Poisson integral to solve this problem is that the Poisson geometry requires that the data to be upward continued refer to points on the surface of a sphere. Conceptually, what could be done would be to first analytically continue the surface anomalies Δg_S to level surface anomalies Δg_P^*. A simple conceptualization of this continuation is by Taylor series, wherein certain corrections that depend on the vertical gradients of the field are added to Δg_S to arrive at Δg_S^* (see equation (1.1) of the Introduction):

$$\Delta g_P^* = \Delta g_S + \frac{\partial \Delta g}{\partial H}(H_P - H_S) + \frac{1}{2}\frac{\partial^2 \Delta g}{\partial H^2}(H_P - H_S)^2 \ldots \qquad (3.2.1)$$

It is to be expected that the rougher the anomaly field (from which Δg_S and Δg_P^* are samples) the larger will be the difference between Δg_S and Δg_P^*, because high degree frequencies are affected much by downward/upward continuation (see, for example, Rummel, 1975, pp. 42-43) while low frequencies are not as critically affected.

There is a theoretical problem in the case of downward continuation of Δg_S (Δg_P^* lies below Δg_S), namely, that very high irregularities in the field caused by very high irregularities in the topography may cause the solution Δg_P^* to diverge, or, at least, be very unstable in the sense that small errors in Δg_S will amplify tremendously to errors in Δg_P^*. Another, now practical, problem is that the computation of the vertical gradients of the field, even just the first gradient and the more so the higher the gradients, places rather severe requirements on the density and accuracy of the given Δg_S.

The above problems reduce for the case of a smooth anomaly field. The corrections ($\Delta g_P^* - \Delta g_S$) will be small, the downward continuation stable, and simpler computational procedures for the corrections may be devised. It is then the central strategy of what we would call the indirect method of upward continuation to explain away most of the high frequencies present in Δg_S as being the effect Δg^t (see section 2.5) of certain shallow topographic masses, in order to be left only with a relatively low frequency residual field ($\Delta g_S - \Delta g^t$) which can then be upward continued less problematically by the Poisson integral. The missing upward continuation of Δg^t to space points is then carried out essentially by an equivalent source technique, which says that the field for which Δg^t are boundary values has the topographic masses as "sources" and, therefore, the said field can be generated by direct integration of gravitational influences of the masses (see section 2.5). In the next section we will detail the equations that can be used to implement an indirect method of upward continuation of surface anomalies Δg_S.

It is to be noted that the Poisson integration, with its associated problem of requiring data to be located on a level surface, can be altogether avoided

with the use of either least squares collocation or Bjerhammar-type equivalent source technique. In these methods it would still be advisable to reduce the original anomalies Δg_S to the smoothed anomalies $(\Delta g_S - \Delta g^t)$ in order to maximize convergence and economy of solution. The residual anomalies $(\Delta g_S - \Delta g^t)$ are essentially inverted into a new set of parameters (the solution vector $(C+D)^{-1}(\Delta g_S - \Delta g^t)$ in collocation; the fictitious quantities Δg^* on the Bjerhammar sphere, in the Bjerhammar method) and then the new parameters rigorously generate the external gravity field. The rigor of the collocation or Bjerhammar approach lies in that they can handle the fact that the data $(\Delta g_S - \Delta g^t)$ are located on a non-level surface. The main disadvantage of these methods is that they require expensive matrix inversion.

3.3 Direct and Indirect Upward Continuation

A. Direct Method

In what we will call the direct method, either the surface free-air anomalies Δg_S or the terrain-corrected free-air anomalies (Faye anomalies) $\Delta g_S + tc$ are input directly in the Poisson upward continuation integral to model the external gravity anomaly field. Using the planar approximation (2.3.1) we have the following directly upward continued fields:

$$(\Delta g_S)^D_{H_o} = U_p\{\Delta g_S\} = \frac{H_o}{2\pi} \int\int_A \frac{\Delta g_S}{D_o^3}\, dx\, dy \qquad (3.3.1)$$

and

$$(\Delta g_S + tc)^D_{H_o} = U_p\{(\Delta g_S + tc)\} = \frac{H_o}{2\pi} \int\int_A \frac{(\Delta g_S + tc)}{D_o^3}\, dx\, dy \qquad (3.3.2)$$

where the superscript D denotes the direct method; the subscript H_o denotes the upward continuation distance H_o; U_p denotes the Poisson upward continuation operation; Δg_S is given by (3.1.1); and tc is formally given by (2.5.6). Equation (3.3.1) is the usual simple-minded application of the classical upward continuation solution. Equation (3.3.2) is the well-known Pellinen type of approach (see details in the next paragraphs) in which a first order reduction of surface data Δg_S to a level surface is implemented using the terrain correction and an assumption of strong correlation between Δg_S and elevations (Moritz, 1968, pp. 1-2).

Note that in both equations (3.3.1) and (3.3.2), the vertical position of the level surface to which the input anomalies are assumed to refer has no clear-cut theoretical definition. It is only implicitly required that this level surface be close to the earth's surface, in order to minimize the differences between the surface anomalies Δg_S and the level surface anomalies Δg^*. A natural choice for the position of the reference level would be that of some mean elevation in the area covered by the surface anomalies. In the section on numerical investigations (section 9) we present a study of the sensitivity of the upward continuation results to the choice of the position of reference level. Given the reference level, the upward continuation distance H_o to be used in

(3.3.1) and (3.3.2) follows as being equal to the elevation of the computation point above the reference level surface.

The anomalies Δg_S are anomalies on the surface of the earth, and therefore the level surface to which Δg_S refers is strictly changing from point to point. These data with changing level are therefore not directly useable under the problem formulation of the original Poisson integral, namely, that the data must be on the surface of a single level sphere. However, compared with Δg_S, the quantities (Δg_S + tc) are closer to being level surface anomalies. This use of the terrain correction to approximate a reduction of surface data to a level surface is discussed in Moritz, 1966, pp. 104-107. There it is shown that for long wavelengths (n, small) we have:

$$(tc)_n = \left[-\frac{\partial \Delta g}{\partial H} \Delta H \right]_n \tag{3.3.3}$$

where $\Delta H = H_S - H_P$ is the vertical distance between the surface anomaly Δg_S and the level surface anomaly Δg^* and the subscript n denotes the n^{th} surface harmonic of the quantity in parentheses. We therefore have this relation between the harmonics for relatively <u>small</u> n (see (3.2.1)):

$$\Delta g_n^* = (\Delta g_S - \frac{\partial \Delta g}{\partial H} \Delta H)_n = (\Delta g_S + tc)_n \tag{3.3.4}$$

where Δg_n^* is the n^{th} harmonic of the level surface anomalies Δg^*. Equation (3.3.4) with the provision that n is small, means that in the space domain the use of a (Δg_S + tc^S), where now we let tc^S denote a long wavelength form of the actual tc, serves to implement a first order long wavelength reduction of the surface data Δg_S to level surface data Δg^*. Again, as stated in the previous paragraph, the level of Δg^* is not clearly defined under this "tc-technique" of data reduction, and the sensitivity of upward continuation results to a particular choice of reference level for Δg^* will be studied in section 9.

The use of tc instead of a tc^S in (3.3.2) forms a theoretical objection to this equation, because according to the last paragraph the interpretation of the terrain correction as a data reduction to a level surface is theoretically guaranteed to be valid (via (3.3.4)) only at long wavelengths. As one of the desirable features of the indirect method to be discussed next this objection is minimized because a tc^S, i.e., a long wavelength form of tc, is used instead of the tc itself.

B. <u>Indirect Method</u>

In order to explain the <u>indirect method</u> let us first define some quantities.

The surface free-air anomaly is given in (3.3.1) as:

$$\Delta g_S = g - \frac{\partial \gamma}{\partial h} H - \gamma \qquad (3.3.5)$$

A reference free-air anomaly can be generated from potential coefficients to degree N_{max} using (2.2.3) with H_o=0 (see also (2.2.4)):

$$\Delta g^S = \frac{kM}{a^2} \sum_{n=2}^{N_{max}} (n-1) \sum_{m=0}^{n} (\bar{C}^*_{nm} \cos m\lambda + \bar{S}_{nm} \sin m\lambda)\, \bar{P}_{nm}(\sin \phi) \qquad (3.3.6)$$

the superscript s denoting spherical harmonics.

The gravity anomaly on the earth's surface, caused by masses of density ρ lying between the actual topography and the geoid is given from (2.5.4) as:

$$\Delta g^{t1} = 2\pi k\rho H - tc \qquad (3.3.7)$$

The gravity anomaly on the surface of a reference topography, caused by masses of density ρ lying between the reference topography and the geoid is given analogously to (3.3.7) as:

$$\Delta g^{t2} = 2\pi k\rho H^S - tc^S \qquad (3.3.8)$$

where H^S is the orthometric height and tc^S the terrain correction of the reference topography. For our purposes H^S will come from a spherical harmonic expansion of topography to degree and order N_{max}, corresponding to the maximum degree and order of the reference anomalies Δg^S of (3.3.6):

$$H^S = \sum_{n=0}^{N_{max}} \sum_{m=0}^{n} (A_{nm} \cos m\lambda + B_{nm} \sin m\lambda)\, \bar{P}_{nm} (\sin \phi) \qquad (3.3.9)$$

The gravity anomaly caused by positive and negative masses of density ρ lying between the actual topography H and the reference topography H^S can be written as:

$$\Delta g^t = \Delta g^{t1} - \Delta g^{t2} \qquad (3.3.10)$$

Note that Δg^{t1} refers to a point on the earth's topography, whereas Δg^{t2} refers to a point on the reference topography. Since Δg^{t2} is a smooth field it is reasonable to assume that the analytical continuation of Δg^{t2} to the position of

Δg^{t_1} is approximately equal to Δg^{t_2} itself. In this case (3.3.10) therefore gives a Δg^t that refers to the earth's surface.

Substituting (3.3.7) and (3.3.8) into (3.3.10):

$$\Delta g^t = 2\pi\kappa\rho(H - H^s) - (tc - tc^s) \qquad (3.3.11)$$

Now a residual anomaly Δg^r can be obtained by removing from the surface anomaly Δg_s of (3.3.5) the spherical harmonic anomaly Δg^s of (3.3.6) and the topographic anomaly Δg^t of (3.3.11):

$$\Delta g^r = \Delta g_s - \Delta g^s - \Delta g^t, \quad \text{or} \qquad (3.3.12)$$

$$\Delta g^r = \Delta g_s - \Delta g^s - 2\pi k\rho(H - H^s) + (tc - tc^s) \qquad (3.3.13)$$

If the reference quantities (those with superscript s) did not appear in (3.3.13) then this equation would give the expression for a refined Bouguer anomaly (Heiskanen and Moritz, 1967, p. 132); but because of the presence of the reference quantities we will call Δg^r the residual refined Bouguer anomaly. Equation (3.3.13) states that the original anomalies Δg_s are de-trended (1.) in the long wavelength, by subtracting free-air anomalies Δg^s generated from spherical harmonics and (2.) in the short wavelength, by doing a "Bouguer reduction" not with respect to the geoid but with respect to the higher order but still smooth surface H^s from spherical harmonics. Since Δg^r of (3.3.12) is a smooth quantity (as will be shown numerically later) the point on the earth's topography at which Δg^r applies can be moved vertically to the point on the reference topography H^s, so that for subsequent processing Δg^r is assumed to lie on the reference topography.

Considering the above definitions, what we will call the indirect upward continuation method then takes place as follows:

(1) The residual refined Bouguer anomalies Δg^r of (3.3.13) are terrain corrected by tc^s, then upward continued using the Poisson integral given by (2.3.1):

$$(\Delta g^r + tc^s)^{D}_{H_o} = U_p\{\Delta g^r + tc^s\} = \frac{H_o}{2\pi}\int\int_A \frac{(\Delta g^r + tc^s)}{D_o^3}\,dx\,dy \qquad (3.3.14)$$

where the superscript D' denotes the fact that $(\Delta g^r + tc^s)$ is input directly into Poisson integral; H_o is the upward continuation distance and U_p denotes the Poisson integral operator. The use of $(\Delta g^r + tc^s)$ instead of simply Δg^r is in accordance with earlier discussion on the use of long wavelength terrain correction (terrain correction indeed has some long

wavelength power-see p. 74 for a feeling for magnitudes) to approximate the reduction of surface data to a level surface (Δg^r is data lying on the reference topography H^s). Note from equation (3.3.13) that the use of ($\Delta g^r + tc^s$) amounts to the transposition of tc^s to the left side of the equation; this significantly reduces the computational effort needed for the evaluation of the right hand side and is therefore a definite practical advantage.

(2) The spherical harmonic anomalies Δg^s of (3.3.6) are implicitly upward continued using (2.2.3):

$$\Delta g^s_{H_o} = U_s\{\Delta g^s\} = \frac{kM}{a^2} \sum_{n=2}^{N_{max}} (n-1) \left(\frac{a}{a+H_o}\right)^{n+2} \sum_{m=0}^{n} \cdot$$

$$(\bar{C}^*_{nm} \cos m\lambda + \bar{S}_{nm} \sin m\lambda)\, \bar{P}_{nm}(\sin \phi) \qquad (3.3.15)$$

where U_s denotes the upward continuation of the spherical harmonic series.

(3) The topographic anomalies Δg^t of (3.3.11) are implicitly upward continued by integration of the gravitational attractions caused by the masses generating Δg^t, namely, the masses lying between the actual topography and the reference topography (see equation (2.5.3)). In practice the integration can be implemented using prisms as integration elements. This prism integration is implemented in an operational program by Forsberg (see section 7). In symbolic form,

$$\Delta g^t_{H_o} = U_R\{\Delta g^t\} \qquad (3.3.16)$$

where U_R denotes the upward continuation by prism integration of masses.

(4) Adding tc^s on both sides of (3.3.12), applying the Poisson integral operator U_p, and transposing terms, we arrive at:

$$U_p\{\Delta g_s + tc^s\} = U_p\{\Delta g^r + tc^s\} + U_p\{\Delta g^s\} + U_p\{\Delta g^t\} \qquad (3.3.17)$$

The indirect upward continuation method consists of replacing the last two terms in (3.3.17) as follows:

$$(\Delta g_s + tc^s)^I_{H_o} = U_I\{\Delta g_s + tc_s\} = U_p\{\Delta g^r + tc^s\} + U_s\{\Delta g^s\} + U_R\{\Delta g^t\} \qquad (3.3.18)$$

that is, the operator U_p operating on anomaly data Δg^s and Δg^t have been replaced by operators U_s operating on spherical harmonic coefficients and U_R operating on topographic masses. The superscript I in (3.3.18) denotes the indirect upward continuation method, and the U_I symbolizes the (implicit) indirect upward continuation operator. The last two terms of (3.3.18) are given in (3.3.15) and (3.3.16).

Starting from Section 7 and onwards we give the relevant numerical studies on the direct and indirect upward continuation methods, as well as studies on the Fourier transform method of upward continuation. Meanwhile, in the next three section (4, 5, 6) we present a general global study of truncation theory for the anomaly field, spectral characteristics of the anomaly signal, and error analysis for the (Poisson) upward continuation operation.

4. Anomaly Field Truncation Theory at Altitude

We can collect equations from section (2.1) as follows:

$$\Delta g_r(r, \bar{\Phi}, \lambda) = \frac{1}{4\pi} \int\int_{\sigma} K(t, \psi)\, \Delta g(R, \Phi', \lambda')\, d\sigma \tag{4.1}$$

$$K(t, \psi) = \frac{t^2(1-t^2)}{D^3} - t^2 - 3t^3 \cos\psi \tag{4.2}$$

$$K(t, \psi) = \sum_{n=2}^{\infty} (2n+1)\, t^{n+2}\, P_n(\cos\psi) \tag{4.3}$$

$$\Delta g_r(r, \bar{\Phi}, \lambda) = \sum_{n=2}^{\infty} t^{n+2}\, \Delta g_n(R, \bar{\Phi}, \lambda); \qquad t = \left(\frac{R}{r}\right) \tag{4.4}$$

A "truncated" gravity anomaly field can be generated as follows:

$$\overline{\Delta g_r} = \frac{1}{4\pi} \int\int_{\sigma} \bar{K}(t, \psi)\, \Delta g\, d\sigma \tag{4.5}$$

$$\bar{K}(t, \psi) = \begin{cases} 0 & , \quad 0 \leq \psi < \psi_0 \\ K(t, \psi) & , \quad \psi_0 \leq \psi < \pi \end{cases} \tag{4.6}$$

ψ_0 ... truncation cap radius.

This truncated field is generated by data function values Δg outside a cap of radius ψ_0 centered at the computation point. In this sense, this field is really a "remote zone" field being generated by remote zone data. The truncation kernel can be expanded into a series of Legendre polynomials as follows:

$$\bar{K}(t, \psi) = \sum_{n=0}^{\infty} \frac{(2n+1)}{2}\, q_n\, P_n(\cos\psi) \tag{4.7}$$

and the frequency domain generation of the truncated field is then given by (see analogous manipulations in Jekeli, 1980, for example):

$$\overline{\Delta g_r}(r, \bar{\phi}, \lambda) = \frac{1}{2} \sum_{n=2}^{\infty} q_n \, \Delta g_n(R, \bar{\phi}, \lambda) \tag{4.8}$$

The truncation coefficients q_n can be obtained as:

$$q_n = \int_0^{\pi} \bar{K}(t, \psi) \, P_n(\cos \psi) \sin \psi \, d\psi \tag{4.9}$$

$$= \int_{\psi_0}^{\pi} K(t, \psi) \, P_n(\cos \psi) \sin \psi \, d\psi \tag{4.10}$$

Putting $y = \cos \psi$, $y_0 = \cos \psi_0$, we have:

$$q_n(t, y_0) = \int_{-1}^{y_0} K(t, y) \, P_n(y) \, dy \tag{4.11}$$

Substituting (4.2) into (4.11) and using recursive integral evaluations found in Shepperd (1979, p. E-1) we arrive at the following recursive computations for the truncation coefficients:

$$q_n(t, y_0) = t^2(1-t^2) \, L_n(t, y_0) - t^2 \, I_n(y_0) - 3t^3 \, H_n(y_0) \tag{4.12}$$

$$L_n(t, y_0) = \int_{-1}^{y_0} \frac{P_n(y)}{D^3} \, dy \tag{4.13}$$

$$I_n(t, y_0) = \int_{-1}^{y_0} P_n(y) \, dy \tag{4.14}$$

$$H_n(t, y_0) = \int_{-1}^{y_0} y \, P_n(y) \, dy \tag{4.15}$$

$$I_0(y_0) = y_0 + 1$$

$$I_1(y_0) = \frac{1}{2}(y_0^2 - 1)$$

$$I_n(y_0) = \frac{(2n-1)y_0\, I_{n-1}(y_0) - (n-2)\, I_{n-2}(y_0)}{n+1}\ ,\ n \geq 2 \qquad (4.16)$$

$$H_0(y_0) = \frac{1}{2}(y_0^2 - 1)$$

$$H_n(y_0) = \frac{(n+1)\, I_{n+1}(y_0) + n\, I_{n-1}(y_0)}{2n+1}\ ,\ n \geq 1 \qquad (4.17)$$

$$L_0(t, y_0) = \frac{2(1+y_0}{(1+t)(1+t+D))D}$$

$$L_1(t, y_0) = \frac{(1+t)\, y_0 - D}{1+t+D}\ L_0(t, y_0)$$

$$L_n(t, y_0) = \frac{(1+t^2)\, L_{n-1}}{t} - L_{n-2} - \frac{I_{n-1}}{Dt}\ ,\ n \geq 2 \qquad (4.18)$$

The above recursive computations were checked for correctness and stability against other published results (with excellent agreement) as part of the studies of Cruz (1985) on truncation coefficients for various gravimetric quantities in space. The recursive formulas (4.18) for $L_n(t, y_0)$ which is probably the main source of instability of the recursions can be derived either analogously to the way Shepperd (1979, pp. B-1 to B-3) derived his $K_n(t, y_0)$ functions, or as a special case of a general formula given by Jekeli (1982, equations (18) to (22)).

The truncation method expressed by equations (4.5) and (4.6), where the original kernel $K(t, \psi)$ is set to zero for $0 \leq \psi < \psi_0$ is in accordance with what is referred to as an unmodified Molodensky truncation method. Other methods of truncation can be defined by specifying the truncation kernel as in (4.6), and deriving, using (4.9), the truncation coefficients that will enter (4.8). Well-known alternative methods for generating a truncated field include the Meissl truncation method and an improved Molodensky truncation method, all these being discussed in Jekeli (1982).

The interest in truncated fields usually lies in trying to generate the various truncated fields (unmodified, Meissl, or improved Molodensky truncated field) from a finite set of available spherical harmonic coefficients of the earth's gravitational potential. This is in contrast to generating the field from a set of Δg values on a geocentric sphere. The spherical harmonic generation of the truncated field can be accomplished by using in (4.8) the surface harmonics Δg_n generated from potential coefficients to degree N_{max} (see Rapp, 1982, p. 4). Specifically, we can collect the necessary equations for the spherical harmonic generation of a truncated anomaly field at altitude, as follows:

$$\overline{\Delta g_r'}(r, \bar{\varphi}, \lambda) = \frac{1}{2} \sum_{n=2}^{N_{max}} q_n(t, y_o) \cdot \Delta g_n(R, \bar{\varphi}, \lambda) \tag{4.19a}$$

$$\overline{\Delta g_r'}(r, \bar{\varphi}, \lambda) = \frac{kM}{2a^2} \sum_{n=2}^{N_{max}} q_n(t, y_o) \cdot (n-1) \cdot \left\{\frac{a}{R}\right\}^{n+2} \cdot$$

$$\cdot \sum_{m=0}^{n} (\bar{C}^*_{nm} \cos m\lambda + \bar{S}_{nm} \sin m\lambda) \bar{P}_{nm}(\sin \bar{\varphi}) \tag{4.19b}$$

$$t = \frac{R}{R+H_o} = \frac{R}{r} \tag{4.19c}$$

$$y_o = \cos \psi_o \tag{4.19d}$$

where

$r, \bar{\varphi}, \lambda$	geocentric radius, geocentric latitude and "geocentric" longitude of the computation point;
$q_n(t, y_o)$	truncation coefficients;
$\Delta g_n(R, \bar{\varphi}, \lambda)$	surface harmonics of the spatial anomaly field, on a sphere of radius R;
R	a mean earth radius, taken as R=6371 km;
$\frac{kM}{a^2} = \gamma$	an average value of gravity;
$\bar{C}^*_{nm}$, $\bar{S}_{nm}$	fully normalized potential coefficients with even degree zonal reference values subtracted;
a	radius of the sphere to which $\bar{C}^*_{nm}$ and $\bar{S}_{nm}$ refer, usually an equatorial radius;

H_o — height of computation point above the sphere of radius R;

ψ_o — angular radius of the truncation cap

The truncated spherical harmonic field $\Delta\bar{g}_r$, given in (4.19b) contains two types of errors: the commission error, which is the error due to errors in the potential coefficients being used, and the omission error, which is the error due to the use of only a finite set of potential coefficients and the consequent omission of the higher frequencies which may exist in the actual truncated field $\Delta\bar{g}_r$ being represented. The combined global mean square value of commission and omission errors can be expressed as (Jekeli, 1980, p. 16; see also (4.19a):

$$\overline{m_r^2} = \frac{1}{4} \sum_{n=2}^{N_{max}} q_n^2 \, \delta C_n + \frac{1}{4} \sum_{n=N_{max}+1}^{\infty} q_n^2 \, C_n \qquad (4.20)$$

where

q_n — truncation coefficients as found from equations (4.12)-(4.18);

δC_n — anomaly error degree variances referred to a sphere of radius R (R=6371 km, the mean earth radius). δC_n is caused by potential coefficient errors $\varepsilon\bar{C}^*_{nm}$ and $\varepsilon\bar{S}_{nm}$. Considering (4.19b) we have:

$$\delta C_n = \gamma^2 (n-1)^2 \left(\frac{a}{R}\right)^{2n+4} \sum_{m=0}^{n} [(\varepsilon\bar{C}^*_{nm})^2 + (\varepsilon\bar{S}_{nm})^2]; \qquad (4.21a)$$

C_n — modeled anomaly degree variances referred to a sphere of radius R. According to the Tscherning/Rapp (1974) model (with R=6371 km):

$$C_n = \frac{425.28\ (n-1)}{(n-2)(n+24)}\ (0.999617)^{n+2} \qquad (4.21b)$$

Optimization of truncation method usually means modifying the definition (4.6) for the kernel $\bar{K}(t, \psi)$ (and therefore modifying the truncation coefficients q_n) such that the mean square error $\overline{m_r^2}$ in (4.20) is reduced compared with the unmodified case, for a given number and accuracy (N_{max} and δC_n) of potential coefficients and given model (C_n) for anomaly degree variances. Jekeli (1982) has shown that for the upward continued gravity anomaly field, optimization of truncation method by using the Meissl or improved Molodensky technique does not offer a significant improvement over the unmodified Molodensky method defined by (4.5) and (4.6). In this report we limit ourselves to the use of the unmodified truncation method.

As an application of the important equations (4.19) and (4.20) of this section, we considered the main interest in this report, namely, the upward continuation of anomalies in the New Mexico area to an approximate altitude of 28.5 km. We first applied (4.19) by modifying program F388 at OSU (see Section 7) to introduce the truncation coefficients $q_n(t, y_o)$. We used:

- the Rapp-180 field (Rapp, 1981)
- H_o = 28.5 km (upward continuation distance)
- γ = 979770 mgals (mean value of gravity)
- ψ_o = 3° (truncation cap radius)
- a = 6378137 m (equatorial radius)
- R = 6371000 m (assumed ground level radius)

The coefficients q_n were computed by a subroutine modified from a subroutine published by Shepperd (1979). The resulting truncated anomaly field for the area of interest in our balloon-borne gravity experiment (Section 8) is given as Figure 1.

If we were using the Rapp-180 field to account for the remote zone outside a 3°-cap centered at the computation point, the values on the map would be added to the result of integration of data inside the 3°-cap. Note that in this case the data cap of integration moves from computation point to computation point. For our final operational procedures, however, we simply used a fixed data cap to compute our anomalies in space and neglected remote zone effects: this neglection is justified by selecting a sufficiently large size for the fixed integration cap. In the case just considered an integration cap of radius 3° is appropriate since the remote zone effects are small as shown in Figure 1.

Let us now turn to an application of equation (4.20). Application of (4.20) yields a global analysis of the effect of remote zone anomalies on the upward continued anomaly and gives an indication of the ability of spherical harmonic model to account for this effect. As a first application we used only the second term of (4.20) and started the summation from n=2. This is equivalent to not using any spherical harmonic model to account for the remote zone effects, the total error being one of pure omission. Using the Tscherning/Rapp (1974) C_n-model (4.21b) the results of summing the second term of (4.20) for altitude 30 km and various truncation angles are shown in Figure 2 as the top curve. This curve shows that a cap of radius 3° is needed to reduce remote zone effects to submilligal level; the 3° cap radius (about 300 km at ground level) is about ten times the upward continuation distance of 30 km and is therefore in accordance with the rule that data out to a distance ten times the upward continuation distance should be used (Hirvonen and Moritz, 1963, p. 68).

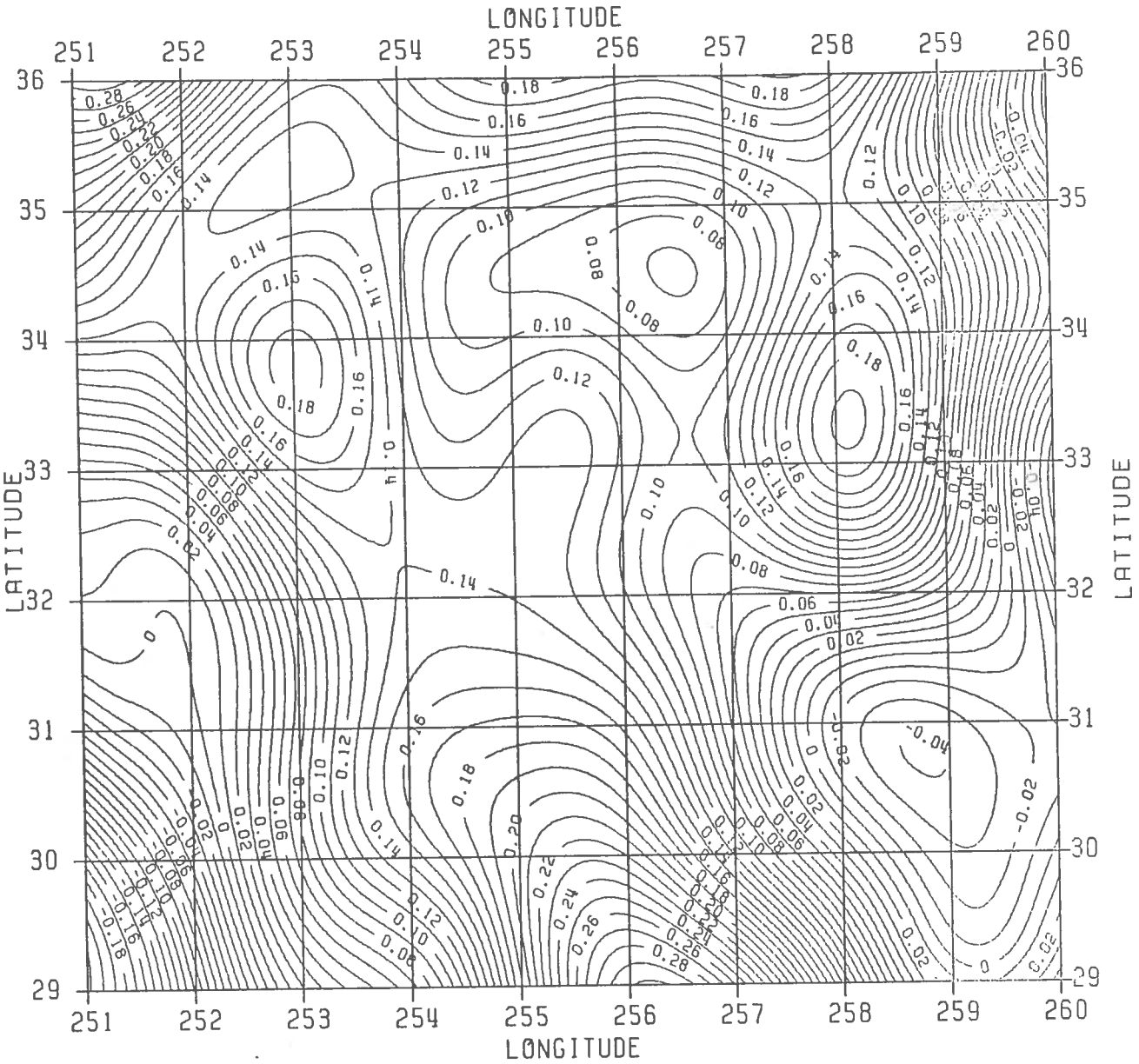

Figure 1. Rapp-180 Truncated Gravity Anomaly Field at 28.5 km Altitude, New Mexico Balloon Gravity Test Site. C.I. = 0.01 mgal; Truncation Cap Radius = 3°.

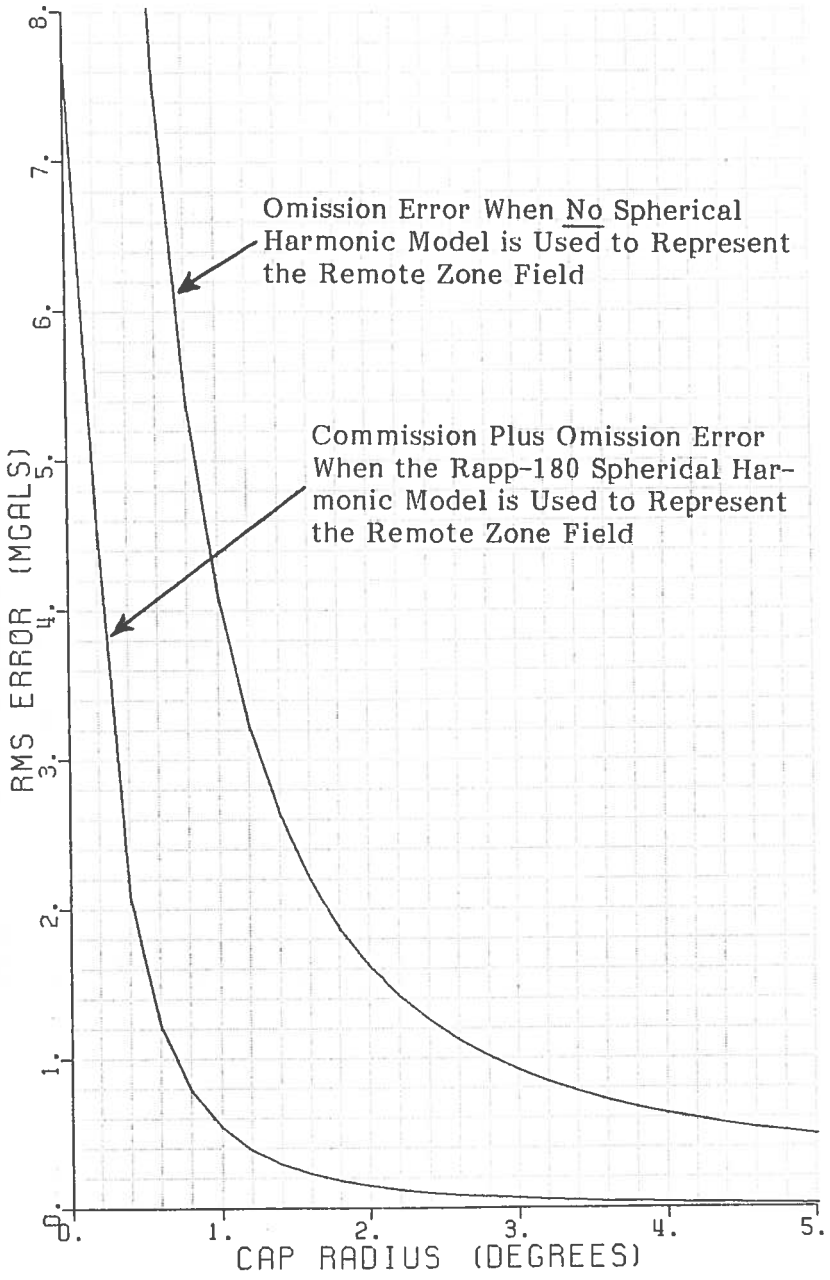

Figure 2. Error Incurred When Not Using and When Using a Spherical Harmonic Model to Represent, at Altitude 30 km, the Remote Zone Field Generated by Data Outside a Cap of Given Radius. C_n-model from Tscherning/Rapp (1974); δC_n from Rapp-180 field with $m_{\overline{\Delta g}}$ = 10 mgals (Rapp, 1981, eq. 30).

For a second application of (4.20) we introduced the Rapp-180 field to account for the remote zone effects (N_{max}=180). In addition we used a more optimistic set of errors associated with the Rapp-180 potential coefficients, found by using $m_{\Delta g}$=10 mgals instead of 20 mgals in equation (30) of Rapp (1981). Again using the Tscherning/Rapp C_n-model and upward continuation distance of 30 km, the total error (commission plus omission) incurred by using the Rapp-180 field to account for remote zones were computed by (4.20) for various truncation cap radii and plotted as the bottom curve of Figure 2. We see that now the total error is drastically reduced compared with the case of the top curve where no spherical harmonic model is used to account for remote zones. For a truncation radius of 3°, the error reduced from RMS 0.9 mgal to RMS 0.1 mgal. For a truncation radius of 1°, the bottom curve of Figure 2 shows that the use of the Rapp-180 field to account for the remote zone field incurs a commission plus omission error of 0.45 mgal global RMS.

Note that Figure 2 represents a global error analysis that may not be representative of a local area. Figure 1 is more suited for analysis of specific areas. For example, Figure 1 says that for a truncation radius of 3° it is immaterial whether we use the Rapp-180 field to account for the remote zone or not because the Rapp-180 truncated contributions are small anyway. On the other hand Figure 2 says that not using the Rapp-180 field at truncation angle of 3° causes an ommission error of 0.9 mgal RMS, and the use of Rapp-180 field decreases this error to 0.1 mgal (commission plus omission error).

5. Global Characterization of Anomaly Fields

A most common statistical characterization of anomaly fields can be made by giving the degree variances of the field, which gives the break down of field power by wavelength. Given the degree variances C_{nR} on a sphere of radius R, the degree variances on an external sphere of radius r is given by using (2.1.5) and analogous derivations to Heiskanen and Moritz (1967, p. 260-261):

$$C_{nr} = s^{n+2}\, C_{nR} \; ; \qquad s = \left(\frac{R}{r}\right)^2 \tag{5.1}$$

The factor s^{n+2} indicates how each component wavelength power of the field attenuates with the upward continuation distance (r-R). Note that the degree variances C_{nR} correspond to the power of field features on a sphere of radius R, these features having a minimum half-wavelength of approximately:

$$\lambda = \frac{\pi R}{n} \qquad \text{(linear units)} \tag{5.2}$$

A second field characterization is obtained by summing the degree variances of the field above a specified degree N. This sum gives a measure of the amount of field information (RMS) beyond the harmonic degree N:

$$\delta\Delta g_r^2(N) = \sum_{n=N}^{\infty} C_{nr} \tag{5.3}$$

The sum (5.3) is important because given the resolution N of a particular field approximation, the sum indicates how much field information (RMS anomaly) is left unresolved by the approximation.

A third method of global characterization is obtained by giving the mean square upward continued anomaly on a spatial sphere, caused by boundary values of Δg outside a cap of radius ψ_o, for various heights of the spatial sphere. This mean square anomaly is the same as the mean square anomaly of the truncated field defined by (4.8) and can be obtained from (4.20) by using only the second term of that formula and starting the summation from n=2:

$$\overline{\delta\Delta g_r^2}(t, \psi_o) = \sum_{n=2}^{\infty} q_n^2(t, \psi_o) C_{nR} \tag{5.4}$$

$$t = \left(\frac{R}{r}\right)$$

The sum (5.4) is important for studying the remote zone effects on upward continued anomalies.

Formulas (5.1), (5.3), and (5.4) were used at altitudes 30, 60, 100 and 150 km, the results being given as Figures 3a, 3b, and 4. The Tscherning/Rapp (1974) C_{nR}-model was used (see (4.21b)). Figure 3a gives the gravity anomaly information beyond degree N: for example, using a 180-field to represent the external anomaly field leaves 5 mgals to be resolved at 30 km, 1.7 mgals at 60 km, 0.4 mgal at 100 km, and 0.1 mgal at 150 km. Figure 3b gives the gravity anomaly information due to data outside a cap of given radius: for example, using a truncation radius of 3° leaves a 0.9 mgal remote zone anomaly at altitude 30 km, 1.8 mgals at 60 km, 2.8 mgals at 100 km, and 3.8 mgals at 150 km. A combined interpretation of Figures 3a and 3b says that the higher the point of upward continuation the larger the data cap needed to maintain a desired accuracy level (Figure 3b), however, at the same time the resolution needed for data inside the cap becomes less and less with altitude (Figure 3a) - this conclusion is well-known and is true for the computation of all gravimetric quantities in space. Finally, Figure 4 gives the degree variances of the anomaly field at altitudes 30, 60, 100 and 150 km to show the effect of upward continuation on component powers of the field.

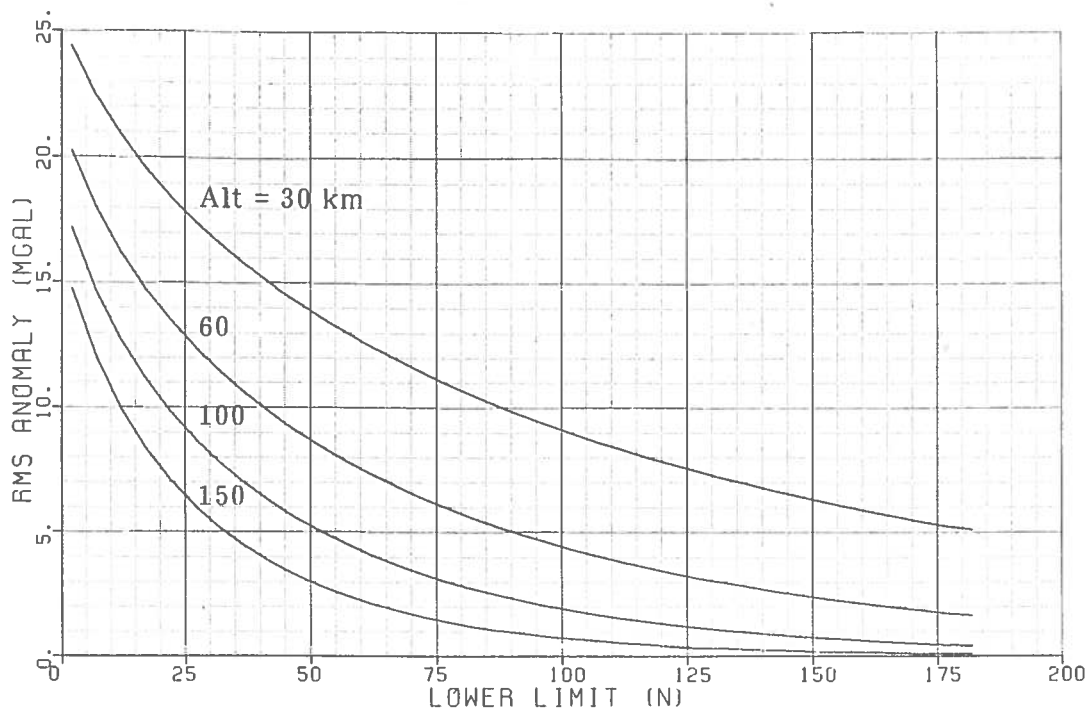

Figure 3a. Gravity Anomaly Information Beyond Degree N, for Altitudes 30, 60, 100, and 150 km. Tscherning/Rapp (1974) Anomaly Degree Variance Model Used.

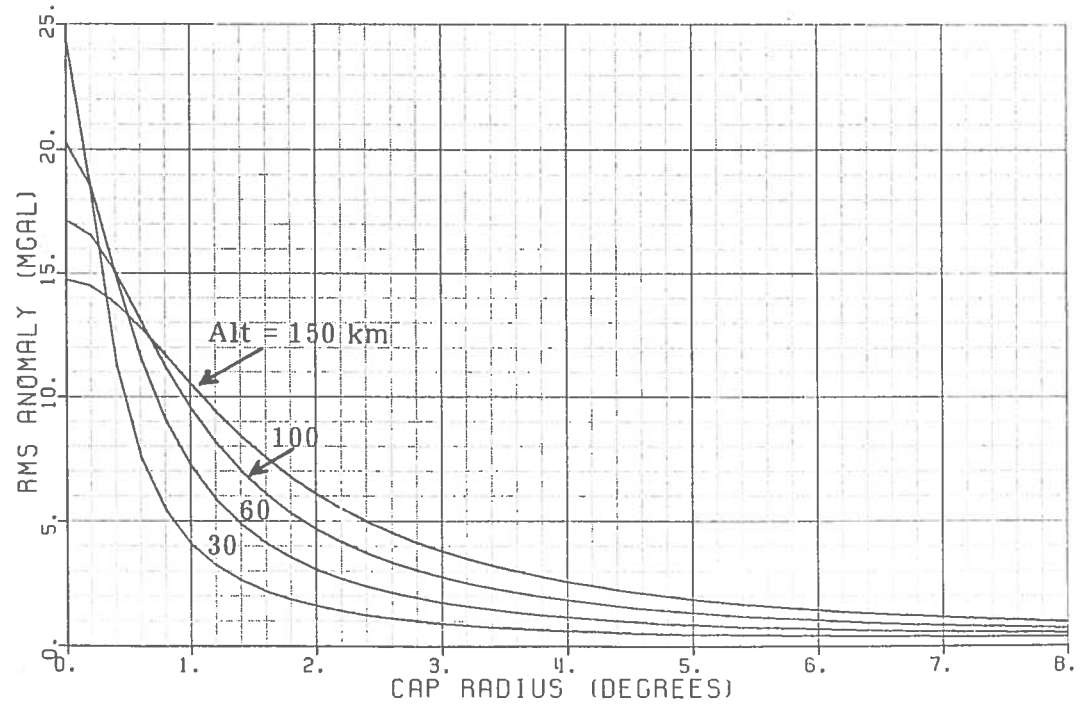

Figure 3b. Gravity Anomaly Information Generated by (Remote Zone) Data Outside a Cap of Given Radius, for altitudes 30, 60, 100, and 150 km. Tscherning/Rapp (1974) Anomaly Degree Variance Model Used.

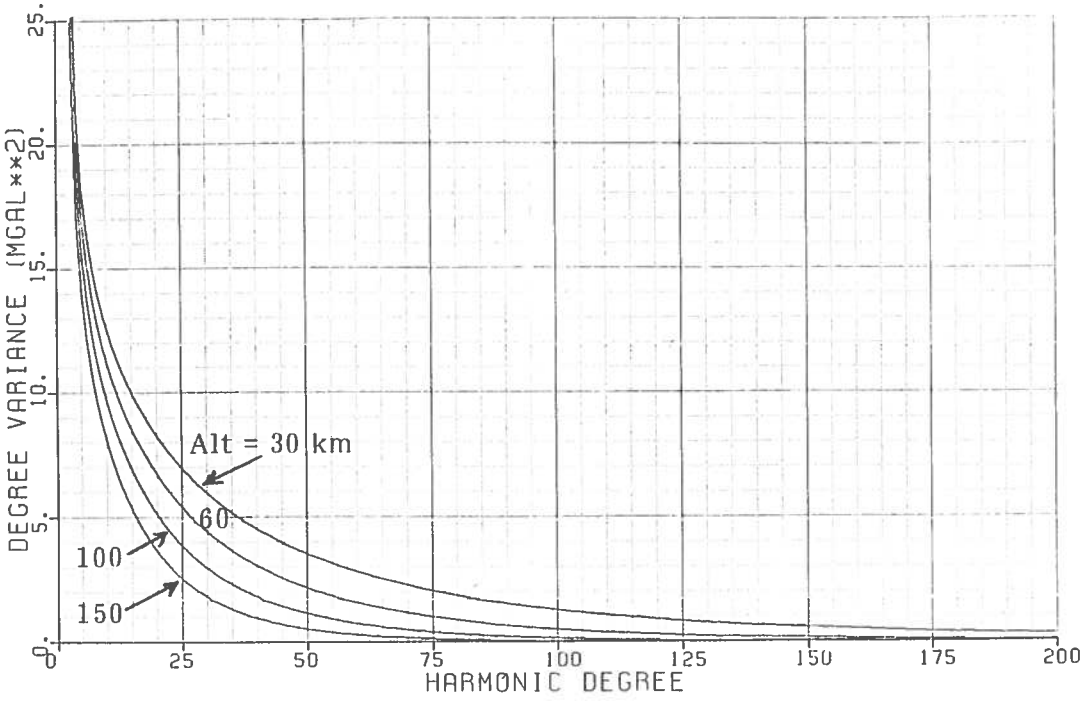

Figure 4. Anomaly Degree Variances at Altitudes 30, 60, 100, and 150 km. Tscherning/Rapp (1974) Anomaly Degree Variance Model Used.

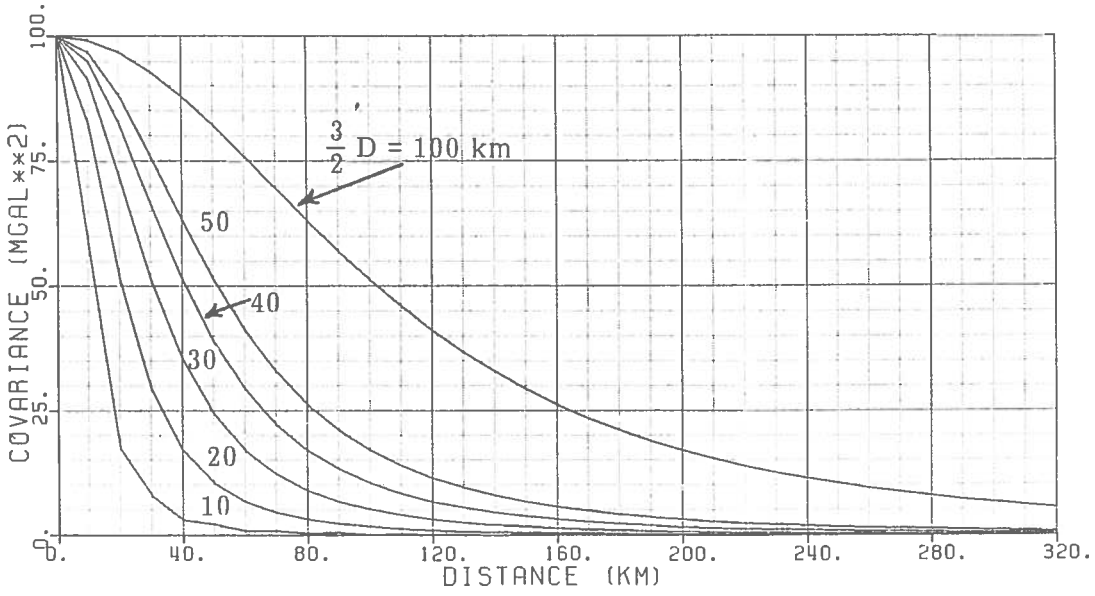

Figure 5. Attenuated White Noise Covariance Functions (scaled), for White Noise Depth D=(2/3)(10, 20, 30, 40, 50, 100 km). Note that the Resulting Correlation Length ξ = 3/2 D.

6. Error Propagation for Upward Continuation Operator

6.1 Flat-Earth Data Error Propagation

Based on (Moritz, H., 1962) we can formulate the problem in the following way.

The upward continuation integral (in planar form) for gravity anomalies is:

$$\Delta g_H(x, y) = \frac{H}{2\pi} \int_{-\infty}^{\infty}\int \Delta g(x', y') \frac{dx'dy'}{D^3} \qquad (6.1.1)$$

where x'y' are variables of integration,

$$D^2 = H^2 + (x-x')^2 + (y-y')^2$$

H is the upward continued distance.

Then formally any error $\varepsilon(x, y)$ in terrestrial Δg will propagate as:

$$\varepsilon_H(x, y) = \frac{H}{2\pi} \int_{-\infty}^{\infty}\int \varepsilon(x', y') \frac{dx'dy'}{D^3} \qquad (6.1.2)$$

Equation (6.1.2) has the exact form of the original Poisson's integral with gravity anomalies Δg replaced by the error function ε. As the computational point (x, y) sweeps the particular level plane at the elevation H above the reference datum plane, the function $\varepsilon_H(x, y)$ describes the variation of the directly propagated (upward continued) error.

Formula (6.1.2) describes the sensitivity of the upward continuation operation to the uncertainties in the data. It assures that the errors attenuate according to exactly the same law (upward continuation law) as the original data. The frequency domain equivalent of formula (6.1.2) is: (see eq. 2.4.4)

$$E_H(k_x, k_y) = e^{-H2\pi\sqrt{k_x^2 + k_y^2}} \cdot E(k_x, k_y) \qquad (6.1.3)$$

where ε, E and ε_H, E_H are Fourier transform pairs and k_x, k_y are spatial frequencies along x and y directions (Robinson E.A., M.T. Silvia, Chap. 2.4,

1981). Equation (6.1.3) shows that the weakly correlated (white) noise in the data will attenuate very rapidly with the elevation H, whereas the long wavelength widely correlated components of the noise will propagate almost unattenuated into upward continued gravity field.

This discussion shows that the correlation length of the errors present in the gravity material will play the major role in the upward continuation error analysis.

As a statistically appropriate measure of the upward continued error function (6.1.2) we choose (after Moritz, H., 1962) the mean square error defined as:

$$M(\varepsilon^2_H) = m^2_H = \frac{H^2}{4\pi^2} \int_x \int_y \int_{x'} \int_{y'} \sigma(x, y, x', y') \frac{dxdy}{D^3} \frac{dx'dy'}{D^3} \qquad (6.1.4)$$

where $\sigma(x, y, x', y') = M(\varepsilon, \varepsilon')$ is the error covariance function, which is a statistical description of the errors $\varepsilon(x, y)$ in Δg. M is the suitable averaging operator.

In (Moritz, 1962) it is shown that introducing some specific model of the error covariance function we can produce explicit expressions for the upward continued mean square error (6.1.4).

Suppose we model the error covariance function present in Δg to be (Moritz, 1962, p. 3):

$$\sigma(x, y, x', y') = \sigma_0 \, e^{-c^2 s^2} = \sigma(s) \qquad (6.1.5)$$

which is a function of distance only (stationarity and isotropy). In eq. (6.1.5):

$s = \sqrt{(x-x')^2 + (y-y')^2}$ is the Cartesian distance between two locations on the plane.

σ_0 is the error variance (square of the standard error present in the datum surface anomalies Δg)

The constant $c \equiv \sqrt{\ell n 2}/\xi$ is inversely proportional to the correlation length ξ of the error function present in Δg (ξ has to be in the same units as s and H).

Using this model (Moritz, 1962) shows that the mean square error (6.1.4) present in the upward continued field takes the simple form:

$$m^2_H = \frac{1}{8H^2} \frac{\sigma_0}{c^2} \qquad (6.1.6)$$

Now we can evaluate (6.1.6) using different trial correlation lengths ξ at different elevations H. The results are shown in Table 1 using the parameter σ_o=(10 mgal)^2. The closed formula (6.1.6) was derived under the assumption that the ratio ξ/H remains small (see Moritz, 1962, p. 7). For that reason the numbers in the lower right-hand portion of Table 1 have been crossed-out as they are considered not to have any physical meaning.

To overcome this assumption see below for a spherical earth analysis.

Table 1

Square root of upward continued error variance at different elevations
m_H in [mgal]; σ_o = 100 mgal ^{2}
(crossed-out values have no physical meaning)

Assumed correlation distance in error function at zero level (ξ in [km])	H = 30 km	H = 10 km	H = 5 km
2	0.28	0.85	1.70
5	0.71	2.12	4.25
10	1.42	4.25	~~8.49~~
30	4.25	~~12.74~~	~~25.48~~

6.2 Spherical-Earth Data Error Propagation

Let us now study the propagation of data error through the upward continuation operation, using as error model an attenuated white noise process (see Heller and Jordan, 1979, for interesting geodetic applications of such process). The degree variances of white noise can be written as:

$$d_n = \sigma_o^2 \ (2n+1) \qquad (6.2.1)$$

where the unit variance σ_o^2 is a constant and is equal to the variance of a single harmonic of degree n and order m of the white noise process. White noise is useful for approximating an uncorrelated noise process.

The covariance function corresponding to (6.2.1) is:

$$D(P, Q) = \sigma_0^2 \sum_{n=2}^{\infty} (2n + 1)\, P_n(\cos \psi) \qquad (6.2.2)$$

where we start the summation from n=2 in anticipation of inputting D(P, Q) to an upward continuation operation that starts with n=2. D(P, Q) represents a dirac delta function (Rummel, 1982, p. 30):

$$D(P, Q) = \begin{cases} \infty & \text{for } P = Q \\ 0 & \text{for } P \neq Q \end{cases} \qquad P, Q \in \sigma \qquad (6.2.3)$$

that is, the total variance is infinite and the correlation length is undefined. To obtain a finite variance and correlation length we upward continue the noise process, resulting in the attenuated covariance function (note that we are using the gravity anomaly upward continuation operation):

$$D_r(s, \psi) = \sigma_0^2 \sum_{n=2}^{\infty} s^{n+2}\, (2n+1)\, P_n(\cos \psi) \qquad (6.2.4)$$

where $s = \left(\frac{R_b}{r}\right)^2$, and

we visualize that the white noise process is located on a sphere of radius R_b internal to the earth sphere of radius R, and the attenuated white noise process described by (6.2.4) is located on a sphere of radius r with $r > R_b$.

Two important quantities to characterize the covariance function D_r are its variance v_r and correlation length ξ_r. A numerical study of (6.2.4) reveals the following good approximations:

$$(r - R_b) = \frac{2}{3}\, \xi_r \qquad (6.2.5)$$

$$v_r = \frac{\text{const.}}{(r - R_b)^2} \qquad (6.2.6)$$

that is, the correlation length ξ_r is 1.5 times the upward continuation distance $(r-R_b)$, and the variance of the attenuated white noise process attenuates with the square of the upward continuation distance. The same relations were found by Sunkel (1981, p. 12, 14) for a slightly different covariance function

from (6.2.4). In Figure 5 we show the covariance function (6.2.4) for r=R (i.e., on the surface of the earth) and varying depths ($R-R_b$) to the white noise process. Figure 5 shows clearly the relation (6.2.5); the graphs were scaled to yield the variance v_r=100 mgal^2.

The functions (6.2.4) such as shown in Figure 5 can be used as error models, on the earth sphere, and it is of interest to see how these functions propagate through the upward continuation operator for gravity anomalies. We have the following procedure for applications:

1. we have, given, the error variance v_R and error correlation length ξ_R of the error process that we want to model on the earth sphere R.

2. the depth D (not to be confused with the same symbol in (6.2.2)) of the white noise process generating ξ_R is then found from (6.2.5):

$$D = (R-R_b) = \frac{2}{3}\,\xi_R \qquad (6.2.7)$$

3. the constant of proportionality in (6.2.6) is found from

$$\text{const.} = v_R(R-R_b)^2 = v_R\,D^2 \qquad (6.2.8)$$

4. the upward continued error variance at altitude H above the earth sphere R is found by applying (6.2.6) with r=R+H and R_b=R-D:

$$v_r = \frac{\text{const.}}{(r-R_b)^2} = v_R\left[\frac{D}{H+D}\right]^2 \qquad (6.2.9)$$

5. the upward continued correlation length ξ_r is found from (6.2.5):

$$\xi_r = \frac{3}{2}\,(r-R_b) = \frac{3}{2}\,(H+D) \qquad (6.2.10)$$

We applied (6.2.7) - (6.2.10), starting with v_R=100 mgal^2 and various correlation lengths ξ_R. The upward continued values v_r and ξ_r for various upward continuation distances are shown in Table 2. The values $(v_r)^{1/2}$ in the table are directly comparable with the values m_H in Table 1, and we see a reasonable agreement; note that $(v_r)^{1/2}$ has no specific problems associated with large correlation lengths ξ_R whereas m_H has problems with this as mentioned in Section 6.1. The conclusion from Table 2 is that error correlations in the

terrestrial data should be avoided as much as possible, because these cause errors to show up significantly in the upward continued anomaly field. Note from Table 2 that the larger the error correlation length the slower the rate at which the error loses its total energy (variance) with altitude, an expected result.

Table 2

Upward Continued Error Variance and Correlation Length,
for Attenuated White Noise Error Model.
v_R = 100 mgal²

	H=30 km		H=10 km		H=5 km	
ξ_R (km)	ξ_r (km)	$\sqrt{v_r}$ (mgal)	ξ_r (km)	$\sqrt{v_r}$ (mgal)	ξ_r (km)	$\sqrt{v_r}$ (mgal)
2	47	0.42	17	1.18	10	2.10
5	50	1.00	20	2.50	12	4.00
10	55	1.82	25	4.00	18	5.71
30	75	4.00	45	6.67	38	8.00

6.3 Flat-Earth Representation Error Propagation

The effect of representation error can also be evaluated. This error is committed when the continuous function Δg is replaced by the step function composed of the mean values representing it over rectangular blocks used in computation. See (Sunkel, 1981). Following (Moritz, 1962) where the same error was considered (but under the name of integration error) we pose the problem in the following way:

Instead of the exact Poisson's integral (6.1.1) in the actual computation we use the summation:

$$\Delta g_H = \frac{H}{2\pi} \sum_i \overline{\Delta g_i} \frac{A}{\overline{D_i}^3} \qquad (6.3.1)$$

where D_i is defined by the relation:

$$\frac{1}{\overline{D_i^3}} = \frac{1}{A_i} \int\int_{A_i} \frac{dA}{D^3} \qquad \text{with } D^2 = H^2 + (x-x')^2 + (y-y')^2$$

and A_i is the area of the rectangular block which is represented by the mean value $\Delta\overline{g_i}$.

Define the error of representation ε to be the function such that over each rectangular block i the following relation holds:

$$\varepsilon\big|_i = \Delta g\big|_i - \overline{\Delta g_i} \tag{6.3.2}$$

which is the difference between Δg and the constant $\overline{\Delta g_i}$ over the rectangular block i. Then, from (6.1.2) the propagated error of representation due to single block i is:

$$\eta_i = \frac{H}{2\pi} \int\int_{A_i} \frac{\Delta g - \overline{\Delta g_i}}{D^3} \, dA \tag{6.3.3}$$

where the total representation error is the sum of η_i's.

Similarly to (6.1.4) the mean square representation error due to single block (a_i x b_i) is:

$$M(\eta_i^2) = \mu_i^2 = \frac{H^2}{4\pi^2} \int_{x_o-\frac{a_i}{2}}^{x_o+\frac{a_i}{2}} \int_{y_o-\frac{b_i}{2}}^{y_o+\frac{b_i}{2}} \int_{x_o-\frac{a_i}{2}}^{x_o+\frac{a_i}{2}} \int_{y_o-\frac{b_i}{2}}^{y_o+\frac{b_i}{2}} F(x, y)\, F(x', y')\, C(s)\, dxdy\, dx'dy' \tag{6.3.4}$$

where $s^2 = (x-x')^2 + (y-y')^2$ is the Cartesian distance on plane

$$F(x, y) = \frac{1}{D^3} - \frac{1}{\overline{D^3}} \quad \left(\text{so consequently } \int\int_{A_i} F(x, y)\, dxdy = 0\right)$$

$C(s) = M(\Delta g \Delta g')$ is the covariance function of actual gravity anomalies, that is a statistical characterization of Δg field itself (and not the errors in Δg)

After (Moritz, 1962) assume the following model covariance function for gravity anomalies:

$$C(s) = \frac{C_0}{1+(\frac{s}{d})^2} \tag{6.3.5}$$

where C_0 is the assumed gravity anomaly variance.

If we define a constant α such that $\alpha^2 = \frac{C_0}{d^2}$ then in first approximation (6.3.5) reduces to:

$$C(s) = C_0 - \alpha^2 s^2 \tag{6.3.6}$$

Assume also all blocks are squares having the area $A_i = a_i^2 = a^2 = A$.

Then (Moritz, 1962) gives the following closed expression for the mean square representation error (6.4.3)

$$\mu_i = \frac{\alpha H}{4\pi\sqrt{2}} \frac{a^4 r_0}{D_0^5} \tag{6.3.7}$$

where

$$r_0^2 = x_0^2 + y_0^2 \ , \ D_0^2 = H^2 + r_0^2$$

Equation (6.3.7) gives the effect due to a single compartment. Next, neglecting again correlations between compartments we can find variance of the total effect just by summing variances of each contributors:

$$m_H^2 = \sum_i \mu_i^2 = \frac{\alpha^2}{384\pi} \frac{A^3}{H^4} \tag{6.3.8}$$

or $m_H = 0.0288\, \alpha \sqrt{a^3 b^3}/H^2$ where a and b form the sides of the block.

This is the square root of error variance of upward continued representation error.

With the numerical values of C_o = 683 (mgal^2), d = 40 km and A implied by 5'x5' blocks we compute

$$m_H = 11.6/H^2 \text{ mgal} \qquad (H \text{ in km}).$$

So for flight elevation H = 30 km

$$m_{30km} = 0.013 \text{ mgal}$$

which is a much smaller contribution than any of the effects given in Table 1 or 2. A spherical-earth analysis of the representation error for gravity anomaly upward continuation may also be done based on Sunkel (1981, p. 17); however, the effect of representation error is so small (using 5'x5' mean values) that we do not repeat this type of analysis here.

7. Operational Program for the Generation of Anomaly Fields

In this section we summarize the programs that can be used to operationally generate the different types of anomaly fields we use in this report. These anomalies are the Poisson anomaly, the spherical harmonic anomaly, the topographic anomaly, and the Fourier anomaly.

What we call the Poisson anomaly field is generated in planar approximation as (2.3.1). A Poisson anomaly field can be operationally generated using a FORTRAN program fully documented in Rapp (1966). The program accepts 5'x5' mean anomalies as boundary values in the flat-earth upward continuation. For a more detailed field generation smaller blocks of 2!5x2!5 mean anomalies may be input near the computation points, and the program then automatically rejects any 5'x5' mean anomalies covered by the input 2!5x2!5 values. The program also has the useful feature of rigorously computing the normal gravity corresponding to the anomalies being computed, the sum of these two quantities being a model for observed total gravity. The program exists as program F499 in the OSU program library.

For the generation of spherical harmonic fields, there are two types of existing operational programs that can be used. If the intention is to generate anomaly values at individual points not on a grid, the program described in Rapp (1982) can be used. If, however, values on a limited grid are desired then the program described in Rizos (1979) can be used. The program by Rapp, to generate values at individual points, exists as program F477 in the OSU program library, and the program by Rizos, to generate values on a grid exists as program F388. A comparison of these and other spherical harmonic programs is given in Tscherning et al. (1983). The input to F477 and F388 are the set of potential coefficients and the geodetic latitude, longitude and height above the reference ellipsoid (ϕ, λ, h) of computation points. The set-up of the programs is to implement equation (2.2.2); however, for reasons stated below equation (2.2.2), we have slightly modified F477 and F388 for our applications to compute (2.2.3) instead.

Another anomaly field of interest to us is the topographic anomaly field, generated by intergrating the gravitational effects of topographic masses of assumed density. The operational generation of a topographic anomaly field can be done using the FORTRAN program described in Forsberg (1984) and existing as OSU program 489. There are various modes under which the program runs, as detailed in Forsberg (ibid.), but the most important one for the purpose of our studies is that for computing the external gravity anomaly field generated by the (positive and negative) residual masses lying between the actual topography defined by a digital elevation model, and a reference topography such as the topography to 180 spherical harmonic expansion. Another mode of interest to the procedures recommended in this report is the terrain correction (tc) computations which will be needed in case the tc are not given on the gravity data records.

Finally, by Fourier anomaly we mean an anomaly which is upward continued using Fourier transform techniques. For the generation of a Fourier anomaly field we used a simple program given in Appendix B and existing as OSU program F498. The theory behind this program is detailed in Section 2.4 and

tests are conducted in Section 9.3. A more extended program for Fourier upward continuation exists in the OSU Department of Geology (R. von Freese, private communication), and this program has options to choose from among several different windowing techniques. However, our tests with this program have not shown a need for the application of windowing for gravity anomaly upward continuation.

8. Data Preparation for Upward Continuation Tests in New Mexico

For testing alternative models for the operational upward continuation of surface free-air anomalies, we prepared data in a 7°x9° area in New Mexico. The location of the area is such that it centers the site of the balloon-borne gravity project coordinated by the AFGL (Lazarewicz, et al., 1983), with surface data coverage extending 300 km on all sides of the balloon flight.

8.1 Available Gravity and Elevation Data

Our gravity and elevation data was based on that supplied to us earlier (April, 1983) by the National Geodetic Survey (NGS). The gravity data were in the form of irregularly distributed point values of surface free-air anomalies, as shown in Figure 6. The gravity data record included the following items (Hittelman et al., 1982):

(1) Geodetic latitude (ϕ), geodetic longitude (λ), and orthometric height (H) of the station.

(2) Measured gravity (g) referenced to a recoverable base station. Base stations had been adjusted to the International Gravity Standardization Network 1971 (Morelli, et al., 1972).

(3) Normal gravity (γ) at the Geodetic Reference System 1967 (GRS67) reference ellipsoid, computed as:

$$\gamma = 978031.85(1 + 0.005278895 \sin^2 \phi + \\ + 0.000023462 \sin^4 \phi) \text{ mgals} \qquad (8.1.1)$$

(4) Surface free-air anomaly (Δg_S) computed as:

$$\Delta g_S = g + 0.3086\ H - \gamma \qquad (8.1.2)$$

where 0.3086 mgal/m is the normal gradient of gravity.

(5) Simple Bouguer anomaly ($\Delta g'_B$) computed as:

$$\Delta g'_B = \Delta g_S - 0.1119\ H \qquad (8.1.3)$$

where the term 0.1119 H is the attraction of a Bouguer plate of standard continental density of 2.67 g/cm^3.

(6) Terrain correction (tc) formally given by (Moritz, 1966, p. 88):

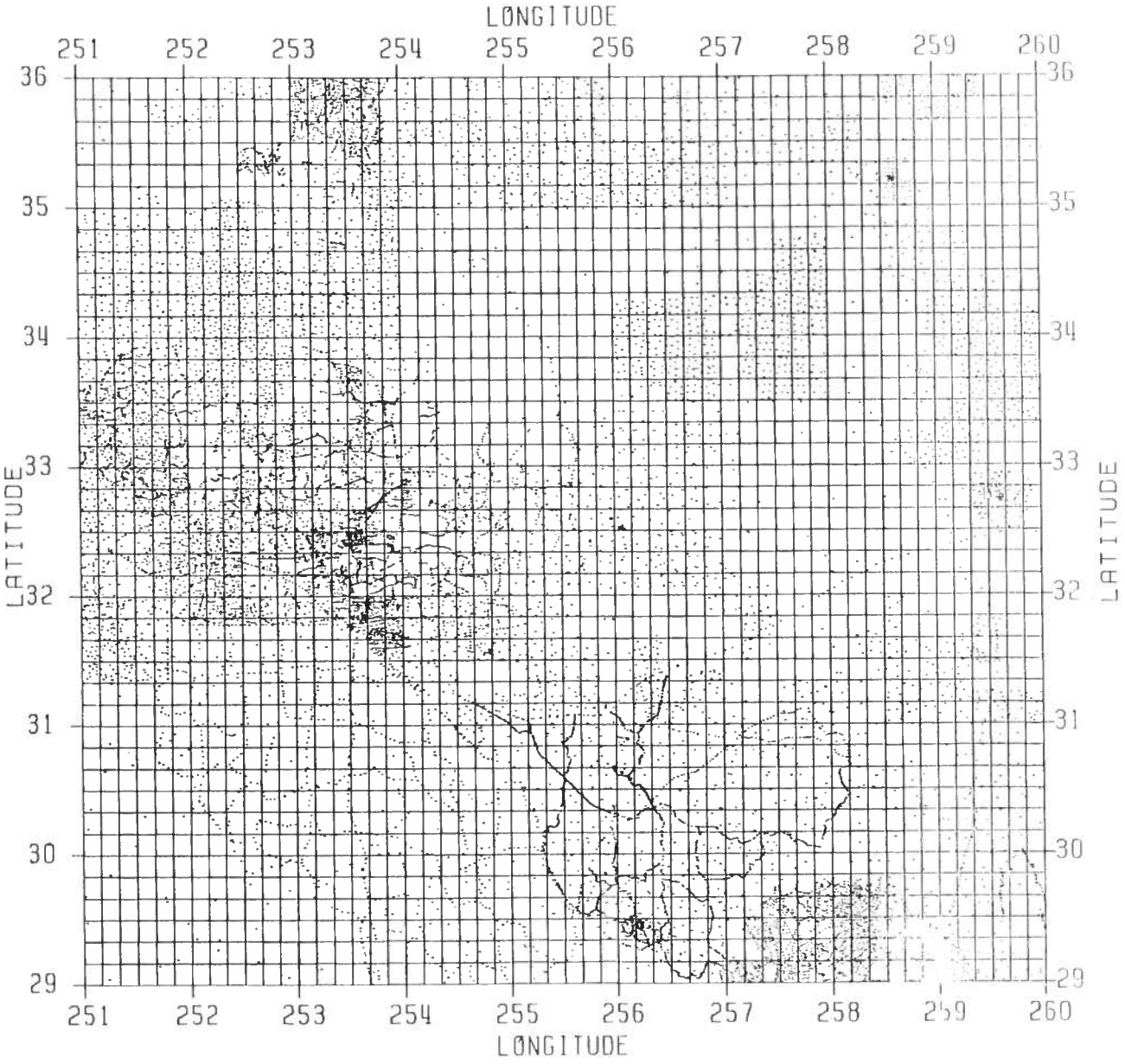

Figure 6. Point Location of Original NGS Gravity Data Before Thinout Procedure, New Mexico Balloon Gravity Test Site

$$tc = \frac{1}{2} k\rho R^2 \int_\sigma \int \frac{(H-H_p)^2}{\ell_0^3} d\sigma \qquad (8.1.4)$$

where k = Newtonian gravitational constant, ρ = density; R = mean earth radius; H = elevation; P = point to which tc refers; σ = unit sphere; $d\sigma$ = element of solid angle; $\ell_0 = 2R \sin \psi/2$; ψ = angular distance between P and $d\sigma$.

(7) Standard error of Δg_B and $\Delta g'_B$.

(8) Various codes: Agency code, quality code, elevation code, and source code.

There were a total of 18,386 original gravity points in our area. Out of these, 13,455 were NGS coded as 'ACCEPTED' while 3,931 were coded as 'NOT EDITED'. We decided to consider all the 18,386 points regardless of code as input to the data thinning step (see Section 8.2 below).

The elevation data were in the form of 30x30 arcsec grid point values. The data covered our 7°x9° New Mexico area except at three 1°x1° blocks in the southwest corner from latitude 29° to 30° and longitude 251° to 254°. We decided to fill these missing blocks by 5'x5' mean elevations from data supplied by the Defense Mapping Agency (DMA). The NGS data were used in our procedures both as the original 30"x30" point values and to obtain 5'x5' averaged values. The 5'x5' mean elevaions were formed by straight averaging all 30"x30" values that fell inside the 5'x5' block (disjoint averages). A contour map of the topography in our area based on 5'x5' mean elevations is shown in Figure 7 for a contour interval of 50 meters.

8.2 Data Thinning

The original set of 18,386 NGS points shown in Figure 6 were input into a data thinning procedure. This step was done to make the data distribution more uniform and to later avoid collocation inversion problems associated with data points that are very close together. To thin out the data a single pass was made to select only the first point that fell inside each element of a 3.5 km 3.5 km ($\Delta\phi$ = 2!0, $\Delta\lambda$ = 2!5) grid mesh. After the thin out procedure a total of 10,208 data points were left. Of these, 2 points were later discovered as blunders and removed leaving a final selection of 10,206 points which are shown in Figure 12 of Section 8.7.

8.3 5'x5' Mean Anomalies

A mean anomaly can be derived by first subdividing the mean block into pxq sub-blocks, predicting point anomalies at the centers of the sub-blocks, then averaging the predicted point anomalies. A predicted point anomaly is given by least squares collocation as follows: (Rapp, 1978, p. 134):

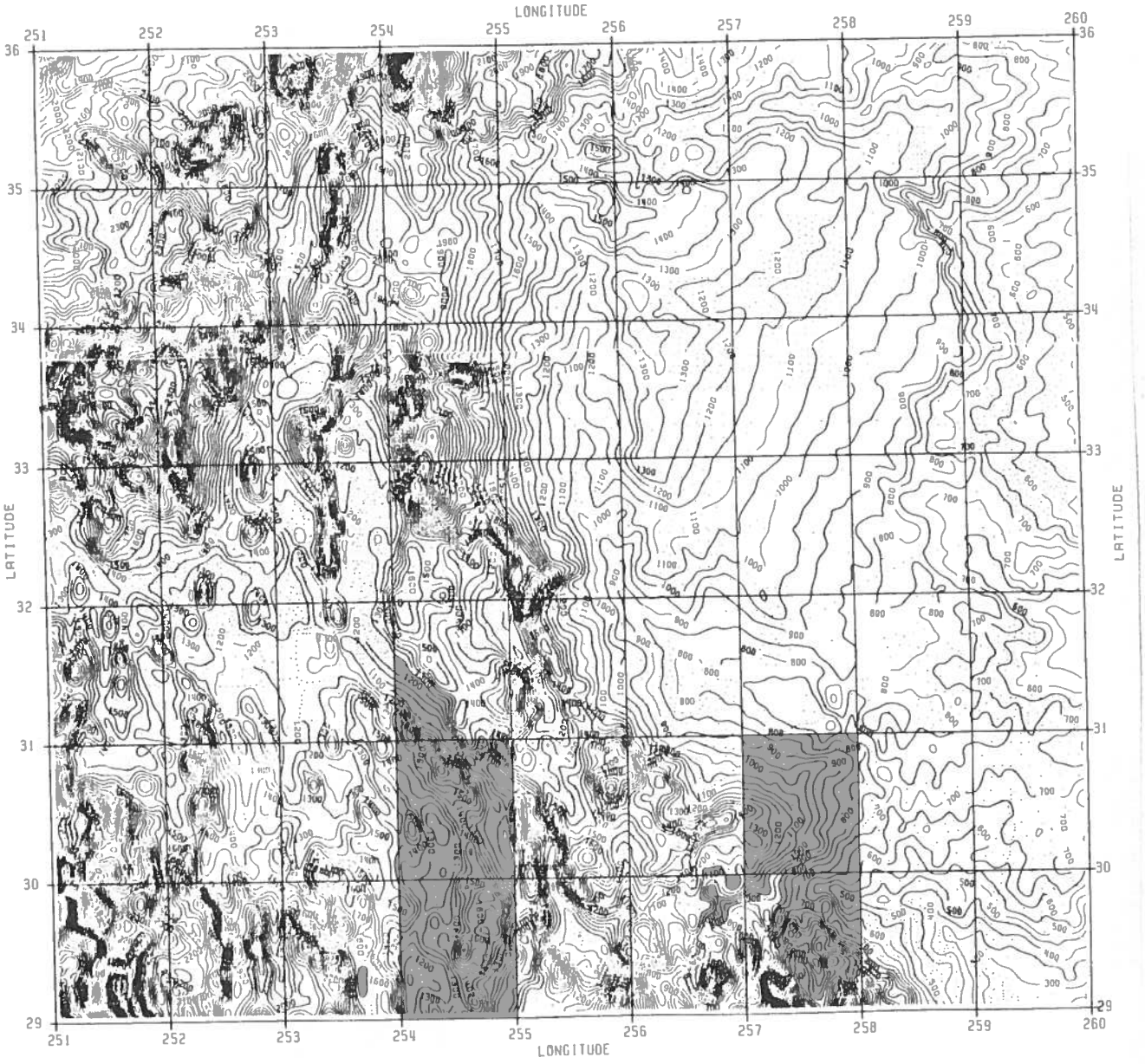

Figure 7. Topography, New Mexico Balloon Gravity Test Site. C.I. = 50 meters.

$$\Delta g_i = C_{ij}^T \, (C_{jj} + D_{jj})^{-1} \, \Delta g_j \qquad (8.3.1)$$

where

C_{ij} anomaly covariance vector between the point i being predicted and the data points j.

C_{jj} anomaly covariance matrix of the data points

D_{jj} error covariance matrix of the data points, taken as diagonal with elements the variances of the data points.

Aspects on the covariance function to use in (8.3.1) and on the removal of known trends in Δg_j are discussed separately in Sections (8.4), (8.5), and (8.6).

The mean anomaly is related to the pxq center point values inside the block by

$$\overline{\Delta g} = \frac{1}{pxq} \sum_{i=1}^{pxq} \Delta g_i \qquad (8.3.2)$$

Substituting (8.3.1) into (8.3.2) we get

$$\overline{\Delta g} = C_{\overline{\Delta g j}}^T \, (C_{jj} + D_{jj})^{-1} \, \Delta g_j \qquad (8.3.3)$$

where

$$C_{\overline{\Delta g j}}^T = \left[\frac{1}{pxq} \sum_{i=1}^{pxq} C_{ij} \right] \qquad (8.3.4)$$

is nothing but the covariance vector between the mean value and the data points j. Equation (8.3.4) expresses a numerical integration procedure (Heiskanen and Moritz, 1967, p. 277) for the determination of mean value to point value covariance using a pxq subdivision of the mean block. Equation (8.3.3) expresses the direct prediction of the mean anomaly from given point anomaly data. The standard error of the predicted $\overline{\Delta g}$ is the square root of:

$$m^2_{\overline{\Delta g}} = C_{\overline{\Delta g \Delta g}} - C_{\overline{\Delta g j}}^T \, (C_{jj} + D_{jj})^{-1} \, C_{\overline{\Delta g j}} \qquad (8.3.5)$$

where $C_{\overline{\Delta g \Delta g}}$ is the variance of the mean value being predicted, given by

$$C_{\overline{\Delta g \Delta g}} = \frac{1}{(pxq)^2} \sum_{i=1}^{pxq} \sum_{k=1}^{pxq} C_{ik} \qquad (8.3.6)$$

that is, $C_{\overline{\Delta g \Delta g}}$ is the average of all covariances between subdivision block center points inside the mean block.

For our applications to be detailed later (Section 8.7) we used equations (8.3.3) to (8.3.6) to predict 5'x5' mean anomalies from the the thinned out data of Section 8.2. We used a 2x2 block subdivision (p=2, q=2) and only the ten closest data points to the center of the 5'x5' block being predicted. The limitation to ten data points was motivated by the computer expense required to invert the matrix in (8.3.3) with dimension equal to the number of data points. This (approximate) collocation from the ten closest data points was compared with a more rigorous but much slower collocation, giving a mean difference of 0.1 mgal and an RMS difference of 2.7 mgals for a 12x12 array of prediction points in the data sparse 1°x1° area from latitude 30° to 31° and longitude 254° to 255° (See Figure 12 for data distribution). The predicted quantities were refined Bouguer anomalies with roughness (standard deviation from the mean = 15 mgals for the 1°x1° test area) shown in Figure 13. The differences between the rigorous and approximate collocation are expected to get smaller in the immediate area of the balloon flight because of the increased density of data there. The rigorous collocation used a one-time inversion of a matrix of size 524x524, giving data coverage out to 0.5 away from the prediction points while the approximate collocation used 144 inversions, with each inversion involving a 10x10 matrix. The rigorous collocation was about 100 times slower than the approximate collocation in this test case.

Theoretical and practical aspects on the choice of covariance functions to use in (8.3.3) and ways to de-trend the data are discussed in the next three sections.

8.4 Covariance Function

The covariance function to use in (8.3.1) or (8.3.3) is well-defined only in the global case. However, for local applications the choice of covariance function to use is rather arbitrary. This arbitrariness comes from the fact that the covariance function to use should be tailored to approximate the local empirical covariance function, and this local function has no clear-cut theoretical definition. The most important questions are: what size of local area should be used to derive the function?, and what trends should be removed from the data? Once a practical decision has been made on these two items, however, the estimation procedure becomes clear: The empirical covariance function is first derived by averaging products of de-trended data samples in the specified area, according to the definition of covariance function (Heiskanen and Moritz, 1967, p. 253). The derived empirical covariance function is then usually approximated by a simple analytical function that lends itself to closed form covariance propagation if needed, resulting in a self-consistent system for the estimation of various linear functionals of the earth's anomalous potential. The way to approximate an empirical covariance function by an

analytical function of specified form, is by satisfying the three essential parameters of the empirical function, namely, the variance, correlation length, and curvature parameter (Moritz, 1980, p. 174).

For our applications we used a simple tailoring procedure for the covariance function. We took the global anomaly covariance function of Tscherning and Rapp (1974) and first subtracted the first 36 harmonics. This resulted in a new covariance function with a correlation length of about 20 km, approximating the correlation length of the de-trended data (see below) used in our estimation procedures. The covariance function was then scaled to satisfy the variance of the de-trended data. This scaling would not affect the previously tailored correlation length. For the cuvature parameter, there was no specific treatment given to satisfy the data; the practical problems associated with the empirical computation of the curvature parameter, as well as its approximate computation by finite differences, can be found in Schwarz and Lachapelle (1980).

8.5 Data De-Trending at High Frequencies

It is well-known that short wavelength free-air anomalies are strongly correlated with short-wavelength topography - for an instructive physical interpretation of this fact using a simple crustal density and isostatic compensation model, see Moritz 1968, p. 28. Therefore, the computational removal of the attraction caused by topographic masses is certain to remove most of the roughness that may be present in an anomaly field.

This removal of roughness of the field is very important in interpolation problems. With the removal of as much roughness as possible, the correlation length of the residual field will be enlarged as much as possible. This implies that the ratio

$$\rho = \frac{\text{correlation length}}{\text{mean data spacing}}$$

will also be enlarged as much as possible, and this is a key to strengthening the interpolation of the residual field (see Sunkel, 1981, pp. 88-93, where values of ρ of at least ρ=3 are indicated to be desirable). Of course, once the interpolated value from the residual field has been obtained,the total field value can be obtained by adding back the influence of topographic masses. This influence is computable from detailed topographic height data which are assumed to be readily available in the prediction area.

Anomaly data de-trended at high frequencies can be the simple or the refined Bouguer anomalies. The simple Bouguer anomaly is given by (8.1.3):

$$\Delta g'_B = \Delta g_S - 0.1119\ H \qquad (8.5.1)$$

where -0.1119 H means the removal from surface data Δg_S of the gravitational attraction of a moving Bouguer plate of standard density 2.67 g/cm^3. The refined Bouguer anomaly is given by:

$$\Delta g_B = \Delta g_S - 0.1119\ H + tc \qquad (8.5.2)$$

where tc is the gravimetric terrain correction formally given by (8.1.4). Whereas (8.5.1) represents the removal of a moving Bouguer plate, the application of tc to (8.5.1) to arrive at (8.5.2) means that now in (8.5.2) the gravitational attraction of the actual (non-moving, fixed) topography is removed from Δg_B. The tc were given for our NGS gravity data; if they had not been given, we would have had to compute them using the operational program by Forsberg (see Section 7). Such computations of tc tend to be expensive (about 0.2 CPU sec per point on the Amdahl 470 V/6 system) if they have to be done for all observation points. In this respect the studies by Sideris (1984) on the computation of tc by Fast Fourier Transforms (FFT) should prove to be very important.

8.6 Data De-Trending at Low Frequencies

The Bouguer anomalies produced by (8.5.1) or (8.5.2) are much smoother than the original Δg_B field but are biased, having large and systematically negative values in mountainous areas - again, it is instructive to see Moritz (1968, p. 28) for a physical explanation of this fact using isostatic compensation theory. In accordance with the statistical aspect of the least squares collocation interpolation procedure, gross trends should first be removed from the data before interpolation (see Moritz, 1980, Sec. 38: "The Meaning of Statistics in Collocation"). To de-trend the Bouguer anomaly data, one way would be to postulate a low order trend surface and fit this surface to the data, possibly in the context of least squares collocation with systematic parameters (Sunkel, 1983), or possibly in the context of a simple least squares adjustment. For our purposes we de-trended the Bouguer anomaly data using available spherical harmonic expansions to 180 of free-air anomaly and topography. The effect that the de-trending at low frequencies has on interpolation results is described later under Section 8.7, step (7).

The free-air anomaly on an equatorial sphere can be generated from potential coefficients to degree N_{max}, using (2.2.3) with H_o=0:

$$\Delta g^S = \frac{kM}{a^2} \sum_{n=2}^{N_{max}} (n-1) \sum_{m=0}^{n} (\bar{C}^*_{nm} \cos m\lambda + \bar{S}_{nm} \sin m\lambda)\, \bar{P}_{nm} (\sin \phi) \qquad (8.6.1)$$

(the superscript s denotes spherical harmonics). The topography can also be expanded in terms of spherical harmonics to degree N_{max}:

$$H^S = \sum_{n=0}^{N_{max}} \sum_{m=0}^{n} (A_{nm} \cos m\lambda + B_{nm} \sin m\lambda) \bar{P}_{nm} (\sin \phi) \qquad (8.6.2)$$

We then have a Bouguer anomaly to resolution corresponding to harmonic degree N_{max}:

$$\Delta g^S_B = \Delta g^S - 0.1119 H^S \qquad (8.6.3)$$

Subtraction of the reference Bouguer anomaly Δg^S_B from the Bouguer anomaly in (8.5.1) and (8.5.2) gives, respectively, the residual Bouguer anomaly (8.6.4) and terrain corrected residual refined Bouguer anomaly (8.6.5) (see equation (3.3.13) for a fuller understanding of equation (8.6.5)):

$$\Delta g^{r'} = (\Delta g_S - 0.1119 H) - (\Delta g^S - 0.1119 H^S) \qquad (8.6.4)$$

$$(\Delta g^r + tc^S) = (\Delta g_S - 0.1119 H + tc) - (\Delta g^S - 0.1119 H^S) \qquad (8.6.5)$$

The last two equations can also be written as

$$\Delta g^{r'} = \Delta g_S - \Delta g^S - 0.1119 (H - H^S) \qquad (8.6.6)$$

$$(\Delta g^r + tc^S) = \Delta g_S - \Delta g^S - 0.1119 (H - H^S) + tc \qquad (8.6.7)$$

The last two equations state that the original anomalies Δg_S are de-trended (1) in the long wavelength, by subtracting free-air anomalies Δg^S generated from spherical harmonic expansion; and (2) in the short wavelength, by doing "Bouguer reduction" not with respect to the geoid but with respect to the higher order but still smooth surface H^S from spherical harmonics.

8.7 Actual Predictions of 5'x5' Mean Anomalies

In accordance with the previous discussions we took the following steps to predict 5'x5' mean anomalies, for use in our anomally upward continuation procedures. The starting anomaly data were the point surface free-air anomalies (look ahead to Figure 12 for point location), resulting from the thin out procedure of Section 8.2. As stated in Section 8.1 the gravity record also contained the elevation H of the station and the terrain correction tc. Here are the various steps:

(1) Reference free-air anomalies Δg^S (8.6.1) were generated on a 0.25x0.25 grid using the Rapp-180 (Rapp, 1981) potential coefficients with N_{max}=180. A contour map of this data is shown in Figure 8 with a contour interval of 5 mgals.

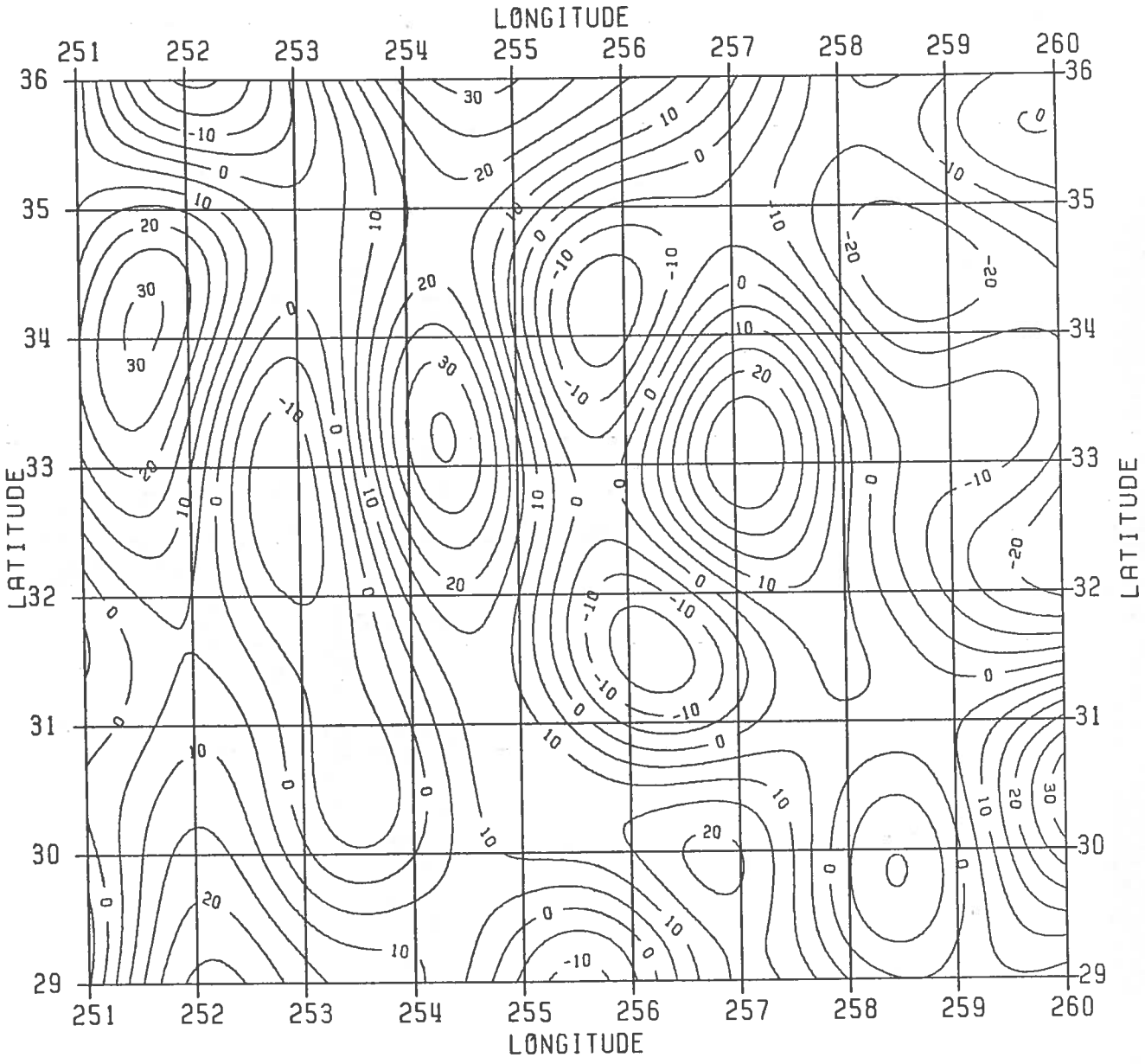

Figure 8. Rapp-180 Gravity Anomalies at Zero Altitude, New Mexico Balloon Gravity Test Site. C.I. = 5 mgals.

(2) Reference elevations H^s (8.6.2) were generated on a 0.25x0.25 grid using topographic coefficients available at OSU (tape GS140, file 15) with N_{max}=180. A contour map of this data is shown in Figure 9 with a contour interval of 50 meters.

(3) Reference Bouguer anomaly values Δg^s_B (8.6.3) were generated on a 0.25x0.25 grid from the Δg^s and H^s of steps (1) and (2). This data is contoured in Figure 10 with a contour interval of 5 mgals. In our procedures we could also generate Δg^s_B directly in one step because we had combined the two series in (8.6.1) and (8.6.2) to produce a Bouguer anomaly series to degree 180, with its own Bouguer anomaly spherical harmonic coefficients.

(4) Refined Bouguer anomalies Δg_B (8.5.2) were computed at the irregularly distributed data points using Δg_s, H and tc given on the gravity records. The RMS value of the original irregularly distributed Δg_s was 26 mgals. The RMS value of the refined Bouguer anomalies Δg_B with the mean removed was higher, 49 mgals, because although Δg_B was smooth it had significant long wave trend.

(5) Terrain corrected residual refined Bouguer anomalies $\Delta g^r + tc^s$ (8.6.5) were computed at the irregular data points by first interpolating the 0.25x0.25 grid of Δg^s_B from step (3) to obtain the reference Bouguer anomaly at the data point, then subtracting this reference value from the refined Bouguer anomaly of step (4).The RMS value of the irregularly distributed anomalies ($\Delta g^r + tc^s$) was a smooth and centered 15 mgal.

(6) 5'x5' mean values of terrain corrected residual refined Bouguer anomalies (8.6.5) were predicted from the data of step (5) using the "collocation from the closest 10 points" procedure described in Section 8.3. To repeat, a 2x2 subdivision of the 5'x5' block was used. The covariance tailoring procedure used is described in Section 8.4. A contour map of the predicted 5'x5' mean residual refined Bouguer anomalies is shown in Figure 11, with a contour interval of 5 mgals. Note that this de-trended anomaly surface is much smoother and, therefore, much more reasonable to interpolate than the trended original Δg_s surface (look ahead to Figure 14). The point location of the irregularly distributed data from which 5'x5' predictions were made, as well as the formal standard errors of predicion coming out of the collocation procedure, are shown in Figure 12. The collocation error estimates shown are at least correct on a relative basis, but also their absolute values are expected to be meaningful because of the use of an empirically tailored covariance function (Schwarz and Lachapelle, 1980, p. 33).

(7) A "back solution" could now be made starting from the predicted 5'x5' mean values of step (6). 5'x5' grid point values of Δg^s_B (8.6.3) were first interpolated at the centers of the 5'x5' mean blocks of step (6) using the 0.25x0.25 grid of Δg^s_B values from step (3). These interpolated values were then added to the values in (8.6.5) from step (6) to produce 5'x5' mean values of refined Bouguer anomalies Δg_B (8.5.2), contoured in Figure 13 with a contour interval of 5 mgals. The difference between the Bouguer anomalies in Figures 13 (from this step) and 11 (from step (6)) is the presence of long wave Bouguer anomaly trend in Figure 13.

To test the significance of de-trending at low frequencies we repeated the predictions of the quantity shown in Figure 13, this time using the simple data average as reference value, instead of the "Bouguer anomaly to 180". The covariance function of step (6) was accordingly scaled to reflect the variance

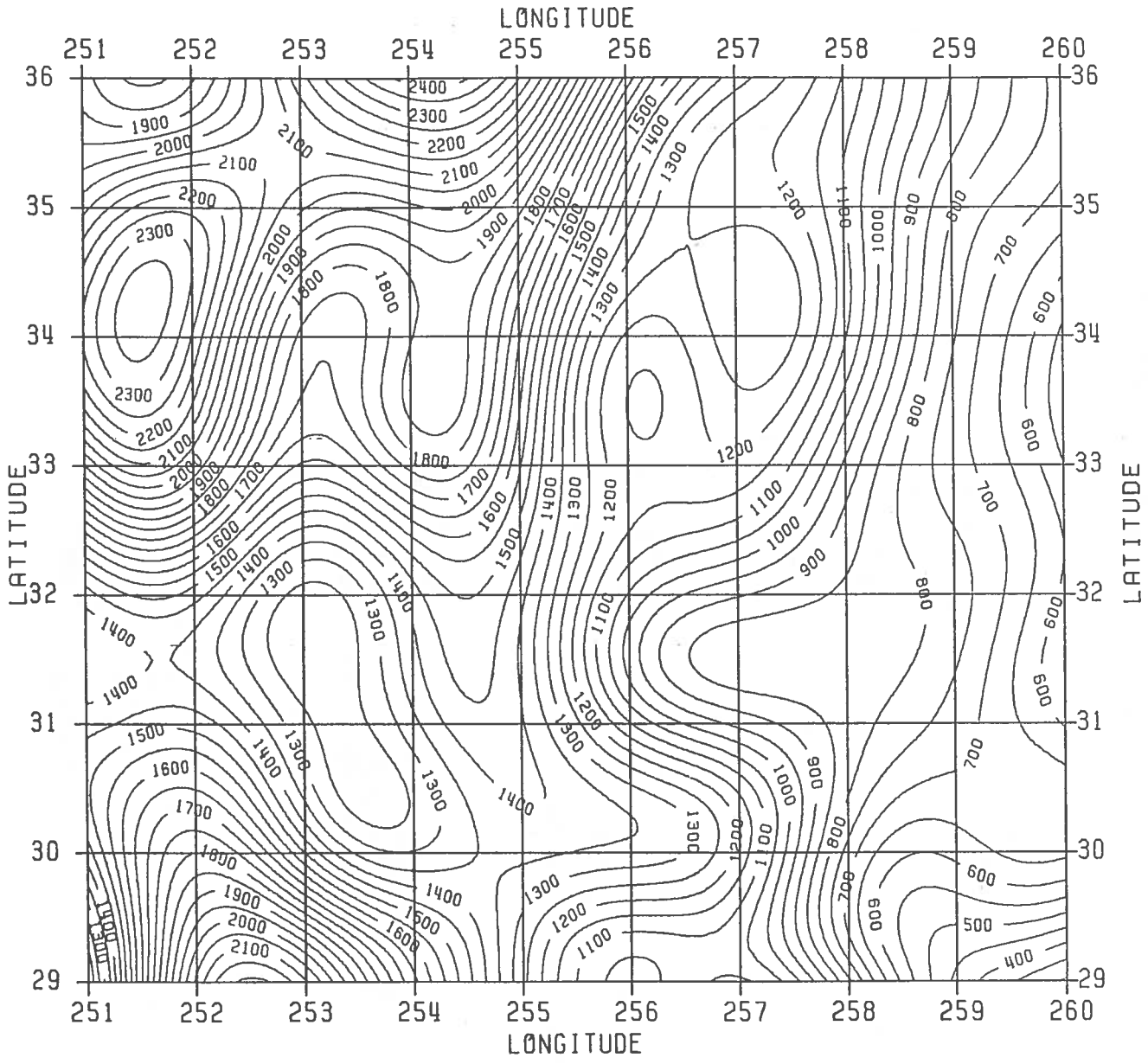

Figure 9. 180 x 180 Spherical Harmonic Expansion of the Topography, New Mexico Balloon Gravity Test Site. C.I. = 50 meters.

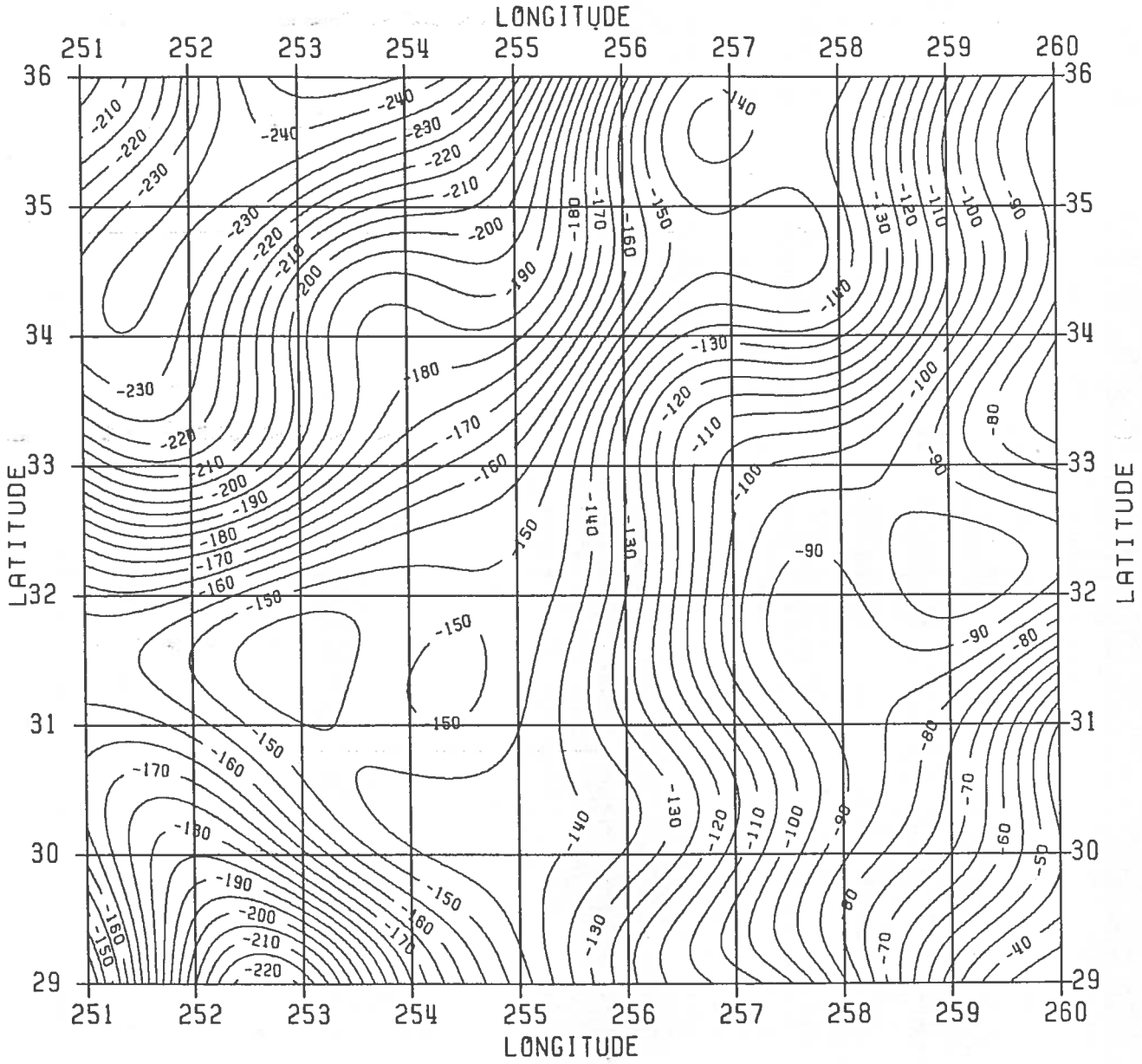

Figure 10. 180 x 180 Spherical Harmonic Expansion of Bouguer Anomalies, New Mexico Balloon Gravity Test Site. C.I. = 5 mgals.

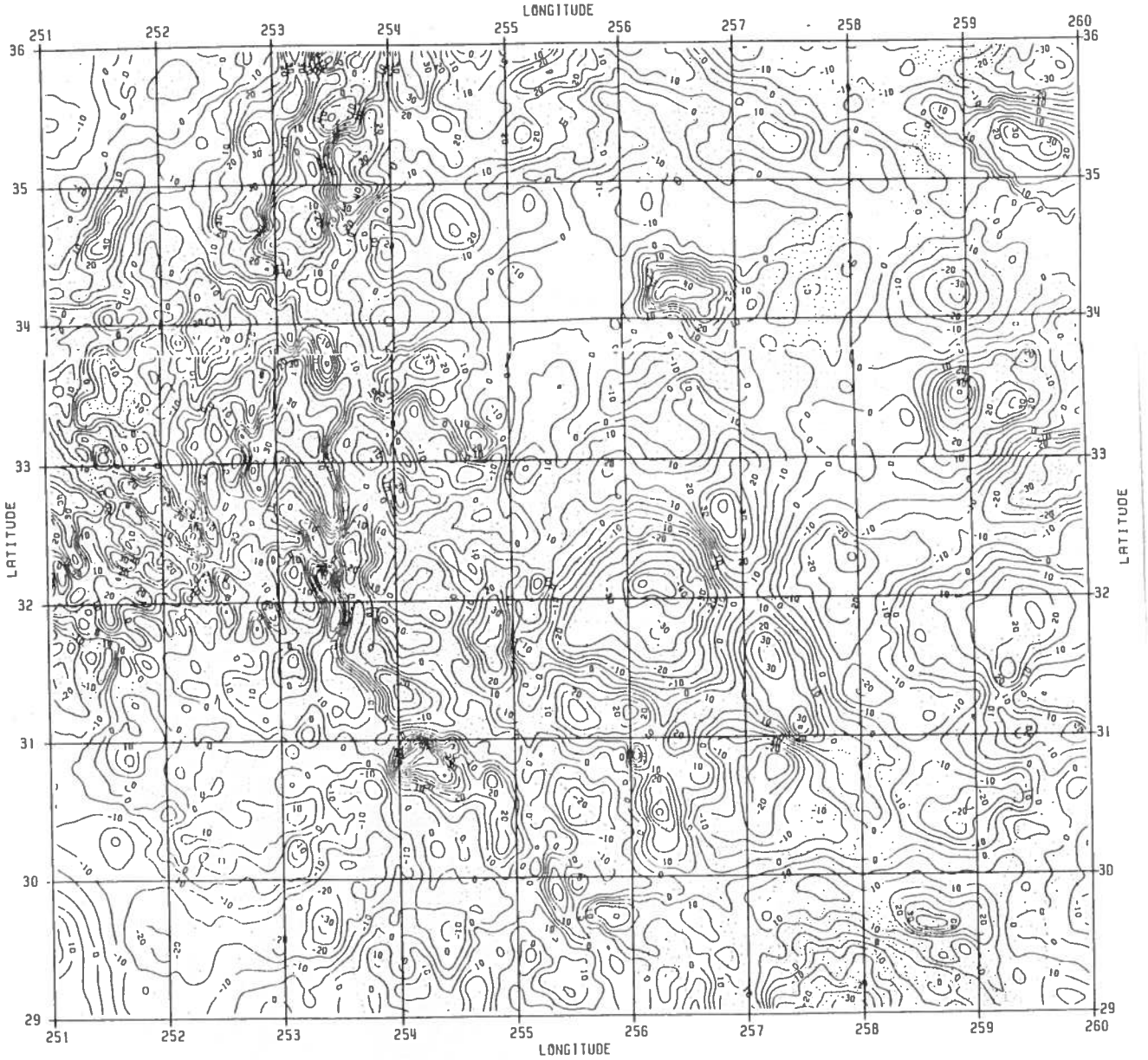

Figure 11. Residual Refined Bouguer Anomalies, New Mexico Balloon Gravity Test Site. C.I. = 5 mgals.

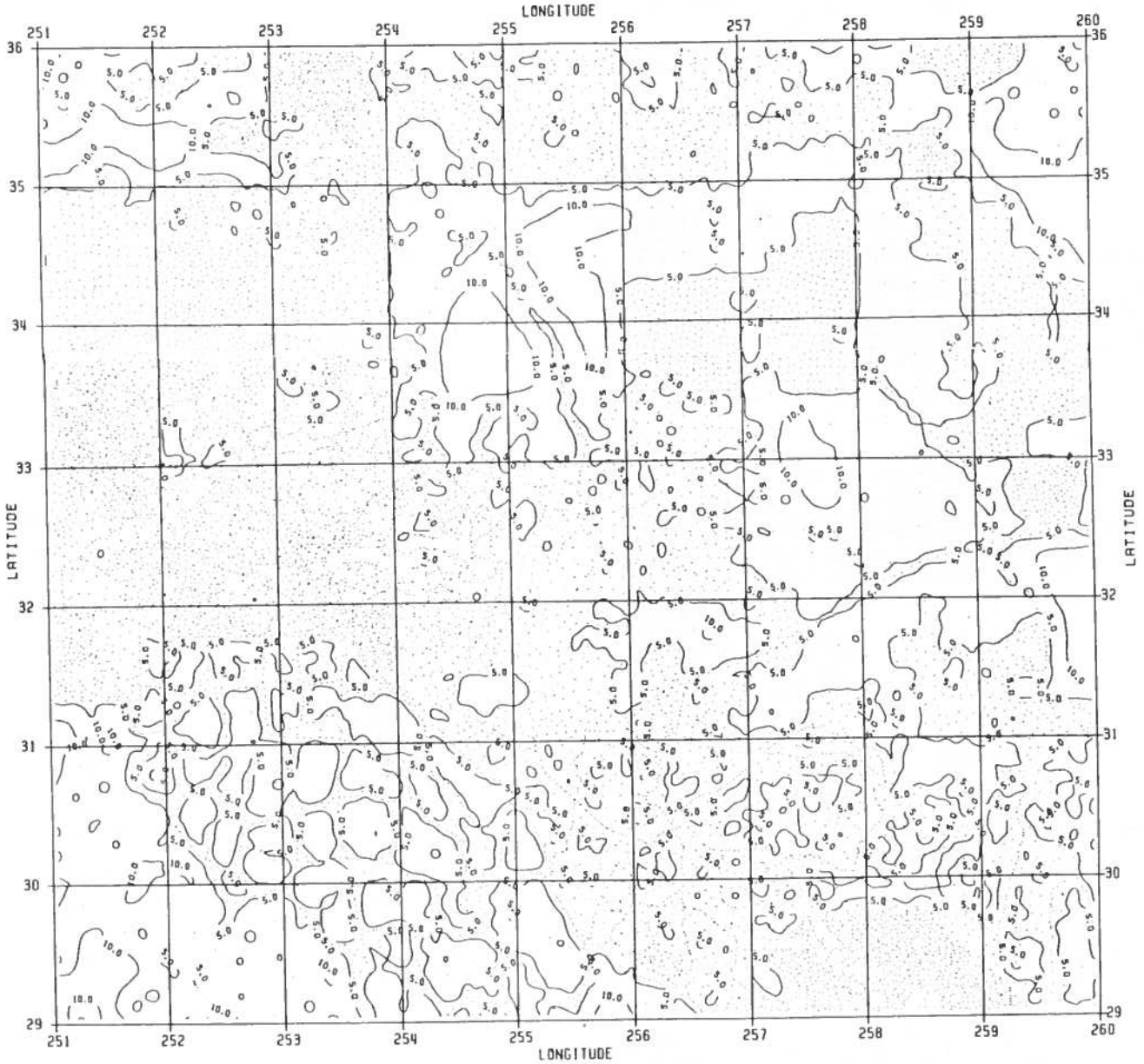

Figure 12. Point Location of Gravity Data, and Formal Standard Errors of Prediction of 5'x5' Mean Residual Bouguer Anomalies Using Collocation from the Ten Closest Data Points. New Mexico Balloon Gravity Test Site. C.I. = 5 mgals.

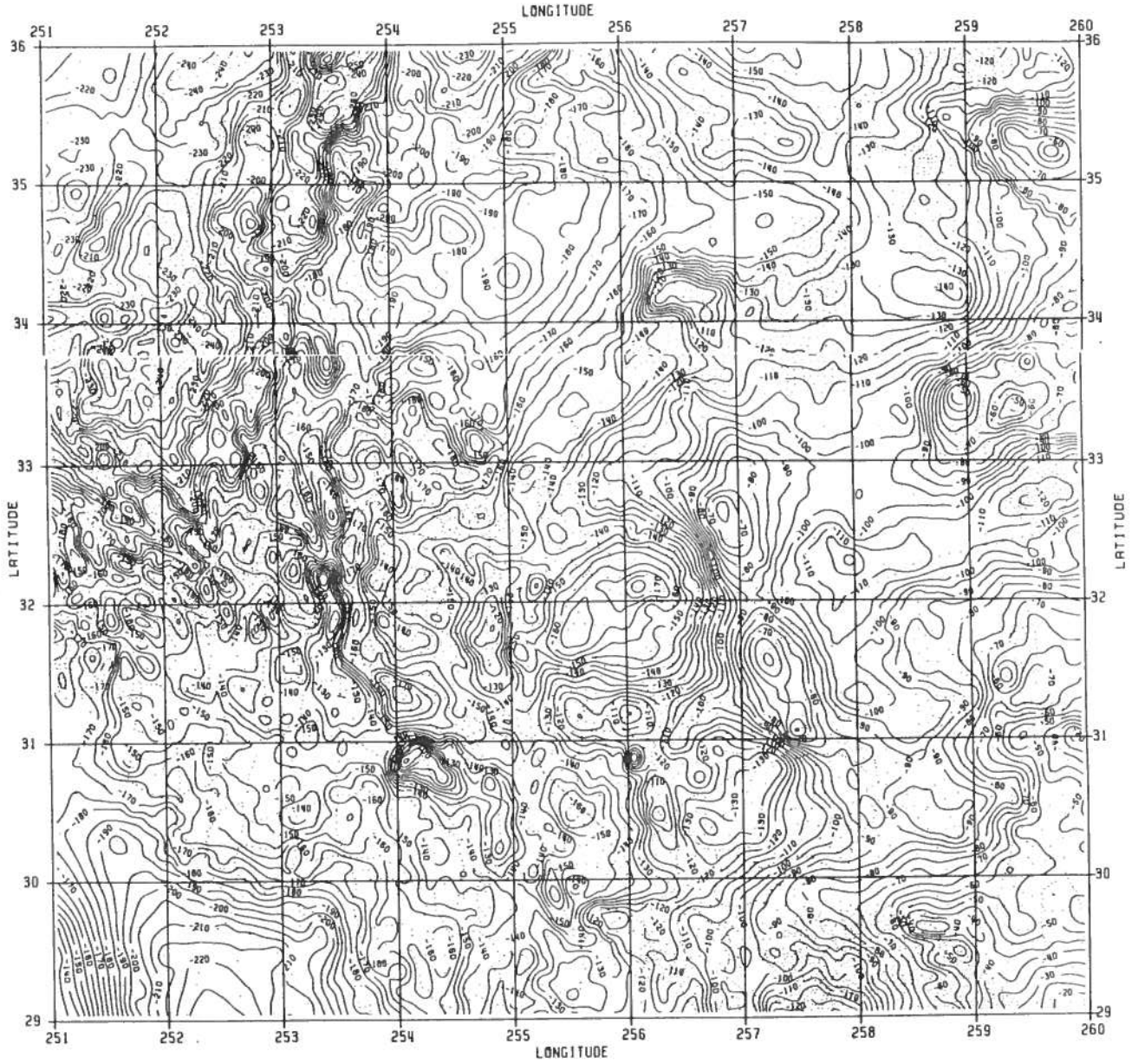

Figure 13. Refined Bouguer Anomalies, New Mexico Balloon Gravity Test Site. C.I. = 5 mgals.

of the "mean-value centered" data, which was 2400 mgal^2. For comparison, let us distinguish two prediction procedures as follows:

Method A: Bouguer anomaly to 180 used as a reference surface. Variance of data used in predictions: 225 mgal^2.

Method B: Simple average used as a reference value. Variance of data used in predictions: 2400 mgal^2.

We observed the following:

(a) In areas with good data coverage (i.e., areas with standard error of prediction less than or equal to 5 mgals as shown in Figure 12), the predicted values from Methods A and B generally agreed to better than 0.2 mgal.

(b) In areas with poor data coverage (standard error greater than or equal to 10 in Figure 12), differences of 7 mgals were observed between Methods A and B. In these areas the used reference value "anchors" the predicted value, in the sense that the predicted value tends to approach the reference value.

(c) The most significant difference between Methods A and B, affecting both areas of good and of poor data coverage, was the scaling of the formal error estimates. Error estimates from Method B were more pessimistic than Method A, by the ratio $(2400/225)^{\frac{1}{2}}$.

From the above we conclude that the advantage in using a higher order trend surface than the simple-average surface lies in a better scaling of the error estimates; the predicted values themselves are not critically affected by the choice of trend surface for areas of reasonable data coverage.

(8) To the 5'x5' refined Bouguer anomalies (8.5.2) from step (7) we added 0.1119 H, where the elevations H were the 5'x5' mean elevations mentioned at the end of Section 8.1. In accordance with (8.5.2), the results would be 5'x5' mean values of terrain corrected (i.e. Faye) surface anomalies (Δg_S + tc), contoured in Figure 14 with a contour interval of 5 mgals. Throughout our procedures we of course assumed that 5'x5' mean values of free-air anomalies referred to 5'x5' mean elevations, and this assumption is justified because of the strong local correlation between point free-air anomalies and elevations; for a further discussion of correspondence between mean free-air anomalies and mean elevations, see Sunkel, 1981, p. 5.

(9) It was also of interest to our studies to predict 5'x5' mean anomalies without having first applied the terrain corrections to the irregular data Δg_S in step (4). In other words, we essentially repeated all the de-trending, prediction, and back solution steps working with simple Bouguer anomalies given by (8.5.2). The end results analogous to those of step (8) were 5'x5' mean values of (terrain uncorrected) surface free-air anomalies Δg_S.

REMARK: Note that implicitly in step (9) we carried the quantity "-tc" (present in the original Δg_S data) through the prediction procedure. Therefore, implicitly we attempted to predict 5'x5' mean values of "-tc" which would have to be very inaccurate because of the very short correlation length associated with the terrain correction (correlation lengths on the order of only 2!5 were

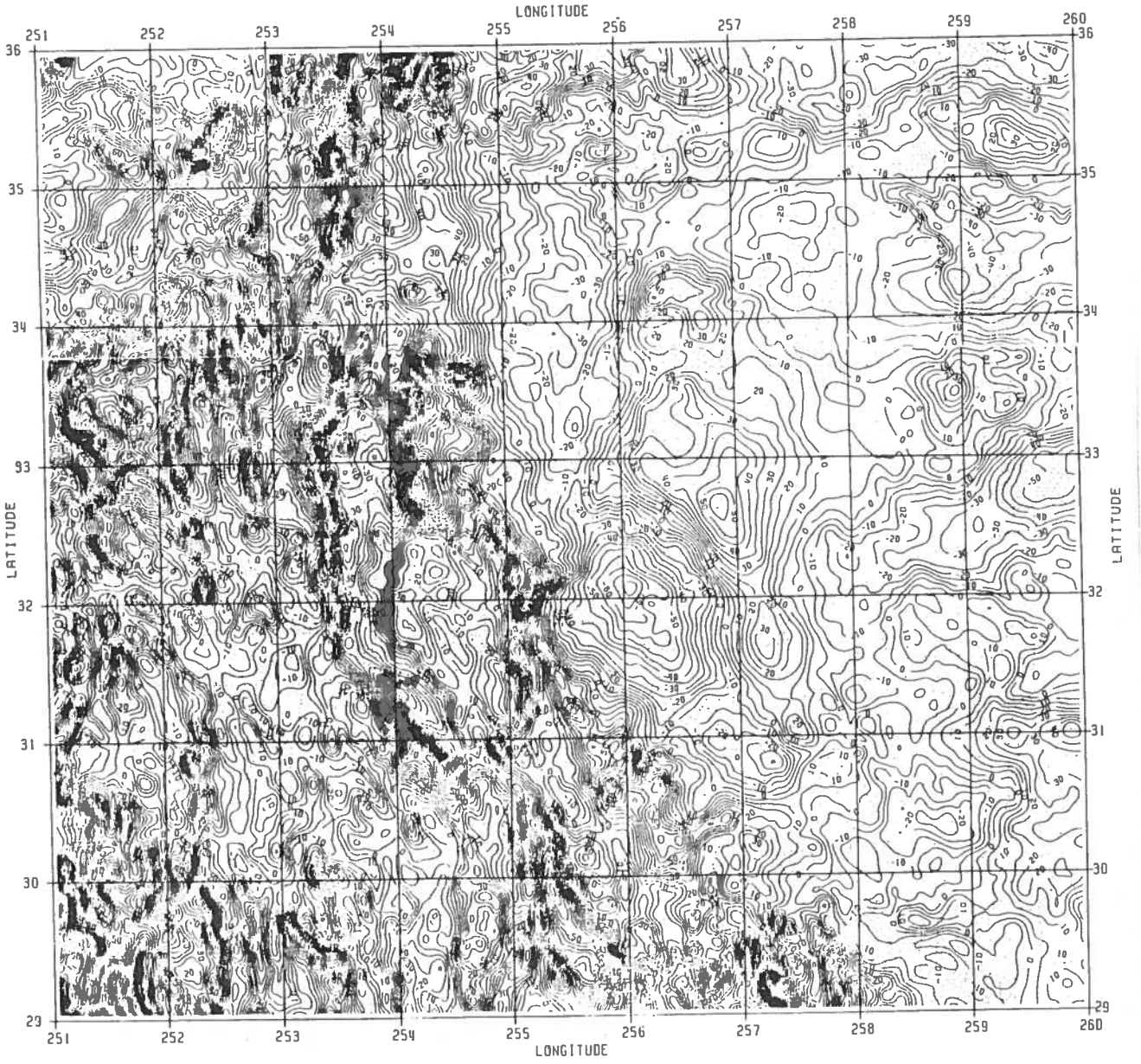

Figure 14. Faye Anomalies, New Mexico Balloon Gravity Test Site. C.I. = 5 mgals.

found by Forsberg, 1984, p. 82). A theoretically better alternative would have been to take the Faye anomalies of step (8) and subtract rigorously computed tc values using Forsberg's (Section 7) program, but this alternative would be prohibitively expensive at the present time. A possible way out of this expense would be the development of FFT techniques to compute tc (Sideris, 1984).

The "predicted" tc of step (9) was brought to light as follows:

$$tc_{(predicted)} = (\Delta g_S + tc)_{STEP(8)} - \Delta g_{S_{STEP(9)}} \qquad (8.7.1)$$

Values of tc(predicted) were taken in the 1°x1° area from latitude 32° and 33° and longitude 254° to 255°, and these values compared with rigorously computed tc from Forsberg's program. We found the following statistics using a 6x6 grid of comparison points (units: mgals):

Statistics	Difference tc(predicted) - tc(rigorous)	Actual Value tc(rigorous)
Mean	-1.18	2.68
Std. Dev.	±2.69	±2.95
RMS	2.06	3.99
Maximum Absolute Value	6.06	14.38

On average, one can say from the above table that 50% of the true tc-information has been recovered in the prediction. Inspection of the actual differences which are not given here reveals that the general shape of the tc-function can be reasonably predicted, but that a reasonable prediction of detailed features basically relies on the chance that there is a data point close to the prediction point. One could expect that for a reasonable prediction of detailed features of tc the data spacing would have to be much less than the correlation length of tc in the area, say, one-third the correlation length; this is indicated from the discussions of Sunkel (1981, pp. 88-93) who gives general data density requirements as a function of the correlation length of the function being interpolated.

9. Numerical Investigations

9.1 Comparison of Direct and Indirect Upward Continuation Results

We applied the indirect and direct upward continuation methods described in Section 3.3 to our 7°x9° study area in New Mexico. Figure 7 on page 52 shows the topographic features in the area. Upward continuations were done for a 60-point profile running east-west from longitude 253° to 258°. Upward continuation distances used were H_0=28.5, 8.5, and 3.5 km. These rather odd values of H_0 resulted from considering the data to be at a mean elevation of 1.5 km and the uplifted profiles to be at 30, 10 and 5 km elevation. The 60 upward continuatuation points were located at the centers of the 5'x5' mean data blocks directly beneath the profile. Although 60 points were used, it was sufficient to present results only for every 6^{th} point giving 11 presentation points.

The entire 84x108 grid of 5'x5' mean anomaly data (Section 8.7) and 5'x5' mean elevation data (Section 8.1) covering the 7°x9° area were used in upward continuations. The types of anomalies used were the terrain corrected residual refined Bouguer anomalies ($\Delta g^r + tc^s$) for the indirect method, and the surface anomalies Δg_s and terrain-corrected surface anomalies (Δg^s + tc) for the direct method. The detailed 1km x 1km point elevation data (Section 8.1) were used near the computation points for the prism integration of the attraction of topographic masses needed in the indirect method. Also for the purpose of the indirect method, the Rapp-180 potential coefficients and a set of degree 180 spherical harmonic coefficients for the topography (Section 8.6) were used to generate reference values of gravity anomalies and topography. The operational programs used in the numerical investigations are described in Section 7.

Tables 3 to 5 give the results of the indirect and direct upward continuations for the 11 presentation points, for H_0=28.5, 8.5, and 3.5 km. Columns 1 to 3 of the tables give the three components of the indirect method, namely (1) anomaly contribution from the medium wavlength part of terrestrial data, (2) anomaly contribution from the long wavelength spherical harmonic field, and (3) anomaly contribution from shallow topographic masses. Column 4 gives the total anomaly (Δg_s + tc^s) from the indirect method (see page 20 for the rationale behind the use of tc^s).

The results from the indirect method were compared with those from the direct method, with differences shown in columns 5 and 6 of Tables 3 to 5. Column 5 shows that the direct method using the surface anomalies alone (Δg_s) produces a profile that is systematically too low compared with the expectedly more rigorous profile of the indirect method. The biases have mean values of 0.64 mgal (H_0=28.5 km), 0.54 mgal (H_0=8.5 km), and 0.71 mgal (H_0=3.5 km). Column 6 shows that the use of terrain-corrected surface anomalies (Δg_s+tc) in the direct method improves the bias of column 5 down to 0.03 mgal (H_0=28.5 km), 0.11 mgal (H_0=8.5 km), and 0.06 mgal (H_0=3.5 km). The standard deviation of the differences of columns 5 and 6 (direct method) with column 4 (indirect method) also improves slightly with the use of (Δg_s+tc) instead of Δg_s in the direct upward continuations. In the next section we will make further studies

Table 3. Comparison of Upward Continued Anomalies. Upward Continuation Distance H_o = 28.5 km. (Superscript I: Indirect Method; D: Direct Method).
Units: mgals

Point Sequence	1 $(\Delta g^r+tc^s)^D_{Ho}$ eq. (3.3.14)	2 Δg^s_{Ho} eq. (3.3.15)	3 Δg^t_{Ho} eq. (3.3.16)	4 $(\Delta g_s+tc^s)^I_{Ho}$ 1 + 2 + 3	5 $(\Delta g_s)^D_{Ho}$-col(4) eq. (3.3.1)	6 $(\Delta g_s+tc)^D_{Ho}$-col(4) eq. (3.3.2)
1	7.91	-4.27	-5.51	-1.87	-0.50	0.27
7	3.98	3.83	-8.44	-0.63	-0.94	0.06
13	0.82	14.37	-6.72	8.47	-1.72	-0.54
19	1.28	17.21	7.33	25.82	-1.56	-0.46
25	2.73	10.51	1.63	14.87	-0.69	0.18
31	2.21	2.45	-8.11	-3.45	-0.24	0.22
37	-2.44	1.61	-6.91	-7.74	-0.34	-0.07
43	2.38	7.61	-1.39	8.60	-0.25	-0.08
49	9.13	12.73	-2.17	19.69	-0.52	-0.15
55	-1.50	11.05	-2.35	7.20	-0.35	-0.01
60	-5.60	5.23	-1.59	-1.96	0.06	0.02
				Mean	-0.64	-0.03
				Std. Dev.	±0.53	±0.27

Table 4. Comparison of Upward Continued Anomalies. Upward Continuation Distance H_o = 8.5 km. (Superscript I: Indirect Method; D: Direct Method).
Units: mgals

Point Sequence	1 $(\Delta g^r+tc^s)^D_{H_o}$ eq. (3.3.14)	2 $\Delta g^s_{H_o}$ eq. (3.3.15)	3 $\Delta g^t_{H_o}$ eq. (3.3.16)	4 $(\Delta g_s+tc^s)^I_{H_o}$ 1 + 2 + 3	5 $(\Delta g_s)^D_{H_o}$–col(4) eq. (3.3.1)	6 $(\Delta g_s+tc)^D_{H_o}$–col(4) eq. (3.3.2)
1	9.00	9.82	-7.36	-8.18	-0.16	0.46
7	5.77	2.74	-4.92	3.59	-0.77	0.86
13	-1.10	19.45	-21.11	-2.76	-1.72	-0.63
19	0.56	23.79	19.41	43.76	-1.68	-0.52
25	1.28	12.92	9.31	23.51	-0.01	1.10
31	5.37	0.39	-16.30	-10.54	-0.01	0.30
37	-4.99	-0.09	-11.69	-16.77	-0.44	-0.24
43	3.77	10.27	-0.05	13.99	-0.07	-0.01
49	20.84	18.57	-3.04	36.37	-0.64	-0.21
55	-4.05	15.75	-3.56	8.14	-0.47	-0.05
60	8.44	6.88	-1.52	-3.08	0.01	0.12
				Mean	-0.54	0.11
				Std. Dev.	±0.60	±0.51

Table 5. Comparison of Upward Continued Anomalies. Upward Continuation Distance H_o = 3.5 km. (Superscript I: Indirect Method; D: Direct Method).
Units: mgals

Point Sequence	1 $(\Delta g^r+tc^s)^D_{Ho}$ eq. (3.3.14)	2 Δg^s_{Ho} eq. (3.3.15)	3 Δg^t_{Ho} eq. (3.3.16)	4 $(\Delta g_s+tc^s)^I_{Ho}$ 1 + 2 + 3	5 $(\Delta g_s)^D_{Ho}$−col(4) eq. (3.3.1)	6 $(\Delta g_s+tc)^D_{Ho}$−col(4) eq. (3.3.2)
1	9.62	−11.71	−9.52	−11.61	0.35	0.89
7	8.71	2.33	2.94	13.98	−2.05	0.35
13	−2.38	21.11	−30.41	−11.68	−0.88	0.00
19	0.18	25.92	27.84	53.94	−4.03	−2.94
25	−0.38	13.64	12.81	26.07	0.37	1.55
31	6.33	−0.37	−19.57	−13.61	0.51	0.76
37	−6.23	−0.68	−13.19	−20.10	−0.12	−0.01
43	3.54	11.16	−0.68	15.38	−0.26	−0.24
49	24.86	20.49	−3.43	41.92	−0.87	−0.57
55	−4.74	17.23	−4.02	8.47	−0.72	−0.38
60	−8.27	7.31	−1.37	−2.33	−0.15	−0.06
				Mean	−0.71	−0.06
				Std. Dev.	±1.26	±1.09

into the causes of the numerical differences between the direct and indirect methods.

For visualization Figure 15a shows the 60-point terrestrial anomaly profile and its upward continued version at altitude H_o=28.5 km. Correspondingly the Rapp-180 anomaly profile at the ground level and at altitude 28.5 km are shown in Figure 15b.

9.2 Other Studies

This section presents other studies that we conducted using the data in New Mexico. The objective is to give more information on the numerical aspects of various procedures related to upward continuation of surface free-air anomalies.

9.2.1 Formally Upward Continued Terrain Correction

For the direct method we had the terrain-uncorrected version:

$$(\Delta g_S)^D_{H_o} = U_p\{\Delta g_S\} = \frac{H_o}{2\pi} \iint_A \frac{\Delta g_S}{D_o^3}\, dxdy \qquad (9.2.1)$$

and the terrain-corrected version:

$$(\Delta g_S + tc)^D_{H_o} = U_p\{\Delta g_S + tc\} = \frac{H_o}{2\pi} \iint_A \frac{(\Delta g_S + tc)}{D_o^3}\, dxdy \qquad (9.2.2)$$

The numerical difference between these two versions of the direct method is:

$$(\Delta g_S + tc)^D_{H_o} - (\Delta g_S)^D_{H_o} = (tc_1)^D_{H_o}\ , \qquad (9.2.3)$$

that is, the upward continued terrain correction. The subscript "1" is used in (9.2.3) to indicate that the terrain correction tc_1 is not equal to the true terrain correction but is rather a terrain correction that contains errors caused by the errors in the individual predicted quantities Δg_S and $(\Delta g_S + tc)$. In other words tc_1, formed as the differences between predicted Δg_S and $(\Delta g_S + tc)$, can be called a "predicted" terrain correction. A comparison of tc_1, with the rigorously computed tc has already been given in Section 8.7. For the upward continued tc_1, i.e. $(tc_1)^D_{H_o}$ we found the statistics shown in Table 6. The statistics were found for various upward continuation distances H_o, using the 60-point upward continuation profile described in the previous section and 5'x5' tc_1 data in the 7°x9° New Mexico test area.

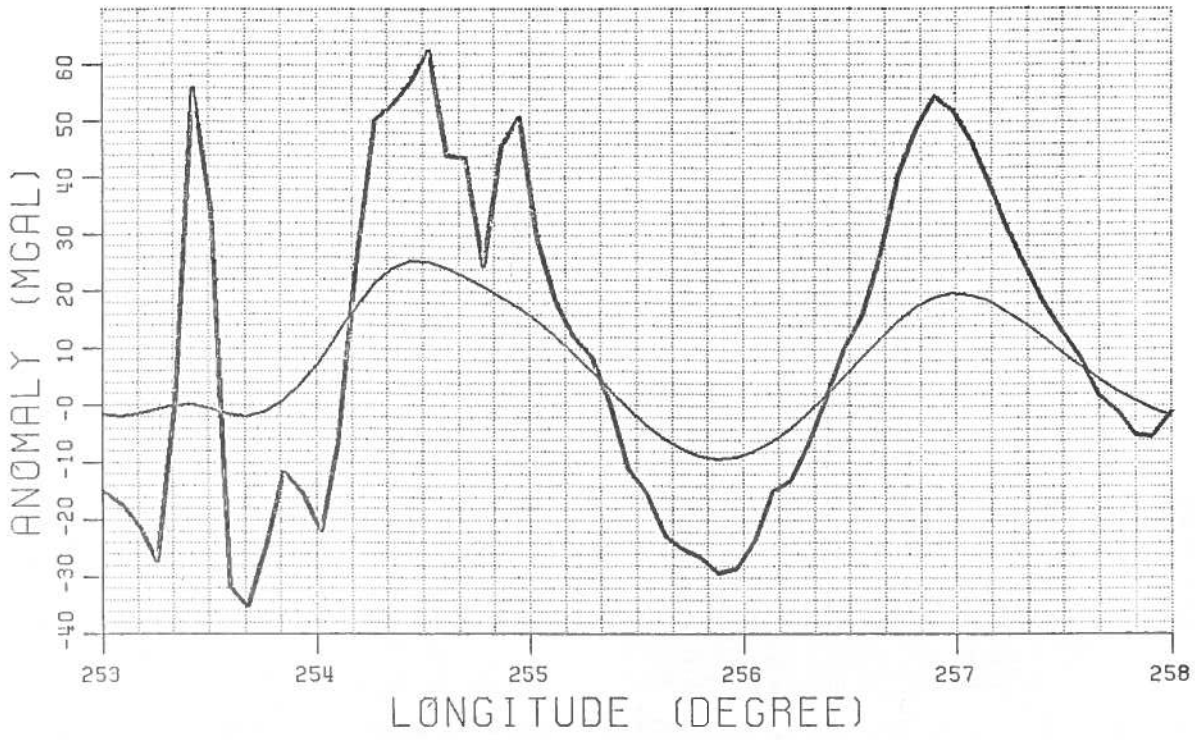

Figure 15a. Terrestrial Anomaly Profile and its Uplifted Version at 28.5 km Altitude, New Mexico Balloon Gravity Test Site. Profile Latitude = 32:5417.

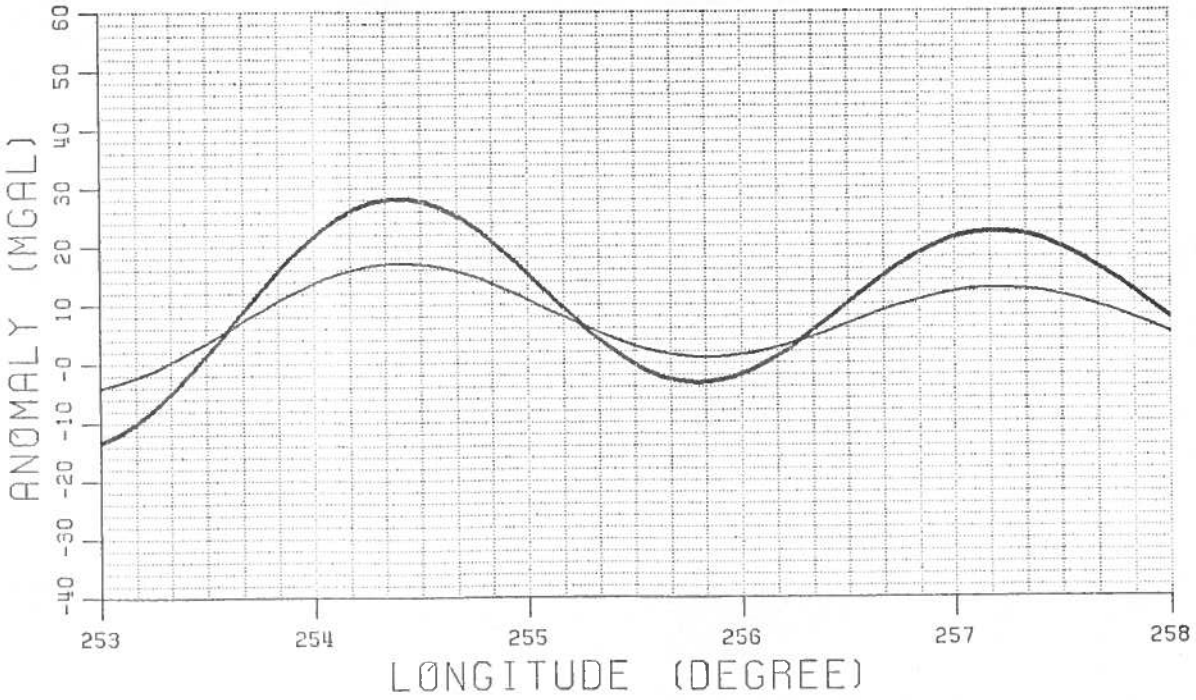

Figure 15b. Rapp-180 Anomaly Profile and its Uplifted Version at 28.5 km Altitude, New Mexico Balloon Gravity Test Site. Profile Latitude = 32:5417.

Table 6. Statistics of Upward Continued Terrain Correction, $(tc_1)^D_{H_o}$

Altitude of Upward Continuation (H_o)	Mean	Std. Dev.	RMS
28.5 km	0.38 mgal	±0.61 mgal	0.71 mgal
8.5	0.52	±0.65	0.82
3.5	0.70	±0.66	0.94
0.0	0.72	±1.16	1.32

The relatively fast decrease of standard deviation from ±1.16 mgals (H_o=0 km) to ±0.66 mgals (H_o=3.5 km), illustrates that tc_1 has energy in the very high frequency range, and this energy gets lost by attennuation at a very short upward continuation distance H_o.

As stated in Section 8.7, the terrain correction has a very short correlation length, but it also contains a weak long wavelength signal. This long wavelength signal attenuates rather slowly with altitude, and shows up in Table 6 as some significant effect (RMS 0.71 mgal) even at 28.5 km altitude.

9.2.2 Direct vs. Indirect Upward Continuation Terms

To analyze further the numerical differences between the direct and indirect upward continuation methods, let us first review what we did in the indirect method. First we performed the following split of the surface free-air anomalies:

$$\Delta g_S = \Delta g^r + \Delta g^s + \Delta g^t \qquad (9.2.4)$$

where Δg^s is the spherical harmonic contribution, Δg^t is the influence contributed by topographic masses, and Δg^r is the residual anomaly. Then to both sides of (9.2.4) we added the terrain correction tc^s of the reference topography H^s (for H^s we used a topography to spherical harmonic expansion 180):

$$(\Delta g_S + tc^s) = (\Delta g^r + tc^s) + \Delta g^s + \Delta g^t \ . \qquad (9.2.5)$$

Then we indirectly upward continued $(\Delta g_S + tc^S)$ as follows:

$$(\Delta g_S + tc^S)^I_{Ho} = (\Delta g^r + tc^S)^D_{Ho} + \Delta g^s_{Ho} + \Delta g^t_{Ho} \ , \qquad (9.2.6)$$

that is, the indirectly upward continued value is the sum of three separately upward continued terms: the <u>first term</u> is a direct upward continuation by the Poisson integral; the <u>second term</u> is an upward continuation in the spherical frequency domain; and the <u>third term</u> is an upward continuation by the prism integration of the gravitational influence of topographic masses.

In the comparison stage (Tables 3, 4, and 5) we get a good mean value agreement between the set of results from the indirect method and those from the direct method that used the terrain-corrected surface anomalies $(\Delta g_S + tc)$. The latter set of results could be <u>conceptually</u> obtained by adding tc to both sides of (9.2.4) then applying direct upward continuation:

$$(\Delta g_S + tc)^D_{Ho} = (\Delta g^r + tc)^D_{Ho} + (\Delta g^s)^D_{Ho} + (\Delta g^t)^D_{Ho} \qquad (9.2.7)$$

Therefore, to explain the numerical differences shown in Tables 3 to 5 between $(\Delta g_S + tc^S)^I_{Ho}$ and $(\Delta g_S + tc)^D_{Ho}$ we need to examine the differences between the corresponding terms on the right hand side of equations (9.2.6) and (9.2.7).

A. Comparison of First Terms

The difference Δ_I between the two terms is:

$$\Delta_I = (\Delta g^r + tc)^D_{Ho} - (\Delta g^r + tc^S)^D_{Ho} = (tc - tc^S)^D_{Ho} \qquad (9.2.8)$$

As stated in (9.2.3) we were able to obtain some sort of predicted tc denoted by tc_1. On the other hand, the determination of the quantity of tc^S was problematic in terms of computer time requirements; the set-up of Forsberg's program that we were using (Section 7) required 0.2 cpu sec. per point on our AMDAHL 470 V/6 system, and we needed at least 84x108=9072 values of tc^S. Therefore, we did not specifically perform an evaluation of $\Delta_I = (tc-tc^S)^D_{Ho}$. However, the numerical comparison of the third terms below show that on average Δ_I is canceled out by the difference (denoted by Δ_{III}) between the third terms (see equation (9.2.20)). In any case, we would expect $(tc-tc^S)^D_{Ho}$ to be small, because the long wavelength quantity tc^S will tend to cancel the long wavelengths of tc $(tc-tc^S)$; as we have seen in Table 6 only these long wavelengths (and not the very short ones) would have had the chance to filter through the upward continued value $(tc-tc^S)^D_{Ho}$.

B. Comparison of Second Terms

The second term of (9.2.7), which is $(\Delta g^S)^D_{H_o}$, uses the spherical harmonic series derived Δg^S and upward continues this using the Poisson integral. The second term in (9.2.6) conceptually uses the same quantity Δg^S but upward continues it using the spherical harmonic series, upward continuation being efffected by multiplying the spectrum of Δg^S by the factor $(R/r)^{n+2}$. To compare these terms we took the Rapp-180 field used in Section 9.1 and, with program F388 of Section 7, generated 5'x5' center-point values of Δg^S on the equatorial sphere level. These values, taken as 5'x5' mean values, covered the 7°x9° test area in New Mexico. We then upward continued the 5'x5' mean values by Poisson integration (program F499, Section 7):

$$(\Delta g^S)^D_{H_o} = \frac{H_o}{2\pi} \int\int \frac{\Delta g^S}{D_o^3}\, dxdy \qquad (9.2.9)$$

and compared the results with the rigorously upward continued values (program F388, Section 7):

$$(\Delta g^S)^D_{H_o} = \frac{kM}{a^2} \sum_{n=2}^{180} (n-1) \left[\frac{a}{a+H_o}\right]^{n+2} \sum_{m=0}^{n} (\bar{C}^*_{nm} \cos m\lambda + \bar{S}_{nm} \sin m\lambda)\, \bar{P}_{nm} (\sin \phi) \qquad (9.2.10)$$

The implementation of equation (9.2.9) was done in two versions. In the first version (called center-point kernel version) the contribution of a 5'x5' Δg^S to the upward continued value was obtained by multiplying Δg^S by the step function evaluation of the integral kernel at the center point of the 5'x5' block. In the second version (called integrated kernel version) the 5'x5' Δg^S was multiplied by the rigorously integrated value of the kernel inside the area covered by the 5'x5' block (see Rapp, 1966, for specific equations). The statistics of the differences $\Delta_{II} = (\Delta g^S)^D_{H_o} - \Delta g^S_{H_o}$ are shown in Table 7. The statistics were obtained for the same eleven presentation points of the profile used in Section 9.1. We observe that the integrated kernel implementation of equation (9.2.9) can keep the error of $(\Delta g^S)^D_{H_o}$ under 1% of true value $\Delta g^S_{H_o}$. This is true down to the lowest upward continuation altitude tested which was H_o=1 km. The center-point kernel implementation, on the other hand, can keep the relative error under 1% down to 10 km, but below 10 km the use of the integrated form is necessary since the tests show that the errors of the center-point form reach 15% at 5 km and blow up at 1 km.

To conclude, the second term $\Delta g^S_{H_o}$ of equation 9.2.6 and the second term $(\Delta g^S)^D_{H_o}$ of equation 9.2.7 are in close agreement, and therefore their difference Δ_{II} is not a major contributing factor to the differences found in Section 9.1 (Tables 3 to 5) between the direct method and the indirect method of upward continuation. However, in spite of the small differences found

between $\Delta g^S_{H_o}$ and $(\Delta g^S)^D_{H_o}$, the rigorous quantity $\Delta g^S_{H_o}$ is still advisable to use (in an indirect method setting) because its evaluation does not increase the computational burden very much and it has the advantage that in principle it uses continuous and global data whereas $(\Delta g^S)^D_{H_o}$ (which is the implicit evaluation in the direct method) uses a step function approximation of the terrestrial data and a limitation of integration to within a finite data cap.

Table 7. Statistics of the Absolute Error Incurred in Using the Poisson Integral for the Upward Continuation of the Rapp-180 Anomaly Field. 5'x5' Center Point Rapp-180 Anomalies Used as Data, Covering the 7°x9° New Mexico Test Area. Units: mgals.

Altitude of Upward Continuation	True $\Delta g^S = \Delta g^{180}$	Error (Center Point Kernel Used)	Error (Integrated Kernel Used)
H_o=30 km	Mean= 7.38	0.05	0.03
	S.D.=±6.17	±0.08	±0.07
	RMS = 9.43	0.09	0.08
10 km	9.02	0.05	0.08
	±9.83	±0.06	±0.13
	13.01	0.08	0.15
5 km	9.52	1.31	0.10
	±11.05	±1.63	±0.13
	14.20	2.03	0.16
1 km	9.94	107.46	0.03
	±12.15	±132.98	±0.03
	15.27	166.20	0.04

C. Comparison of Third Terms

Finally let us now turn to a comparison of the third terms, i.e. $\Delta g^t_{H_o}$ in (9.2.6) and $(\Delta g^t)^D_{H_o}$ in (9.2.7). The quantity $\Delta g^t_{H_o}$ is the indirect, and

$(\Delta g^t)^D_{H_o}$ the direct, upward continued value of Δg^t. In turn Δg^t is given by equation (8.7):

$$\Delta g^t = 0.1119\ (H - H^s) - (tc - tc^s)\ , \qquad (9.2.11)$$

where in our case the reference elevations H^s and terrain corrections tc^s refer to a 180-expansion of the topography. We have the indirect quantity:

$\Delta g^t_{H_o}$ found by integration of the attractions caused at the computation point by residual topographic masses subdivided into prism integration elements (see Section 7 for operational program used);

and the direct quantity:

$$(\Delta g^t)^D_{H_o} = \frac{H_o}{2\pi} \iint_A \frac{0.1119\ (H - H^s) - (tc - tc^s)}{D_o^3}\ dxdy \qquad (9.2.13)$$

As we indicated under equation (9.2.8) we did not evaluate tc^s because of computer time limitations. Therefore, we also did not evaluate (9.2.13) where tc^s appears. However, tests of interest could still be conducted by dropping some terms in (9.2.13); we used two versions:

$$(\Delta g^t_1)^D_{H_o} = \frac{H_o}{2\pi} \iint_A \frac{\Delta g^t_1}{D_o^3}\ dxdy \qquad (9.2.14a)$$

with $\Delta g^t_1 = \Delta g^t - tc^s = 0.1119\ (H - H^s) - tc$; (9.2.14b)

and

$$(\Delta g^t_2)^D_{H_o} = \frac{H_o}{2\pi} \iint_A \frac{\Delta g^t_2}{D_o^3}\ dxdy \qquad (9.2.15a)$$

with $\Delta g^t_2 = \Delta g^t + (tc - tc^s) = 0.1119\ (H - H^s)$ (9.2.15b)

Using our 5'x5' data in New Mexico, various upward continuation distances (H_o=28.5, 8.5, 3.5 km), and the eleven presentation points of Section 9.1, we compared (9.2.14) and (9.2.15) against (9.2.12) and obtained the statistics shown in Table 8. The statistics are given for the results of (9.2.12) and for the

differences: [equation (9.2.14) or (9.2.15)] minus [result of (9.2.12)]. We should note that in view of the results of Table 7 we used the integrated kernel evaluation for H_o = 3.5 km, and simply used the center point kernel evaluation for H_o = 8.5 and H_o = 28.5 km to implement (9.2.14) and (9.2.15).

Table 8. Statistics of $\Delta g^t_{H_o}$, and of the Differences $((\Delta g^t_1)^D_{H_o} - \Delta g^t_{H_o})$ and $((\Delta g^t_2)^D_{H_o} - \Delta g^t_{H_o})$, in mgals. See equations (9.2.14), (9.2.15), and (9.2.12).

Altitude of Upward Continuation	(1) $\Delta g^t_{H_o}$ (9.2.12)	(2) $(\Delta g^t_1)^D_{H_o} - \Delta g^t_{H_o}$ (9.2.14)−(9.2.12)	(3) $(\Delta g^t_2)^D_{H_o} - \Delta g^t_{H_o}$ (9.2.15)−(9.2.12)
H_o=28.5 km	Mean=−3.11	−0.63	−0.02
	S.D.=±4.74	±0.51	±0.24
	RMS = 5.49	0.80	0.23
8.5 km	−3.71	−0.64	0.06
	±11.24	±0.62	±0.58
	11.34	0.87	0.55
3.5 km	−3.39	−1.58	0.08
	±15.57	±1.22	±1.04
	15.23	1.30	0.99

The small mean differences in Table 8, column 3 imply that numerically:

$$M\{\Delta g^t_{H_o}\} = M\{(\Delta g^t_2)^D_{H_o}\} \ , \qquad (9.2.16)$$

where M denotes the straight averaging operator, operating on the test point samples. Therefore, for the difference (let us denote this difference by Δ_{III}) between the third terms (9.2.12) and (9.2.13) we have the approximation:

$$M\{\Delta_{III}\} = M\{(\Delta g^t)^D_{H_o} - \Delta g^t_{H_o}\} \cong M\{(\Delta g^t)^D_{H_o} - (\Delta g^t_2)^D_{H_o}\} \ . \qquad (9.2.17)$$

By virtue of (9.2.15b),

$$M\{(\Delta g^t)^D_{H_o} - (\Delta g_2^t)^D_{H_o}\} = M\{-(tc - tc^{D_s})_{H_o}\} \qquad (9.2.18)$$

Combining ((9.2.17) and (9.2.18) we finally have the approximate mean difference between the <u>third</u> terms $(\Delta g^t)^D_{H_o}$ and $\Delta g^t_{H_o}$:

$$M\{\Delta_{III}\} = M\{(\Delta g^t)^D_{H_o} - \Delta g^t_{H_o}\} \cong M\{-(tc - tc^s)^D_{H_o}\} \qquad (9.2.19)$$

Combining (9.2.19) and (9.2.8) we have:

$$M\{\Delta_{III}\} \cong -M\{\Delta_I\}, \text{ or}$$

$$M\{\Delta_I + \Delta_{III}\} \cong 0. \qquad (9.2.20)$$

From the discussions related to Table 7 we also learned that $M\{\Delta_{II}\} \cong 0$, and therefore the mean of the total difference $\Delta = \Delta_I + \Delta_{II} + \Delta_{III}$ is small, i.e.,

$$M\{\Delta\} = M\{\Delta_I + \Delta_{II} + \Delta_{III}\} \cong 0 \qquad (9.2.21)$$

Equation (9.2.21) repeats the results of Tables 3, 4, and 5, namely, that the mean difference between the indirect method, on the one hand, and the direct method that uses terrain corrected surface anomalies (Δg_s + tc), on the other hand, is small.

9.2.3 Sensitivity of Anomaly Fields to Changes in Upward Continuation Distance H_o

As mentioned in Section 3.3 (A) there is an uncertainty as to what value of upward continuation distance H_o to use in the Poisson integral. Recall that H_o is theoretically the vertical distance between the computation point P in space and the level surface to which the anomaly data are assumed to refer. The uncertainty in H_o is caused by the fact that the given surface anomaly data refer to a varying level surface, rather than to a single level surface. Even in the case when the terrain correction is applied to implement an approximate data reduction to a level surface, the position of the final reference level is uncertain (see Section 3.3 (A)). In our final procedures we simply assume that the reference level coincides with the mean elevation surface in the area covered by our anomaly data. The error in upward continuation distance H_o that results from this assumption is expected to be

related to the deviation of the actual topography from the mean elevations surface. In this section we give a feeling for the sensitivity of our results to the choice of value for H_o.

The mean elevation in our New Mexico study area is about 1.5 km. For sensitivity analysis we compared upward continuation results for the case when the reference level for the data is assumed to be at the 1.5 km level, and for the case when this level is assumed to be at the geoid (i.e., the 0 km-level). The difference between the two cases is, therefore, the use of upward continuation distances H_o that differ by 1.5 km. We performed our comparisons using the eleven presentation points of the profile in Section 9.1. The statistics of the comparisons, for various values of H_o and various types of anomaly fields, are shown in Table 9.

Table 9 says, for example, that in the direct method that uses the total field $(\Delta g_B + tc)^D{}_{H_o}$, (see (3.3.2)), an uncertainty of 1.5 km in H_o for H_o=30 km directly causes an uncertainty of 0.43 mgal (3.8% of computed value) in the upward continued anomaly. If data reductions are used, as in the indirect method, such that only the residual part $(\Delta g^r + tc^s)^D{}_{H_o}$ is used (see (3.3.14)), the uncertainty reduces to 0.19 mgal (4.2% of computed residual value). Table 9 also shows that the residual topographic field $\Delta g^t{}_{H_o}$ (see (3.3.16)) is the part of the total field that is most sensitive to changes in H_o, the reason being that Δg^t contains the high frequency part of the field. This last sensitivity does not introduce any error into the computations, since $\Delta g^t{}_{H_o}$ has no problem associated with defining an "upward continuation distance". Finally, Table 9 also shows that the spherical harmonic (long wavelength) component of the field is the least sensitive to altitude changes.

Table 9. Sensitivity of Sample Profile Anomalies to a 1.5 km Change in Upward Continuation Distance H_o, for Various Values of H_o and Various Types of Anomaly Fields.*

Upward Continuation Distance	Total Field $(\Delta g_s + tc)^D_{H_o}$ (3.3.2)	Residual Field $(\Delta g^s + tc)^D_{H_o}$ (3.3.14)	Spherical Harmonic Field $\Delta g^s_{H_o}$ (3.3.15)	Residual Topographic Field $\Delta g^t_{H_o}$ (3.3.16)
H_o = 30 km	11.32	4.49	9.65	5.49
	0.43	0.19	0.24	0.27
	3.8%	4.2%	2.5%	4.9%
H_o = 10 km	19.92	8.02	13.35	11.34
	1.35	0.51	0.37	1.14
	6.8%	6.4%	2.8%	10.1%
H_o = 5 km	23.70	9.41	14.59	15.23
	2.15	0.73	0.41	2.29
	9.1%	7.8%	2.8%	15.0%

*Key to entries in table for each box:

(1) RMS value of profile anomalies at height H_o (mgals).

(2) RMS change in profile anomalies when height H_o is reduced by 1.5 km (mgals).

(3) Percentage ratio: (2) ÷ (1).

9.3 Fourier Computations

From the numerical point of view it is very attractive to use frequency domain processing. The theoretical equations are summarized in Chapter 2.4. Here we will show how the Fourier Transform principle can be utilized in practice to upward continue the gravity anomaly field from one level surface to another. It should be stressed here that the Fourier technique requires exactly the same assumptions as the flat Earth Poisson's integral. After all these two procedures give the unique solutions to the same Dirichlet problem for half space - one in spatial the other in frequency domain. Fourier technique is much cheaper in computational stage but requires the special care in controlling the edge effects. As our balloon experiment shows, these effects are negligible far from the edges where the upward continued value was computed.

In practice the evaluation of upward continuation operator is done by means of digital Fourier transformation defined by (Robinson and Silvia, 1981, ch. 3.3). (Notice that we define the forward transform with a + sign in the exponent).

$$F(m_x, m_y) = \sum_{n_x=0}^{N_x-1} \sum_{n_y=0}^{N_y-1} f(n_x, n_y)\, e^{i2\pi\left(\frac{n_x m_x}{N_x} + \frac{n_y m_y}{N_y}\right)} \qquad (9.3.1a)$$

$$f(n_x, n_y) = \frac{1}{N_x N_y} \sum_{m_x=0}^{N_x-1} \sum_{m_y=0}^{N_y-1} F(m_x, m_y)\, e^{-i2\pi\left(\frac{n_x m_x}{N_x} + \frac{n_y m_y}{N_y}\right)} \qquad (9.3.1b)$$

$n_x, m_x \in \{0, 1, \ldots, N_x-1\}$

$n_y, m_y \in \{0, 1, \ldots, N_y-1\}$

If we choose N_x, N_y to be powers of 2 we can use the Fast Fourier Transform algorithm to evaluate (9.3.1).

The integers n_x, n_y, m_x, m_y are defined by:

$$x = n_x \Delta x \qquad y = n_y \Delta y$$

$$k_x = m_x \Delta f_x \qquad k_y = m_y \Delta f_y \qquad (9.3.2)$$

$$\Delta f_x = 1/(N_x \Delta x) \qquad \Delta f_y = 1/(N_y \Delta y)$$

where the spatial increments are related to angular increments by

$$\Delta x = R \cos \phi \, \Delta\lambda \qquad \text{(E-W direction)}$$
$$\Delta y = R \, \Delta\phi \qquad \text{(N-S direction)} \tag{9.3.3}$$

Here the regular spatial grid intervals Δx and Δy are computed using the mean latitude $\phi=\bar{\phi}=32.5°$ of the data location. The original data are considered here as the discrete point-measurements of the gravity anomaly field of the surface of the earth using uniform angular spacing $\Delta\phi=\Delta\lambda=5'$. This uniform spacing on the sphere under transformation (9.3.3) becomes strictly speaking non-uniform on the plane due to meridian convergence. Using a fixed value of ϕ in (9.3.3) introduces some distortions to the original spacial distributions of the data. Our study indicates that this distortion produces an essentially negligible effect on the results due to the use of rather fine 5'x5' grid defined on a relatively small portion of the sphere (7°x9° block). In other words the flat earth approximation being valid for the original Poisson space processing of data is also valid for its frequency implementation, at least for small regions as discussed in this report.

Summary of frequency domain digital upward continuation procedures:

1. compute Δx and Δy; (9.3.3)

2. transform the data to the frequency domain as indicated by (2.4.5) using (9.3.1a);

3. multiply the transformed data in the frequency domain by the transfer function A (2.4.6)

4. invert the result back to space domain as indicated by (2.4.7) using (9.3.1b).

The above procedure was applied to our 7°x9° New Mexico study area, to upward continue the entire 84x109 grid of 5'x5' mean Faye anomalies (see Section 8.7). The uplifted grid for an upward continuation distance of 28.5 km is contoured in Figure 16, with a contour interval of 5 mgals. This figure should be compared with Figure 17 in which the corresponding grid from the Rapp-180 field is contoured. The long wave agreement between Figures 16 and 17 is evident, with Figure 16 expectedly showing more detail because of the use of high frequency terrestrial data.

For the Fourier upward continuation we used only a simplified procedure including no windowing of the data or any other regularization routine in frequency domain (i.e., no specialized filters used). We found the results produced by this simplified procedure in satisfactory agreement with the space domain processing of original $\Delta g+tc$ field by means of Poisson's integral. The difference in results on the order of 0.15 mgal at 30 km flight altitude can be associated with the differences in numerical implementation. We employed this

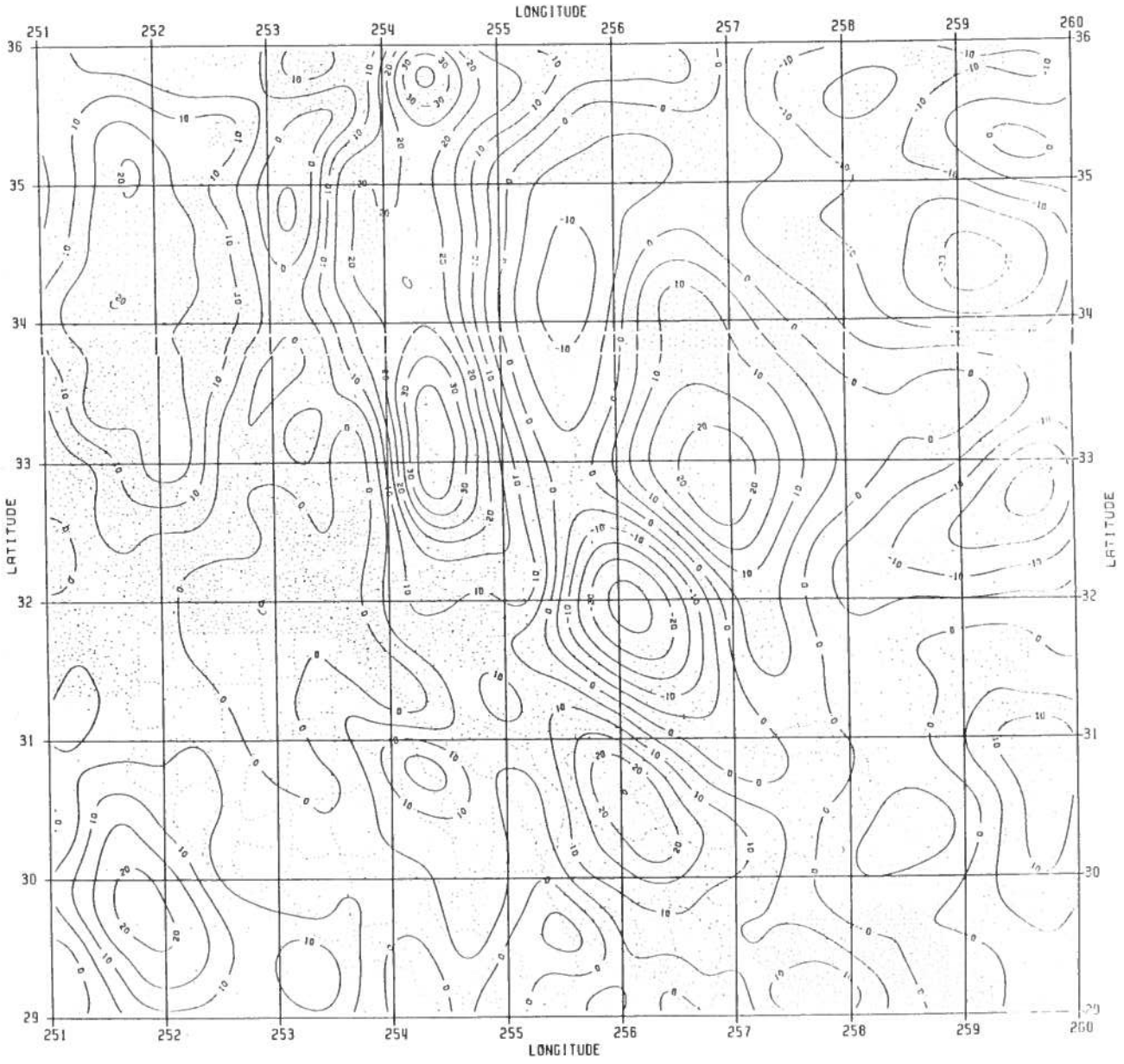

Figure 16. Upward Continued Faye Anomalies Using Fast Fourier Upward Continuation, New Mexico Balloon Gravity Test Site.
C.I. = 5 mgals; Upward Continuation Distance = 28.5 km.

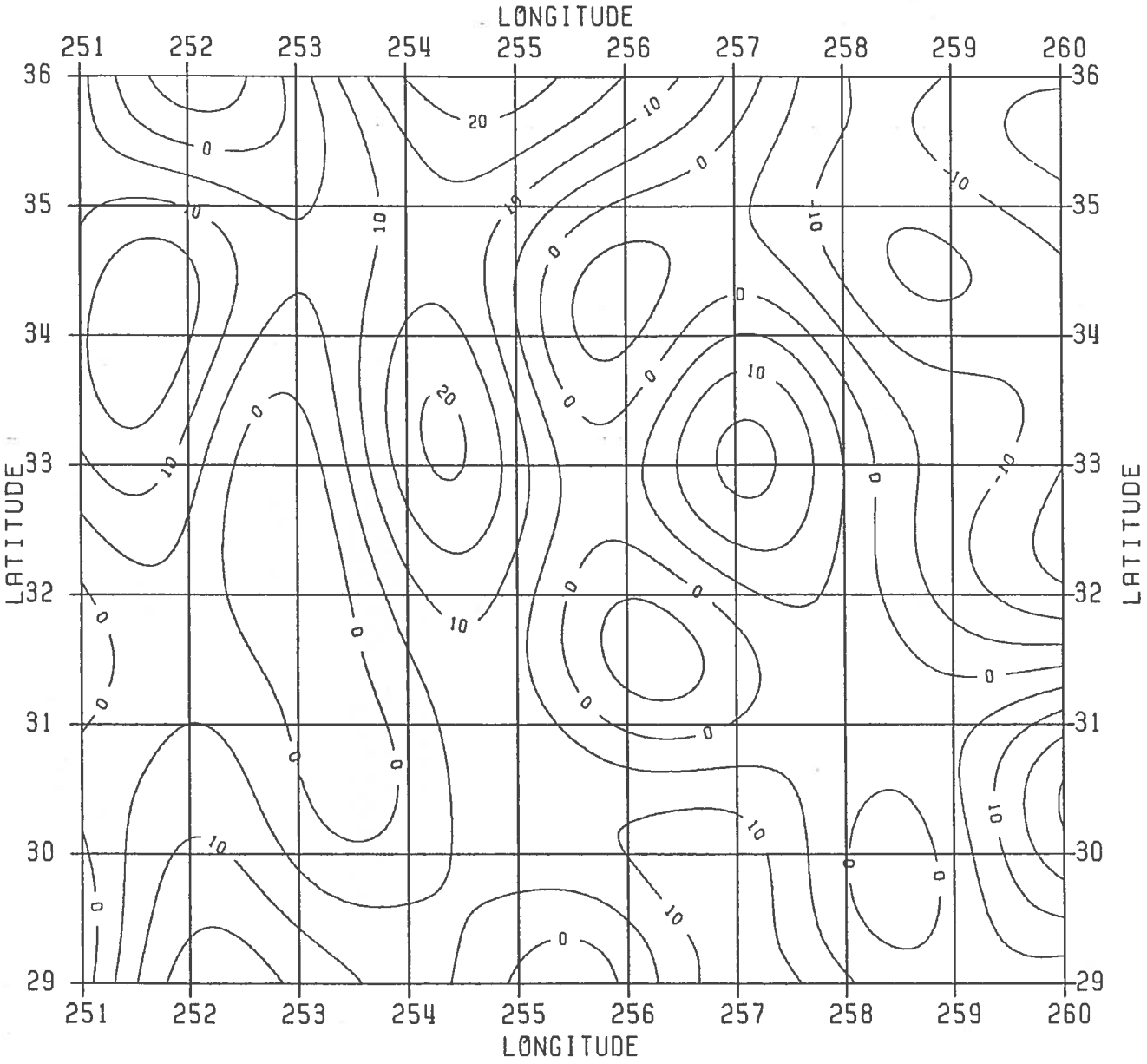

Figure 17. **Rapp-180 Gravity Anomalies at 28.5 km Altitude, New Mexico Balloon Gravity Test Site. C.I. = 5 mgals.**

procedure using the Fast Fourier Transform routine modified from Claerbout (1976, p. 12). The technique was tested using the original terrain corrected free-air anomaly field. The results were compared along E-W test profile with the results of the Poisson's integral operating on the same field.

The RMS difference over the test profile between those two results were 0.12 mgal for the upward continuation distance of 28.5 km. For the upward continuation distance of 8.5 km the RMS difference along the same test profile was 0.32 mgal.

The magnitude of the above differences is in fact on the order of differences between the indirect and direct space domain procedures already discussed. This indicates that the Fourier method can prove to be competetive with the one-step space domain processing (direct method) with respect to accuracy of the results. It can be recommended for fast processing of large volumes of gridded data to produce the image of the field (in a gridded form) at any level surface above the data surface. To get the values at any location outside the grid point the interpolation has to be performed which is a valid routine provided the original data were gridded in accordance with the sampling theorem (Robinson and M.T. Silvia, 1981, ch. 2.6).

On the theoretical side it provides an elegant uniform treatment of all frequencies present in the original signal. On the practical side, it provides a fast numerical procedure to transform the data upward from one level surface to another. As far as accuracy is concerned the edge effects (inherent in Fourier techniques) should be treated with care by appropriate windowing routine or (if possible) the region with data should cover enough grounds surrounding the point of interest.

10. Applications to Balloon Gravity Project

The theory outlined in this report was applied to the Balloon Gravity Project coordinated by the Air Force Geophysics Laboratory, Bedford, Massachusetts. The experiment took place in New Mexico and was designed to test the theory, procedures and instruments used for both the measurements and the prediction of gravity in space.

The comparisons between the observed and predicted gravity will give insight into the accuracy and performance of the theories and techniques of gravity recovery in space which are in the operational stage today. It is also a test of the accuracy and performance of the balloon-borne instruments and techniques that are used today for the measurements of the external gravity field.

In this section some technicalities of the actual gravity prediction procedure used for the Balloon Project are given. The method we chose for the final application is the indirect method described in Section 3.3. To repeat briefly, the rationale behind this method is to extract the high frequency variation in the original surface gravity. Here by high frequency variation we understand the topographic effects (irregular geometry of the terrain plus tc correction). As we have seen in the previous chapters this high frequency component of the gravity signal cannot be conceptually nor practically converted downward to the Poisson's spherical geometry so we did not try to do this. Instead we immediately upward continued this high frequency component (right from the original surface where it was defined) up to the balloon's attitude using partially the ideas of equivalent source method as implemented in the prism integration of topographic effects.

After the removal of this short-wavelength variations, the remaining regular portion of the gravity field was converted downward (formally) to the Poisson's spherical geometry (see Section 3.3). Then the long-wavelength or global portion of this signal is upward continued in the frequency domain (using spherical harmonics) and the mid-frequency portion is upward continued by solving the usual Dirichlet problem for half space (in planar approximation) by means of Poisson's integral.

In the actual computation we used the FORTRAN implementation of the Poisson's integral procedure as described in (Rapp, February 1966). The routine was run using the gridded mid-frequency portion of the gravity anomaly signal as discussed in Section 3.3.

10.1 Preparation of the Balloon Tracking Data for Upward Continuation Procedure

The balloon tracking data were sent on the magnetic tape dated 4 May 1984. The tape name is DUCKY Ia Radar Tracking Data. The tape contained four files, with the float portion of the experiment contained as part of file #3.

The positions of the balloon during the experiment were provided in the form of geodetic coordinates (ϕ, λ, h) with respect to the WGS72 ellipsoid (see Table 10).

The original tape contained 462,200 positions. The original records were parameterized by the time of measurements. On Figure 18 we show the spatial location of the balloon's trajectory. The average spacing of original tracking data for the float portion of the experiment was approximately 0.6 m on the ground. At the first step we reduced the number of data-points spatially by choosing only the clusters of 10 original records spaced every 30" angular distance apart from each other. During this step the false data records were rejected and the remaining set containing 3160 records was checked for blunders. The false data records on the original tape occurred at the end of each file due to technical reasons.

Since we were primarily interested in the flight altitude portion of the experiment (29-30 km altitude) it was sufficient to select only 1 data point every 2' spacing (in angular distance) along the track. The 2' spacing is sufficient for all interpolation purposes at flight elevation because the anomalous gravity field is already very smooth at that altitude (see Figure 15a, for example). The resultant data-set contained 31 values equally spaced in 2' intervals covering the flight portion of the balloon's trajectory, that is the portion of the original data tape (file #3) which falls in the time interval <57445.95, 66955.95>. The time is UTC time in seconds. In the computational stage of this project we used the time only as a convenient parameter to locate the data on tape.

10.2 Reference Systems Used in the Balloon Project

In this section we give the summary of reference systems and conversions used at the stage of data preparation for the balloon project. The geodetic coordinates (ϕ, λ, h) of the balloon positions provided on balloon tape were given with respect to WGS72. The terrestrial gravity anomaly field that we used in this project was given in the GRS67 system. The spherical harmonic expansion of the global gravity field up to degree 180 was assumed to refer to GRS80 (Rapp, 1981) (referred to as Rapp 180 field). The ellipsoid parameters for the reference systems used are given in Table 10.

Ellipsoid	a [m]	1/f
WGS72	6378135	298.26
GRS67	6378160	298.2471674273
GRS80	6378137	298.257222101

Table 10. Parameters of the reference ellipsoids involved in the data preparation for the balloon project.

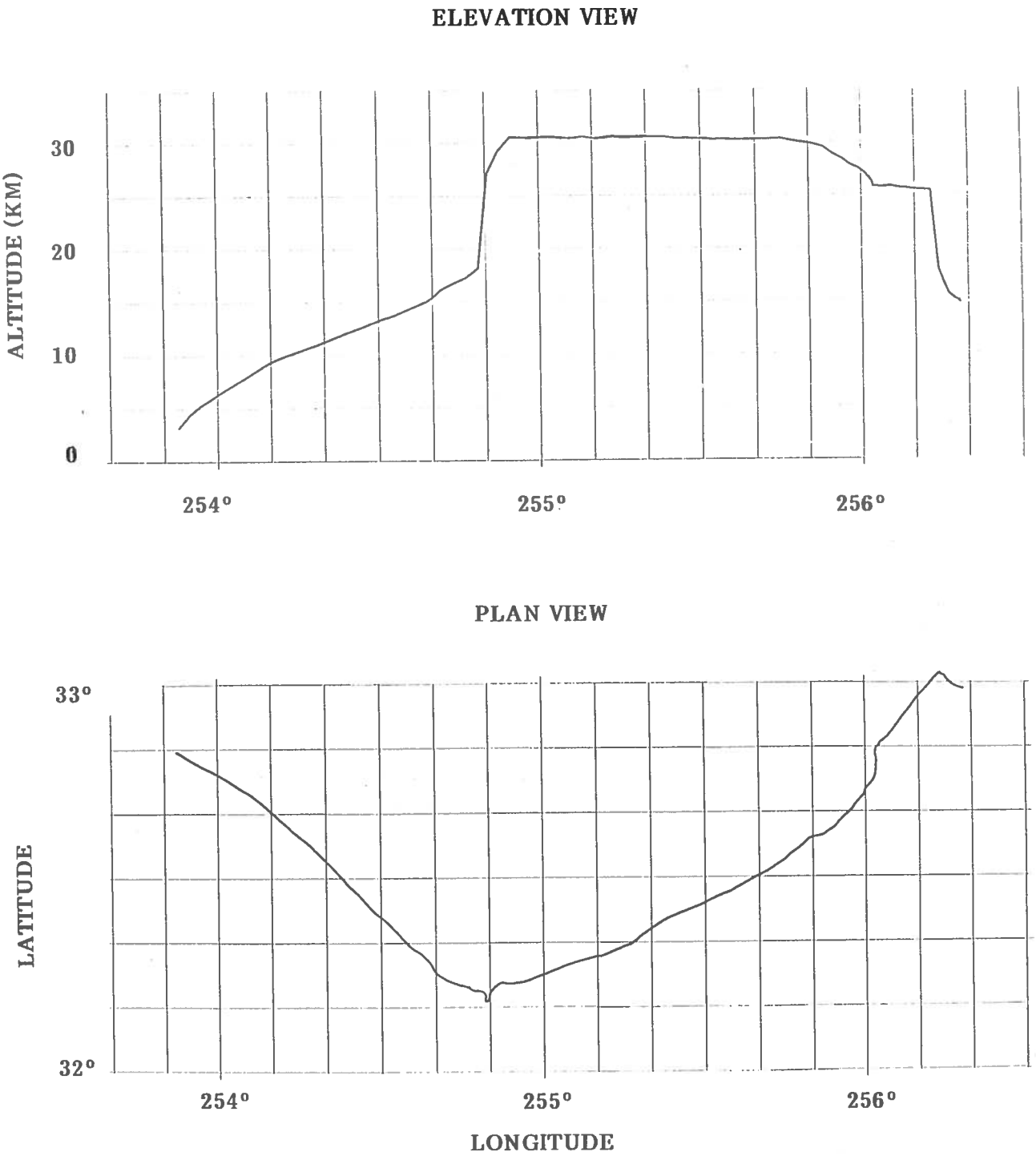

Figure 18. Plan View and Elevation View of the New Mexico Balloon-Borne Gravity Flights.

Now we will summarize the conversions used for upward continuation of gravity anomalies. Since the original gravity anomaly field that we used in our project refers to GRS67 ellipsoid we decided to convert the given geometric heights h_{WGS72} that refer to the WGS72 ellipsoid to the normal heights H^*_{GRS67} that refer to the GRS67 ellipsoid.

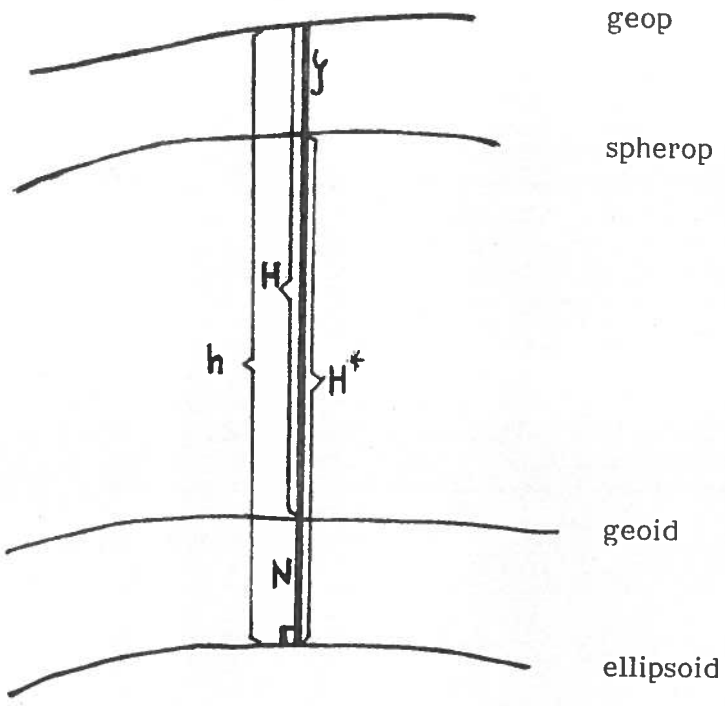

Figure 19. The Spatial Relationship Between Selected Gravimetric Quantities

From Figure 19 we have the relation:

$$H^*_{GRS67} = H + (N - \zeta)_{GRS67} \qquad (10.2.1)$$

where ζ is the geop-spherop separation or height anomaly at balloon's altitude.

Instead of the difference $(N-\zeta)_{GRS67}$ we will actually use $(N-\zeta)_{GRS80}$ in the approximate relation:

$$H^*_{GRS67} \cong H + (N - \zeta)_{GRS80} \qquad (10.2.2)$$

For the orthometric height H appearing in (10.2.2) we can write the relation (see Figure 19):

$$H = h_{GRS80} - N_{GRS80} \qquad (10.2.3)$$

To get h_{GRS80} from a given h_{WGS72} we implement the well known formulas of geometric geodesy (Rapp, 1984, Geometric Geodesy Notes, Vol. 1, pp. 121-122) in the following procedure

$$\left.\begin{array}{ll} \text{input:} & h_{WGS72},\ \phi \\ \text{compute:} & z_{WGS72} = (N(1 - e^2) + h)\sin\phi \quad \text{using WGS72 constants} \\ \text{convert:} & z_{GRS80} = z_{WGS72} + \Delta z \cong z_{WGS72} \\ & \text{here we set the origin shift } \Delta Z \text{ to zero so that the ellipsoid WGS72 and GRS80 have a common center} \\ \text{compute:} & h_{GRS80} = \dfrac{z}{\sin\phi} - N + e^2 N \quad \text{using GRS80 constants} \end{array}\right\} \qquad (10.2.4)$$

where $N = a/\sqrt{1-e^2\sin^2\phi}$, $e^2 = 2f - f^2$.

In practice, instead of converting each data point separately using the above formulas, we applied a single common constant $\Delta h = -1.66$ m to each height given in the WGS72 system:

$$h_{GRS80} = h_{WGS72} + \Delta h \qquad (10.2.5)$$

where the particular value of $\Delta h = h_{GRS80} - h_{WGS72} = -1.66$ m has been evaluated by the sequence of equations (10.2.4) (starting from a nominal h_{WGS72} and computing the equivalent h_{GRS80}) using the mean latitude of the balloons trajectory (32.40°) and the mean altitude of the flight section of the experiment (30 km).

Using (10.2.3) and (10.2.5) we can write (10.2.2) in the final form:

$$H^*_{GRS67} \cong (h_{WGS72} + \Delta h) - \zeta_{GRS80} \qquad (10.2.6)$$

In the actual implementation of equation (10.2.6) we used the Rapp 180 field (based on the spherical harmonic expansion of gravity potential up to degree

and order 180) to generate the required values of height anomalies ζ_{GRS80}. Due to the smoothness of the height anomaly field at flight altitude a single constant mean value of ζ_{GRS80} = -23 m (±0.26 m) was used in formula (10.2.6).

The normal heights (10.2.6) were subsequently used in the FORTRAN subroutine for Normal Field Computations (Rapp, 1966) (see also Section 2.6) to generate normal gravity at the exact balloon positions. The routine was run using GRS67 constants.

10.3 Upward Continuation Results

The upward continuation procedure of gravity anomaly described in this report was actually applied only to the 31 points selected in Section 10.1. The results are shown in Table 11. The position of each point is defined in columns 1 to 4: (1) time tag in the tracking record; (2) latitude; (3) longitude; and (4) height above the WGS72 ellipsoid. Columns 5 to 7 give the upward continued anomaly contribution from: (5) residual defined Bouguer anomalies; (6) spherical harmonic anomalies; and (7) topographic anomalies. Columns 5, 6, 7 were summed to form column 8, which is the total upward continued anomaly from the indirect method of upward continuation. Column 9 gives the normal gravity to be added to the upward continued anomaly to produce the first model for measured gravity at the space point. Columns (10) and (11) give the upward continued anomalies resulting from the direct method of upward continuation of surface anomalies using terrain-uncorrected and terrain-corrected surface anomalies, respectively. Columns (12) and (13) give the errors of columns (10) and (11) relative to the expectedly more rigorous indirect method (column 8) of upward continuation. The mean error and standard deviation of errors are as follows:

	Error of Direct Method without use of tc (col. 12)	Error of Direct Method with use of tc (col. 13)
mean error	-0.51 mgal	0.14 mgal
s.d. error	±0.35 mgal	±0.18 mgal

In agreement with earlier results, we see an improvement with the use of terrain correction in the direct method.

10.4 Interpolation of the Results at Altitude

In the last step the upward continued values were interpolated at all original data-records on the balloon tape that fell in the time interval covering the flight portion of the experiment (190,201 data-points). Only results from the indirect upward continuation method were used (Table 11, Col. 8.). The actual interpolation was done using the one-dimensional cubic spline routine (subroutines SPLINE and SEVAL, Forsythe et al., 1977) applied to the flight sequence which has been parameterized with longitude only.

Table 11. Gravity Anomaly and Normal Gravity Upward Continuation Results at 31 Balloon Points, New Mexico Area. Units: mgals.

(1)	(2)	(3)	(4)	(5)	(6)	(7)	(8)	(9)	(10)	(11)	(12)	(13)
57445.95	32.23065	254.87090	29092.55	5.34	11.24	-3.66	12.91	970577.50	11.82	12.74	-1.09	-0.17
57762.95	32.22806	254.91080	30501.66	5.06	10.46	-2.62	12.90	970148.30	11.81	12.75	-1.09	-0.15
58063.95	32.23602	254.94970	30452.27	4.85	9.93	-1.57	13.21	970164.00	12.14	13.10	-1.07	-0.11
58382.95	32.24597	254.98790	30497.05	4.57	9.40	-0.47	13.50	970151.20	12.46	13.43	-1.04	-0.07
58711.95	32.25821	255.02540	30512.55	4.27	8.87	0.58	13.72	970147.50	12.71	13.69	-1.01	-0.03
59032.95	32.27126	255.06230	30489.45	3.96	8.34	1.48	13.78	970155.50	12.80	13.78	-0.98	0.00
59340.95	32.28166	255.10040	30362.62	3.65	7.76	2.17	13.58	970195.00	12.68	13.65	-0.90	0.07
59626.45	32.29117	255.13870	30512.57	3.32	7.14	2.51	12.96	970150.10	12.15	13.10	-0.81	0.14
59933.95	32.29828	255.17810	30332.64	3.00	6.51	2.64	12.15	970205.40	11.43	12.36	-0.72	0.21
60263.45	32.31088	255.21510	30514.49	2.66	5.94	2.30	10.90	970151.10	10.28	11.17	-0.62	0.27
60610.95	32.32318	255.25240	30522.17	2.34	5.37	1.73	9.44	970149.70	8.92	9.78	-0.52	0.34
60955.45	32.34001	255.28680	30525.83	2.08	4.90	0.89	7.87	970150.00	7.43	8.24	-0.44	0.37
61256.95	32.35934	255.31970	30551.45	1.88	4.48	-0.13	6.23	970143.80	5.86	6.63	-0.37	0.40
61569.45	32.37817	255.35310	30488.89	1.71	4.06	-1.23	4.54	970164.30	4.24	4.95	-0.30	0.41
61869.45	32.39508	255.38760	30487.72	1.53	3.63	-2.33	2.83	970166.10	2.55	3.22	-0.28	0.39
62181.95	32.40819	255.42460	30337.99	1.30	3.16	-3.42	1.05	970212.70	0.79	1.42	-0.26	0.37
62465.95	32.42084	255.46190	30375.28	1.05	2.73	-4.45	-0.67	970202.40	-0.93	-0.33	-0.26	0.34
62758.95	32.43474	255.49850	30302.17	0.83	2.34	-5.46	-2.30	970225.80	-2.53	-1.98	-0.23	0.32
63044.45	32.44913	255.53490	30259.73	0.63	2.00	-6.39	-3.77	970239.80	-4.00	-3.48	-0.23	0.29
63343.95	32.46223	255.57180	30231.00	0.41	1.69	-7.21	-5.11	970249.60	-5.35	-4.86	-0.24	0.25
63627.95	32.47775	255.60730	30229.17	0.27	1.46	-7.92	-6.19	970251.50	-6.43	-5.97	-0.24	0.22
63940.95	32.49326	255.64290	30209.40	0.16	1.27	-8.50	-7.06	970258.80	-7.31	-6.88	-0.25	0.18
64256.95	32.50900	255.67830	30239.82	0.10	1.14	-8.91	-7.67	970250.80	-7.93	-7.53	-0.26	0.14
64615.45	32.52541	255.71340	30251.17	0.09	1.06	-9.16	-8.01	970248.60	-8.29	-7.91	-0.28	0.10
64952.45	32.54475	255.74590	30300.75	0.24	1.06	-9.28	-7.99	970235.20	-8.27	-7.91	-0.28	0.08
65276.45	32.56645	255.77680	30127.15	0.52	1.11	-9.33	-7.70	970289.80	-8.00	-7.67	-0.30	0.03
65606.44	32.58788	255.80770	29976.55	0.84	1.20	-9.24	-7.20	970337.40	-7.50	-7.19	-0.30	0.01
65930.44	32.60358	255.84270	29790.57	1.01	1.29	-9.01	-6.71	970395.30	-7.02	-6.72	-0.31	-0.01
66226.44	32.61519	255.87990	29491.52	1.09	1.40	-8.70	-6.21	970487.30	-6.51	-6.23	-0.30	-0.02
66630.94	32.63475	255.91220	28765.83	1.50	1.58	-8.38	-5.30	970709.80	-5.61	-5.34	-0.31	-0.04
66955.94	32.65994	255.93890	28397.28	2.15	1.83	-7.93	-3.95	970824.10	-4.24	-4.00	-0.29	-0.05

1. TIME (SEC.)
2. LATITUDE (DEG.)
3. LONGITUDE (DEG.)
4. h_{WGS72}(m)
5. $(\Delta g^r + tc^s)^D_{H_o}$, eq. (3.3.14)
6. $\Delta g^s_{H_o}$, eq. (3.3.15)
7. $\Delta g^t_{H_o}$, eq. (3.3.16)
8. $(\Delta g_s + tc^s)^I_{H_o}$ = (5)+(6)+(7)
9. γ_{H_o}
10. $(\Delta g_s)^D_{H_o}$, eq. (3.3.1)
11. $(\Delta g_s + tc)^D_{H_o}$, eq. (3.3.2)
12. $(\Delta g_s)^D_{H_o} - (\Delta g_s + tc^s)^I_{H_o}$
13. $(\Delta g_s + tc)^D_{H_o} - (\Delta g_s + tc^s)^I_{H_o}$

To check the internal accuracy of this interpolation process we removed every other record out from the 31 "master" points and treated the remaining 16 points as the new knots in the spline interpolation procedure. In this way we interpolated values at the removed knots and compared with the "true" values obtained directly from the upward continuation process. The differences were on the order of 0.01 mgal in gravity anomaly.

For the normal gravity computation the chosen 31 grid points were not dense enough to properly recover the normal gravity at flight altitude, mostly due to the vertical gradient of normal gravity. It was evident especially at both ends of the flight portion of the experiment where the balloon changes altitude very rapidly. Therefore we decided not to interpolate normal gravity but to compute it rigorously at every observational point (see Section 2.6).

10.5 Propagation of Positional Errors

On the original balloon tape the positional accuracy of the balloon in all three directions were provided with each data-record. The average accuracy of the 31 points selected for actual upward continuation was on the order of 2 m in all x, y and z coordinates.

Considering that the largest horizontal gradient of the actual computed anomalous gravity field along the flight portion of the balloon trajectory is about 0.0006 mgal/m (this is the actual gradient of the computed results for the balloon project), we assess the maximal error due to the 2 m uncertainty in the horizontal position of the balloon to be 0.0012 mgal in gravity anomaly and 0.0011 mgal in normal gravity (for normal gravity computation, only the uncertainty in N-S direction must be considered).

The uncertainties in altitudes will also produce uncertainties in the computed components of the gravity field. From Table 9 we learn that the vertical gradient of the actual Δg field at 30 km flight altitude is about 0.0003 mgal/m. Therefore the 2 m error in the balloon vertical position will show up as the uncertainty of about 0.0006 mgal in the computed Δg field. Similarly the vertical gradient of normal gravity of 0.3086 mgal/m (Rapp 1982, p. 8) will cause the uncertainty in the computed normal gravity of about 0.6 mgal (due to the 2 m uncertainty in the altitude).

Also, the error in geoid undulation (more precisely in height anomalies) used in the data reduction propagates directly to the uncertainties in the clearance of the balloon above the datum surface. In our project we used the height anomalies field implied by the set of potential coefficients up to degree 180 computed by (Rapp, Dec. 1981) and referred to as the Rapp 180 field. The height anomalies were needed in data reduction process to convert the WGS72 geometric heights given as the data to the normal heights in GRS67 (See Section 10.2).

The Rapp-180 field used in the data reduction process gives the undulations (height anomalies) with the accuracy on the order of ± 1 m (Rapp, Dec. 1981, p. 31). For our actual sub-balloon trace in New Mexico we decided it is sufficient to represent the Rapp-180 height anomaly field in this area by a

constant value of -23 m (±0.26 m) which is the mean height anomaly computed for the flight portion of the experiment only. We conclude that the usage of the Rapp-180 undulation field introduces about 1 m uncertainty into the balloon vertical position. Using the same vertical gradients stated above we find the 0.0003 mgal error in the computed Δg value and the 0.3 mgal error in the computed normal gravity.

In conclusion, we notice that the positional errors in the balloon coordinates and the height anomaly error do not noticeably affect the gravity anomaly computation, but they have an effect on the computed normal gravity and on the predicted observed gravity (mainly due to the altitude error). Therefore, the predicted observed gravity may be contaminated by at least 0.6 mgal uncertainty due to the vertical positional errors.

10.6 Other Sources of Errors

In Section 6 we considered theoretically how the errors present in gravity data propagate through the upward continuation integration. Here we can try to use some of the results of Section 6 to give the rough evaluation of errors that affect the actual procedure.

The main source of the gravity data error probably comes from the gridding procedure of the gravity material by means of the collocation prediction of the mean 5'x5' values. If we assume that the mean values computed by the collocation prediction procedure are contaminated by the error function having error variance of 25 mgal^2 (this number is a rough estimate from the formal errors output by the collocation prediction in the area of the balloon flight; see Figure 12, central portion) and the correlation length of about 10 km (this correlation length is unavoidably due to the gaps in the original gravity data of about this size which cause the adjacent 5'x5' blocks to be correlated), then we can use Table 2 together with (eq. 6.2.9) to conclude that at 30 km flight altitude the propagated effect is about 0.9 mgal (in standard error) with 55 km correlation length. This puts the limit of accuracy on our entire procedure. This limit is due to the quality of the original gravity data mainly in spatial distribution and cannot be overcome by refinements in procedure unless the geometry and quality of original data are improved.

It should be noted here that errors present in the mean anomalies (for which 25 mgal^2 variance and 10 km correlation length at ground level was our rough estimate) are due to both: errors in the original gravity point-values (on input to collocation prediction routine) and errors of interpolation. The error of interpolation comes from the difference between the true gravity anomaly and the gravity anomaly model implemented by the subtraction of the reference field in order to center the original data. Of course where the original data are very dense the computed mean values are (almost) uncorrelated and are affected mainly by the point-gravity data error. If this error in original point-values could be modelled by a weakly correlated noise having correlation length shorter than 5'x5' blocks (used in prediction) then this type of data error would tend to cancel during the computation of 5'x5' means, producing essentially negligible effect at 30 km altitude. If the point-data field is sparse in some areas then the predicted mean values will be

affected by both data error and the interpolation error. In sparse areas the computed mean values tend to be correlated with each other and so will be the interpolation error. The correlation length of this error is dependent on the size of the gaps in the original data - the larger the gaps the wider correlated errors (from this type of analysis comes our rough estimate of 10 km correlation length errors present on output of collocation prediction procedure). As we learn in Section 6 such widely correlated errors do not attenuate very fast with altitude. For example, according to our rough estimate (see Table 2) at 30 km flight altitude the correlated errors produce the effect that can be descibed as the distortion function which is 0.9 mgal in amplitude and 55 km wide in correlation length. This type of effect can very easily be misinterpreted as some sort of systematic error and wrongly associated with errors in the modeling of the upward continuation distance (see Section 9.2.3) or the data reduction error. We consider this type of error as the main limitation of accuracy of final results.

Another effect considered in Section 6 is the representation error due to the conceptual replacement of the true gravity field by the step function composed of the flat patches over 5'x5' blocks. At 30 km flight altitude the rough estimate of this effect in gravity anomaly is only about 0.01 mgal (standard error).

If we assume that the effects considered here act independently of each other we can sum the error variances of each component to get the rough estimate of the total error to be 0.92 mgal (total standard error) in gravity anomaly and about 0.7 mgal error in normal gravity.

In Table 12 we give the summary of errors that affect the actual results of upward continued gravity anomalies and normal gravity for the Balloon Project. Notice that the indirect method is to some extent free of the truncation error (Section 4) since we carry up the complete global long-wavelength information represented by the spherical harmonic expansion of the gravity field up to degree 180.

In order to get a feeling of the actual magnitude of propagated errors it is possible to perform some simplified numerical test. (Rapp, 1966) suggested a simple numerical check (not estimate) on the relative magnitude of propagated uncorrelated errors in the upward continuation process. The trick is to upward continue the estimates of accuracies of gravity material using the same computer program which was used to process the actual gravity data.

In a computer implementation the upward continuation integral (6.1.1) takes the form of summation:

$$\Delta g_H = \frac{H}{2\pi} \sum \sum \Delta g \frac{dxdy}{D^3} \qquad (10.6.1)$$

This is a weighted average operator. Now, if we know the accuracy $m^2_{\Delta g}$ of each component Δg_{ij} used in the summation (10.6.1) we can neglect the

correlations between adjoining blocks (i, j) and simply sum the individual error variances $m^2_{\Delta g}$ over all blocks used according to the formula:

$$m^2_{\Delta g_H} = \frac{H^2}{(2\pi)^2} \sum \sum m^2_{\Delta g} \left(\frac{dxdy}{D^3}\right)^2 \qquad (10.6.2)$$

Table 12. Error Budget of the Gravity Upward continuation for the Balloon Project

Source	Effect at 30 km Altitude	
	Gravity Anomaly	Normal Gravity
The original gravity material error and the error in predicted 5'x5' mean anomalies (interpolation error) (see Section 6) assumed: standard error 5 mgals correlation length 10 km	0.9 mgal standard error 55 km correlation length	unaffected
Errors in the modelling of the upward continuation distance (on the transition from the true earth to the Poisson's spherical geometry). (See Table 9, col. 3). assumed uncertainty: 1.5 km	0.2 mgal uncertainty	unaffected
Representation error (See Section 6)	0.2 mgal standard error	unaffected
Errors in the balloon position (See Section 10.5)		
horizontal errors of 2 m	0.0012 mgal maximal error	0.0011 mgal uncertainty
vertical errors of 2 m	0.0006 mgal uncertainty	0.6 mgal uncertainty
Height anomaly error (See Section 10.5)		
Estimated uncertainty of 1 m	0.003 mgal uncertainty	0.3 mgal uncertainty

This is the quadrature formula similar to (10.6.1) but with the squared kernel. Therefore, we used the actual upward continuation program described in (Rapp 1966) to upward continue the uncorrelated errors in the gravity material due to the prediction of mean values on the 5'x5' grid, using (10.6.2). For programming details see (Rapp, 1966). Computation was performed exactly at the balloon locations giving the accuracies on the order of 0.2 mgal for the flight portion of the balloon trajectory (30 km upward continuation distance). From this single experiment we observe the attenuation of errors from about 4 mgals (on average) at the ground level to about 0.2 mgals at 30 km flight altitude.

It is important to realize that this numerical experiment is valid only for one specific type of error (namely errors due to prediction of the mean gravity anomaly values on the grid, see Section 8.3 for details) assuming the error is uncorrelated. Also the arbitrary scaling of error variances on the ground would produce the respective rescaling of upward continued variances of flight elevation. In that sense only the relative degree of attenuation is a meaningful outcome of that numerical check.

11. Summary and Conclusion

We have presented operational procedures for the upward continuation of gravity anomalies given on the surface of the earth. The main conceptual difficulty is that operationally available anomalies are referred to the earth's surface, which is not an equipotential surface. These surface anomalies can be upward continued using discrete estimation procedures such as collocation or a Bjerhammar-type of approach, but in this report we have avoided such techniques because of the expensive matrix inversions that they require.

Instead, as stated in Section 1 we used collocation only in a preliminary step, to predict an optimal set of mean anomaly values from the available irregularly distributed point anomaly data. This application of collocation is operationally feasible because in contrast to the prediction of upward continued values, the prediction of mean anomalies requires information to be inverted only from a small number of data points around the computation block. After obtaining a complete set of mean anomalies over rectangular blocks we turn to a continuous upward continuation problem, in which it is assumed that at every point on the earth's surface we know the gravity anomaly function, as represented by the mean values.

The upward continuation of a continuous gravity anomaly function given on the (non-level) surface of the earth is by no means a simple problem. The simplest conceptualization of a solution is by means of Taylor series expansion, in which the surface anomalies are first used to derive anomalies on a level surface using the vertical gradients of the anomaly field. Once the level surface anomalies are known classical Poisson integration yields a solution to the upward continuation problem with relative accuracy on the order of the earth's flattening. However, for rough anomaly fields the computation of vertical gradients required for data reduction to a level surface, itself requires such density and accuracy of data that is not usually available in practice (see Noe (1980), for example). Moreover, for such fields downward continuation of surface values cannot be expected to be regular. Therefore, as reasoned out in Section 3 we have resorted to the so-called indirect method of upward continuation.

The most important feature of the indirect method is the extraction and separate modeling of the high frequency irregularities of the original gravity anomaly signal. This high frequency component is due to shallow topographic masses, and can be modeled by directly integrating the gravitational effects of those masses without need for any sort of data reduction to a level surface. Operationally, the topographic effects on gravity anomalies at altitude can be computed by prism integration as stated in Section 2.5 with an operational program mentioned in Section 7, while on the earth's surface the topographic effect on gravity anomaly at a point is conveniently formed as the sum of a "Bouguer plate" effect and a "terrain correction" effect (see (3.3.11)). In this report we modeled the high frequency component of the 3-dimensional gravity anomaly field using as "equivalent sources" the positive and negative topographic masses of assumed density $2.67 g/cm^3$, lying between the actual topography and a reference topography to spherical harmonic degree and order 180. With the extraction and separate modeling of the high frequency anomaly signal we circumvent the major difficulties associated with the

reduction of surface data to a level surface, these difficulties being precisely due to the high frequency irregularities of the field.

The residual field left after removal of topographic effects is much smoother than the original field. From this residual field we decided to further remove and separately model the low frequency component using the Rapp-180 (1981) field. This was done in order to formally free the upward continuation from truncation error caused by neglect of remote zone data. In order to remove the effect of the Rapp-180 field from the surface data, the data points were basically taken at their actual horizontal positions, but an assumption had to be made that the data points all lie on a common level surface and not in their actual vertical positions. The assumption was necessary to keep evaluation time for the Rapp-180 field reasonable. The assumption seems justified because the vertical gradient of a 180-field is expected to be small, but this point can be further studied (see, for example Table 9). The Rapp-180 field was evaluated at ground level using a program for fast generation on a grid, while at isolated computation points at altitude another program suited for single point computations was used (see Section 7).

The medium frequency residual field, left after removing both the high frequency topographic effects and the low frequency spherical harmonic field, was then modeled by the Poisson integral. Since the data points were still located on the earth's surface, a data reduction to a level surface was still called for. However, since the residual field is much smoother than the original field, an approximate reduction can be used. To do this a long-wavelength form of the terrain correction, namely, the terrain correction tc^s of an expansion of the topography to degree 180, was implicitly applied to the residual anomalies. The application of long-wavelength terrain correction to approximate a first order long-wavelength reduction of surface anomaly data to a level surface is discussed in Moritz (1966). Since the final position of the level surface to which the data are reduced is uncertain in this procedure, it was simply assumed that this position coincides with the mean elevation of topography in the area of upward continuation. Such uncertainties in defining the data level directly causes uncertainties in defining the upward continuation distance H_0 which is the vertical clearance between the data level and the upward continuation point in space. The numerical effect of such uncertainties on upward continuation results can be examined from Table 9.

The final upward continued gravity anomaly model of the indirect method was then the sum total of three contributions: low frequency contribution from spherical harmonics, high frequency contribution from topographic mases, and medium frequency contribution from Poisson integration of terrain-corrected residual field. The relative order of magnitude of the three contributions depends on the spectral distribution of power of a particular field,and for the profiles tested in Section 9 the contributions were about the same in magnitude.

As a matter of interest, we compared the results of the indirect method to those of two simpler upward continuation procedures. The first was the direct Poisson integration of the original terrain-uncorrected surface anomalies, simply assuming the anomalies to lie on a common level surface. The second was the direct Poisson integration of terrain-corrected surface anomalies, with

the terrain-corrections intended to effect an approximate data reduction to a level surface. The terrain corrections in the second method originated from the point terrain corrections given in the original data records, these corrections having applied to the original point anomalies before the prediction of the mean anomalies used in Poisson integration.

For the numerical tests we developed 5'x5' mean anomalies and 5'x5' mean elevations in a 7°x9° test area in New Mexico, starting from available irregularly distributed point anomaly data and 30"x30" grid point elevations. The 30"x30" elevations themselves were also used in the final computations, for detailed integration of topographic effects in the immediate vicinity of the computation point. The various operational steps in developing mean anomalies including data thinning, tailoring of covariance function, use of only the ten closest data points in the collocation prediction, and data de-trending at high and low frequencies are discussed in detail in Section 8. The required resolution and area coverage of mean anomalies for given upward continuation distances, as well as the effect of data error propagation, can be assessed based on concepts presented in Sections 4, 5 and 6.

Numerical investigations on upward continuations to test-profiles at 30, 10, and 5 km are presented in Section 9. The test profiles resulting from the direct Poisson integration of terrain-uncorrected anomalies are negatively biased (i.e., too low) by about (0.6, 0.5, 0.7) mgal at elevation (30, 10, 5) km compared with the profiles resulting from the direct Poisson integration of terrain-corrected anomalies. This bias between the two direct methods represents the effect of upward continued terrain corrections (see (9.2.3)). There is no detectable bias between the terrain-corrected direct method and the indirect method; this is mainly due to the fact that in the Poisson integration part, the two methods both use terrain-corrected anomalies (see (9.2.6) and (9.2.7)). The standard deviation of the differences among all three upward continuation methods reach the order of (0.5, 0.6, 1.3) mgal at (30, 10, 5) km elevation (see Tables 3, 4, and 5).

In Section 10 we present the details of applying the upward continuation methods to compute anomalies (and total gravity) at points of the balloon-borne gravity measuring project of AFGL. It is hoped that such projects would provide "aerial truth" assessment of the accuracies of upward continuation models. It is projected in Section 10.6 that values at the balloon points have been recovered with about 0.9 mgal standard error in gravity anomaly with data error propagation as dominating error source, and about 0.7 mgal error in normal gravity with vertical position error as dominating error source.

In another series of tests (Section 9.3) we have shown agreement between Fast Fourier upward continuation and Poisson integration, on the level of (0.1, 0.3) mgal at (30, 10) km elevation. Fast Fourier techniques are useful for very fast generation of complete grids of upward continued values.

We conclude that actual gravity measurements at altitude should be used to validate the various procedures presented in this report. Practical validation will be most important. First, to ascertain the accuracy of the upward continued gravity values, and second, to ascertain the improvements gained by employing the following intended refinements: the use of terrain correction to

approximate data reduction to a level surface, and the modeling of high frequency anomaly components as topographic mass effects. Preferably, actual measurements should be accurate in the milligal level, to validate the small bias and differences observed in our numerical comparisons.

Appendix A

DIGITAL FOURIER TRANSFORM FOR UPWARD CONTINUATION

```
// JOB ,
// REGION=512K,MSGLEVEL=(2,0)
/*JOBPARM V=S
//PROCLIB DD DISP=SHR,DSN=GEODSCI.PROCLIB
// EXEC VSSUPER
//SOURCE DD *
C
C
C
C UPWARD CONTINUATION OF DG BY FOURIER TRANSFORM
      IMPLICIT REAL*8 (A-H,O-Z)
      COMPLEX*16  Z(128,128),CTEMP(128)
      DIMENSION TEMP(108)
      DIMENSION D1(2,128,128)
      EQUIVALENCE (D1(1,1,1),Z(1,1))
      COMMON CTEMP
C
C INITIATE CONSTANTS (LINEAR MEASURE IN KM ANGULAR INITIALLY IN DEC DEG)
      H=28.5D0
      R=6371D0+1.5D0
      AMELEV=1.5D0
      PI=4D0*DATAN(1D0)
      ANGRID=5D0/60D0
      FIAVER=32.5D0
C
C LINEAR INCREMENTS IN E-W AND N-S DIRECTIONS
      DX=R*DCOS(FIAVER*PI/180D0)*ANGRID*PI/180D0
      DY=R*ANGRID*PI/180D0
C
C INPUT THE DATA
      NX=128
      NY=128
      INDX=108
      INDY=84
C
      DO 2 I=1,NY
      DO 2 J=1,NX
    2 Z(I,J)=(0D0,0D0)
      DO 5 I=1,INDY
      READ(1,7001)(TEMP(J),J=1,INDX)
      DO 5 J=1,INDX
      Z(I,J)=TEMP(J)
    5 CONTINUE
 7001 FORMAT(10X,10F7.2/(3X,11F7.2))
C
```

```
C-----------------------------------------------
C FORWARD 2-D TRANSFORM (+SIGN)
      CALL FFT2D(Z,NY,NX,+1)
C
C
C FREQUENCY INCREMENTS
      DFX=1D0/(NX*DX)
      DFY=1D0/(NY*DY)
C
C UPWARD CONTINUATION 2D TRANSFORM ( - SIGN)
      CALL FFT2UP(H,DFY,DFX,Z,NY,NX,-1)
C-----------------------------------------------
C
C OUTPUT
      DO 11 I=1,INDY
      DO 10 J=1,INDX
   10 TEMP(J)=Z(I,J)
   11 IF(I.EQ.42) WRITE(6,7002)(J,TEMP(J),J=1,INDX)
 7002 FORMAT(1X,I3,F7.2)
C
      STOP
      END
      SUBROUTINE FFT2D (H,NX,NY,NSIGN)
C*********************************************************
C     SUBROUTINE FFT2D COMPUTES THE TWO DIMENSIONAL FOURIER TRANSFORM
C     OF A COMPLEX ARRAY H(NX,NY),NX AND NY MUST BE A POWER OF 2.
C
C     NSIGN= +1 INVERSE TRANSFORM
C
C     NSIGN= -1 FORWARD TRANSFORM
C
C*********************************************************
      IMPLICIT REAL*8 (A-H,O-Z)
      COMMON CTEMP
      COMPLEX*16 H(NX,NY),CTEMP(128)
      SIGNI=DFLOAT(NSIGN)
      DO 10 IY=1,NY
   10 CALL FORK(NX,H(1,IY),SIGNI)
      IF(NY.EQ.1) RETURN
      DO 20 IX=1,NX
      DO 30 IY=1,NY
   30 CTEMP(IY)=H(IX,IY)
      CALL FORK(NY,CTEMP,SIGNI)
      DO 40 IY=1,NY
   40 H(IX,IY)=CTEMP(IY)
   20 CONTINUE
      RETURN
      END
      SUBROUTINE FORK(LX,CX,SIGNI)
C*********************************************************
C     FAST FOURIER TRANSFORM, MODIFIED FROM CLAERBOUT,J.F.
C     FUNDAMENTALS OF GEOPHYSICAL DATA PROCESING, MCCRAW-HILL,1976.
C             LX
C     CX(K)=SUM(CX(J)*EXP(2*PI*SIGNI*I*(J-1)*(K-1)/LX))
C             J=1
```

```
C      FOR K=1,2,...,(LX=2**INTEGER)
C      SIGNI= +1 INVERSE TRANSFORM
C      SIGNI= -1 FORWARD TRANSFORM
C      LX MUST BE A POWER OF 2 (LX=2**INTEGER)
C      NORMALIZATION PERFORMED BY DIVIDING BY
C      DATA LENGTH UPON THE FORWARD TRANSFORM
C*************************************************************
       IMPLICIT REAL*8 (A-H,O-Z)
       COMPLEX*16 CX(LX),CARG,CEXP,CW,CTEMP
       PI=4D0*DATAN(1D0)
       J=1
       SC=1D0/DFLOAT(LX)
       DO 30 I=1,LX
       IF(I.GE.J) GOTO 10
       CTEMP=CX(J)
       CX(J)=CX(I)
       CX(I)=CTEMP
    10 M=LX/2
    20 IF(J.LE.M) GOTO 30
       J=J-M
       M=M/2
       IF(M.GE.1) GOTO 20
    30 J=J+M
       L=1
    40 ISTEP=2*L
       DO 50 M=1,L
       CARG=(0D0,1D0)*(PI*SIGNI*DFLOAT(M-1))/DFLOAT(L)
       CW=CDEXP(CARG)
       DO 50 I=M,LX,ISTEP
       CTEMP=CW*CX(I+L)
       CX(I+L)=CX(I)-CTEMP
    50 CX(I)=CX(I)+CTEMP
       L=ISTEP
       IF(L.LT.LX) GOTO 40
       IF(SIGNI.GT.0D0) RETURN
       DO 60 I=1,LX
    60 CX(I)=CX(I)*SC
       RETURN
       END
       SUBROUTINE FFT2UP (ELEV,DFX,DFY,H,NX,NY,NSIGN)
C*************************************************************
C     SUBROUTINE FFT2D COMPUTES THE TWO DIMENSIONAL FOURIER TRANSFORM
C      OF A COMPLEX ARRAY H(NX,NY),NX AND NY MUST BE A POWER OF 2.
C ELEV  IS THE APWARD CONTINUATION DISTANCE (SAME UNITS AS DX DY)
C DFX DFY   FREQUENCY INCREMENTS ASSOCIATED WITH INDEXES NX NY RESP
C               DFX=1/(NX*DX)      DFY=1/(NY*DY)
C
C      NSIGN= +1 INVERSE TRANSFORM
C
C      NSIGN= -1 FORWARD TRANSFORM
C
C*************************************************************
```

```
      IMPLICIT REAL*8 (A-H,O-Z)
      COMMON CTEMP
      COMPLEX*16 H(NX,NY),CTEMP(128)
      PI=4D0*DATAN(1D0)
      SIGNI=DFLOAT(NSIGN)
C
      DO 16 IX=1,NX
      IF(IX-1.GT.NX/2)THEN
      IPX=(IX-1)-NX
      ELSE
      IPX=IX-1
      ENDIF
      DO 15 IY=1,NY
      IF(IY-1.GT.NY/2) THEN
      IPY=(IY-1)-NY
      ELSE
      IPY=IY-1
      ENDIF
      DUMP=DEXP(-ELEV*2D0*PI*DSQRT(DFLOAT(IPX)**2*DFX**2+DFLOAT(IPY)
     $**2*DFY**2))
   15 H(IX,IY)=DUMP*H(IX,IY)
   16 CONTINUE
C
      DO 10 IY=1,NY
   10 CALL FORK(NX,H(1,IY),SIGNI)
      IF(NY.EQ.1) RETURN
C
      DO 20 IX=1,NX
      DO 30 IY=1,NY
   30 CTEMP(IY)=H(IX,IY)
      CALL FORK(NY,CTEMP,SIGNI)
      DO 40 IY=1,NY
   40 H(IX,IY)=CTEMP(IY)
   20 CONTINUE
      RETURN
      END
/*
//GO.FT01F001 DD DISP=SHR,DSN=TS4268.FA5X5B.NEWMEX
//
```

References

Bhattacharyya, B.K., "Some General Properties of Potential Fields in Space and Frequency Domain: A Review," Geoexploration, vol. 5, pp. 127-143, 1967.

Bjerhammar, A., "A New Theory of Geodetic Gravity," Trans. Roy. Inst. Technol. Stockholm, No. 243, 1964.

Claerbout, J.F., Fundamentals of Geophysical Data Processing with Applications to Petroleum Prospecting, McGraw Hill, Inc., New York, 1976.

Colombo, O., "Convergence of the External Expansion of the Gravity Field Inside the Bounding Sphere," Manuscripta Geodaetica, Vol. 7, No. 3, pp. 209-246, October 1982.

Cruz, J.Y., Ph.D. thesis (in preparation), Dept. of Geodetic Science and Surveying, The Ohio State University, 1985.

Forsberg, R., "A Study of Terrain Reductions, Density Anomalies, and Geophysical Inversion Methods in Gravity Field Modeling," Report No. 355, Dept. of Geodetic Science and Surveying, The Ohio State University, April 1984.

Forsberg, R. and C.C. Tscherning, "The Use of Height Data in Gravity Field Approximation by Collocation," J. Geophys. Res., Vol. 86, No B9, pp. 7843-7854, September 1981.

Forsythe, G.E., M.A. Malcolm, C.B. Moler, Computer Methods for Mathematical Computations, series in Automatic Computation, Prentice-Hall, Inc., Englewood Cliffs, New Jersey, 1977.

Heiskanen, W.A. and H. Moritz, Physical Geodesy, W.H. Freeman and Co., San Francisco, 1967.

Heller, W.G. and S.K. Jordan, "Attenuated White Noise Statistical Gravity Model", J. Geophys. Res., Vol. 84, No. B9, pp. 4680-4688, August 1979.

Hirvonen, R.A., "A New Theory of the Gravimetric Geodesy", Publications of the Institute of Geodesy, Photogrammetry and Cartography, No. 9, The Ohio State University, 1960.

Hirvonen, R.A. and H. Moritz, "Practial Computation of Gravity at High Altitudes", Report No. 27, Insitute of Geodesy, Photogrammetry and Cartography, The Ohio State University, May 1963.

Hittelman, A.M., D. Scheibe, and C. Goad, "U.S. Land Gravity," Key to Geophysical Records Documentation No. 18, National Geophysical Data Center, NOAA, Boulder, Colorado, 1982.

Jekeli, C., "Reducing the Error of Geoid Undulation Computations by Modifying Stokes' Function," Report No. 301, Dept. of Geodetic Science and Surveying, The Ohio State University, May 1980.

Jekeli, C., "Optimizing Kernels of Truncated Integral Formulas in Physical Geodesy," presented at IAG, General Meeting, Tokyo, Japan, May 7-15, 1982.

Jordan, S.K., "Fourier Physical Geodesy," The Analytic Sciences Corporation, Report No. 1, AFGL-TR-78-0056, for Air Force Geophysics Laboratory, 1978.

Lazarewicz, et al., "Balloon-borne, High-Altitude Gravimetry," EOS Abstracts for AGU Spring Meeting, Vol. 64, No. 18, May 3, 1983.

Morelli, C., et al., "The International Gravity Standardization Net 1971 (IGSN-71)," Special Publication No. 4, International Association of Geodesy, May 1972.

Moritz, H., "Studies on the Accuracy of the Computation of Gravity in High Elevations," Report No. 21, Institute of Geodesy, Photogrammetry and Cartography, The Ohio State University, April 1962.

Moritz, H., "Linear Solutions of the Geodetic Boundary-Value Problem," Report No. 79, Dept. of Geodetic Science, The Ohio State University, December 1966.

Moritz, H., "On the Use of the Terrain Correction in Solving Molodensky's Problem," Report No. 108, Dept. of Geodetic Science, The Ohio State University, May 1968.

Moritz, H., "Nonlinear Solutions of the Geodetic Boundary-Value Problem," Report No. 126, Dept. of Geodetic Science, The Ohio State University, October 1969.

Moritz, H., "Molodensky's Series and Analytical Continuation," Report No. 145, Dept. of Geodetic Science, The Ohio State University, September 1970.

Moritz, H., "Convergence of Molodensky's Series," Report No. 183, Dept. of Geodetic Science, The Ohio State University, September 1972.

Moritz, H., Advanced Physical Geodesy, Herbert Wichmann Verlag, Karlsruhe, 1980.

Noe, H., "Numerical Invesigations on the Problem of Molodensky," der geodatischen Institute der Technischen Universitat Graz Folge 36, 1980.

Rapp, R.H., "A FORTRAN Program for the Upward Coninuation of Gravity Anomalies," Report No. 62, Dept. of Geodetic Science, The Ohio State University, February 1966.

Rapp, R.H., "A FORTRAN Program for the Computation of the Normal Gravity and Gravitational Field of the Earth," Report No. 52, Dept. of Geodetic Science, The Ohio State University, January 1966.

Rapp, R.H., "Results of the Application of Least-Squares Collocation to Selected Geodetic Problems," in H. Moritz and H. Sunkel (eds): Approximation Methods in Geodesy, H. Wichmann, Karlsruhe, pp. 117-156, 1978.

Rapp, R.H., "Geometric Geodesy," vol. 1 (class notes), Department of Geodetic Science and Surveying, The Ohio State University, 1980.

Rapp, R.H., "The Earth's Gravity Field to Degree and Order 180 Using Seasat Altimeter Data, Terrestrial Data, and other Data," Report No. 322, Dept. of Geodetic Science and Surveying, The Ohio State University, December 1981..

Rapp, R.H., "A FORTRAN Program for the Computation of Gravimetric Quantities from High Degree Spherical Harmonic Expansions," Report No. 334, Dept. of Geodetic Science and Surveying, The Ohio State University, September, 1982.

Rizos, C., "An Efficient Computer Technique for the Evaluation of Geopotential from Spherical Harmonic Models," Aust. J. Geodesy, Photogrammetry and Surveying, No. 31, pp. 161-169, December 1979.

Robinson, E.A., M.T. Silvia, Digital Foundations of Time Series Analysis, vol. 2, Wave-Equation Space-Time Processing, Holden Day, Inc., San Francisco, 1981.

Rummel, R., "Downward Continuation of Gravity Information From Satellite Tracking or Satellite Gradiometry in Local Areas," Report No. 221, Dept. of Geodetic Science, The Ohio State University, April 1975.

Rummel, R., "Gravity Parameter Estimation from Large Data Sets Using Stabilized Integral Formulas and a Numerical Integration Based on Discrete Point Data," Report No. 339, Dept. of Geodetic Science and Surveying, The Ohio State University, September 1982.

Schwarz, K.-P. and G. Lachapelle, "Local Characteristics of the Gravity Anomaly Covariance function," Bulletin Geodesique, vol. 54, pp. 21-35, 1980.

Shepperd, S.W., "Molodenskii-type Coefficients with Application to Gravity Disturbance Vector Truncation Errors at Altitude," Report No. R-139, The Charles Stark Draper Laboratory, Inc., Cambridge, MA, October 1979.

Sideris, M.G., "Computation of Terrain Corrections Using the Fast Fourier Transform," IAG SSG 4.91 handout, January 1984.

Sunkel, H., "Feasibility Studies for the Prediction of the Gravity Disturbance Vector in High Altitudes," Report No. 311, Dept. of Geodetic Science and Surveying, The Ohio State University, March 1981.

Sunkel, H., "The Estimation of Free-Air Anomalies," Report No. 315, Dept. of Geodetic Science and Surveying, The Ohio State University, September 1981.

Sunkel, H., "Point Mass Models and the Anomalous Gravitational Field of the Earth," Report No. 328, Dept. of Geodetic Science and Surveying, The Ohio State University, December 1981.

Sunkel, H., "The Geoid in Austria," in Proceedings of the International Association of Geodesy (IAG), Symposia, Hamburg, FRG, pp. 348-364, August 1983.

Sunkel, H., and G. Kraiger, "The Prediction of Free-Air Anomalies," Manuscripta Geodaetica, Vol. 8, No. 3, pp. 229-248, December 1983.

Tscherning, C.C. and R. Forsberg, "Prediction Test Using Least Squares Collocation and Residual Terrain Reduction," in K.-P. Schwarz (ed.): Techniques to Predict Gravity Anomalies and Deflections of the Vertical in Mountainous Areas, Report No. 30004, Dept. of Surveying Engineering, University of Calgary, Alberta, 1983.

Tscherning, C.C., "Gravity Prediction Using Collocation and Taking Known Mass Density Anomalies into Account," Geophys. J.R. astr. Soc., 59, 147-153, 1979.